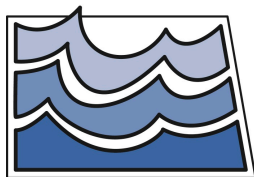


**FIELD AND LABORATORY SOIL HYDRAULIC  
PROPERTY DATA MEASURED FOR THE  
CARRINGTON RECHARGE PROJECT (1987-1993)  
AND THE SARE-ACE PROJECT (1992-1996)**



By  
W.M. Schuh



**Water Resources Investigation No. 59  
North Dakota State Water Commission**

**2017**



This report may be downloaded as a PDF file from  
the North Dakota State Water Commission website at:

<http://swc.nd.gov>

Click on Reports and Publications.

Then, click on Water Resource Investigations, and scroll down to WRI No. 59



## CARRINGTON RECHARGE and SARE-ACE\* EXPERIMENTS 1987 - 1998



RECHARGE



SARE-ACE

### Thanks To

Ron Meyer  
Dr. David Klinkbiel  
Dr. John Gardner  
Dr. Bruce Seelig  
Mike Sweeney  
Staff of the NDSU  
Carrington Research  
Extension Center,  
Carrington, North Dakota  
SWC Technicians



\*ACE – Agriculture in Concert with the Environment grant / USDA  
SARE – Sustainable Agriculture Research and Education grant / USDA



## EXECUTIVE SUMMARY

The purpose of this report is to present the soil hydraulic data for field experiments conducted on the lands of the Carrington Research Extension Center, Carrington, ND, between 1987 and 1996. The data consists of three full profile measurements of in situ hydraulic conductivity and water retention in 6-inch (15.2-cm) increments from the surface to approx. 1 m, with accompanying bulk density and laboratory water retention data to extend the dry range; and laboratory measurements of soil-water retention, bulk density, and unsaturated-hydraulic conductivity from undisturbed core samples collected in the vadose zone below the root zone, at 1 to 1.5 m below land surface. Parametric functions are included for all data.

Two experiments were conducted on the lands of the North Dakota State University Carrington Research Extension center, at Carrington, ND, to measure drainage from the root zone and movement of agricultural chemicals to groundwater under varying cropping practices. The experiments included:

1. The Carrington RECHARGE experiment, was conducted from 1987 through 1993. The purpose of the RECHARGE experiment was to partition and quantify drainage from the root zone, and movement of water and agricultural chemicals to the underlying vadose zone, saturated till, and Carrington aquifer at 20 feet (6 m) below land surface. Field hydraulic properties measured for the experiment included infiltration rates at three sites, unsaturated hydraulic-conductivity, and water-retention curves for 6-inch depth increments on three sites using the instantaneous profile method of Rose et al. (1965) and Hillel et al. (1972), and supplementary measurements of laboratory bulk density and water retention. All data were fitted to the functional format of van Genuchten (1980) for modeling applications.
2. The Carrington SARE-ACE experiment was conducted from 1990 through 1996. The purpose was to determine the effects of three crop management practices, labeled Biological, Conventional, and Integrated, on yield, drainage, and movement of nitrate to the vadose zone, the saturated till, and the underlying Carrington aquifer. The experiment consisted of a randomized block design consisting of 12 replicate blocks (36 sites). Soil hydraulic data measured for the SARE-ACE experiment included laboratory water-retention curves, hydraulic diffusivity, and unsaturated hydraulic conductivities from undisturbed core samples for depths 107, 122, 137, and 152 cm below land surface. All data were fitted to the functional format of van Genuchten (1980) for modeling applications.

In addition,  $^{15}\text{N}$  and  $^{18}\text{O}$  isotope data for nitrate samples were collected and determined to assess denitrification occurrence in the vadose zone, saturated till, and upper aquifer under all treatments. It was concluded that substantial denitrification was occurring in the saturated till and upper aquifer, but most in the saturated till. Isotope data and analysis are included in this report.

This report presents all of the hydraulic data for both experiments in tabular, graphical, and functional format for future use, modeling and comparative analysis by other parties who may wish to do so. I have

attempted to provide sufficient documentation of methods and limitations to enable use of the data with reasonable understanding of its appropriate use and limitations.





## TABLE OF CONTENTS

	Page
<b>INTRODUCTION.....</b>	<b>1</b>
<b>CARRINGTON RECHARGE: 1988-1990.....</b>	<b>5</b>
LAYOUT AND METHODS.....	5
<b>Measurement of In-Situ Hydraulic Properties.....</b>	<b>5</b>
<b>Soil Particle Size, Organic Carbon, and Specific Conductance.....</b>	<b>6</b>
<b>Soil Bulk Density and Water Retention.....</b>	<b>7</b>
<b>Field Measurements.....</b>	<b>8</b>
SUMMARY OF PUBLISHED RESULTS.....	8
RECHARGE EXPERIMENT DATA.....	10
<b>Infiltration.....</b>	<b>10</b>
<b>Laboratory Soil-Water Retention and Bulk Density.....</b>	<b>13</b>
<b>Unsaturated Soil Hydraulic Conductivity Values and Parameters.....</b>	<b>15</b>
<u>In Situ Soil Hydraulic Data and VG Parameters for the NE Site.....</u>	19
<u>In Situ Soil Hydraulic Data and VG Parameters for the NW Site.....</u>	24
<u>In Situ Soil Hydraulic Data and VG Parameters for the SE Site.....</u>	29
<b>CARRINGTON SARE-ACE EXPERIMENT: 1992-1996.....</b>	<b>35</b>
FIELD DESIGN, LAYOUT AND SAMPLING PLAN.....	35
<b>Instrumentation.....</b>	<b>35</b>
<b>Water Sample Collection and Measurement.....</b>	<b>38</b>
<b>Soil Hydraulic Characteristic Sample Collection.....</b>	<b>38</b>
<b>Laboratory Hydraulic Property Measurements.....</b>	<b>38</b>
SUMMARY OF PUBLISHED RESULTS.....	39
SOIL HYDRAULIC DATA, PROPERTIES, AND PARAMETERS.....	40
<b>Soil Bulk Density and Water Retention.....</b>	<b>40</b>
<u>Bulk Density.....</u>	40
<u>Soil Water-Retention Curves.....</u>	42

## TABLE OF CONTENTS

	Page
<b>Soil Saturated Hydraulic Conductivity</b> .....	47
<b>Unsaturated Hydraulic Diffusivity and Conductivity</b> .....	52
<b>Unsaturated Soil Hydraulic Conductivity Parametric Form</b> .....	52
<b>Unsaturated Soil Hydraulic Conductivity Values and Parameters</b> .....	54
<u>Site C3. Evaluation Comments, Hydraulic Data, and VG Functions</u> .....	57
<u>Site C4. Evaluation Comments, Hydraulic Data, and VG Functions</u> .....	61
<u>Site C5. Evaluation Comments, Hydraulic Data, and VG Functions</u> .....	64
<u>Site C6. Evaluation Comments, Hydraulic Data, and VG Functions</u> .....	68
<u>Site C7. Evaluation Comments, Hydraulic Data, and VG Functions</u> .....	72
<u>Site C8. Evaluation Comments, Hydraulic Data, and VG Functions</u> .....	76
<u>Site D6. Evaluation Comments, Hydraulic Data, and VG Functions</u> .....	80
<u>Site D7. Evaluation Comments, Hydraulic Data, and VG Functions</u> .....	85
<u>Site D8. Evaluation Comments, Hydraulic Data, and VG Functions</u> .....	89
<u>Site D9. Evaluation Comments, Hydraulic Data, and VG Functions</u> .....	94
<u>Site D10. Evaluation Comments, Hydraulic Data, and VG Functions</u> .....	98
<u>Site D11. Evaluation Comments, Hydraulic Data, and VG Functions</u> .....	101
<b>Soil Water Retention and Unsaturated Soil Hydraulic Conductivity Parameter: Analysis and Summary</b> .....	<b>105</b>
<b>ISOTOPIC INDICATORS OF DENITRIFICATION</b> .....	<b>109</b>
$^{15}\text{N}$ and $^{18}\text{O}$ vs. Nitrate-N.....	<b>112</b>
$^{15}\text{N}$ and $^{18}\text{O}$ vs. Depth.....	<b>114</b>
$^{5}\text{N}$ and $^{18}\text{O}$ vs. Nitrate-N by Treatment.....	<b>115</b>
<b>Denitrification Conclusions</b> .....	<b>115</b>
<b>CITATIONS</b> .....	<b>117</b>
<b>APPENDIX A-1: Soil Particle Size, Texture, Organic Carbon, Specific Conductance, and 15-Bar Gravimetric Water Content for Recharge Experiment Sites - NW, NE, and SE Hydraulic Measurement Sites</b> .....	<b>pp. A1-A3</b>
<b>APPENDIX A-2: Soil Particle Size, Texture, Organic Carbon, Specific Conductance, and 15-Bar Gravimetric Water Content for Recharge Experiment Sites - Vadose Sampler Sites.</b> .....	<b>pp. A4-A5</b>
<b>APPENDIX B: Soil Water Retention for Individual Samples, SARE-ACE</b> .....	<b>pp. B1-B6</b>

## LIST OF FIGURES

	Page
Figure 1. Location of the RECHARGE and SARE-ACE project sites on the Carrington Station.....	2
Figure 2. Soil Series map for the RECHARGE and SARE-ACE project sites.....	3
Figure 3. Carrington RECHARGE experiment Plot Layout. N, S, E, W labels are monitoring well nests. Southeast, Northeast, and Northwest symbols indicate measurement sites for soil hydraulic properties, including infiltration rates, unsaturated hydraulic conductivity and water retention data; and later used for monitoring ambient moisture conditions.....	6
Figure 4. Sample-plate assembly used for measurement of soil water retention curves.....	7
Figure 5. Infiltration rate (i) and cumulative infiltration (I) for the NE Site.....	10
Figure 6. Infiltration rate (i) and cumulative infiltration (I) for the NW Site.....	11
Figure 7. Infiltration rate (i) and cumulative infiltration (I) for the SE Site.....	12
Figure 8a. Northeast Site water retention and hydraulic conductivity data (Depths 7 through 38 cm). Combined field (wet range) and laboratory (dry range) $\theta(\psi)$ data and field $K(\theta)$ data, with fitted VG function parameters.....	22
Figure 8b. Northeast Site water retention and hydraulic conductivity data (Depths 53 through 137 cm). Combined field (wet range) and laboratory (dry range) $\theta(\psi)$ data and field $K(\theta)$ data, with fitted VG function parameters.....	23
Figure 9a. Northeast Site water retention and hydraulic conductivity data (Depths 7 through 38 cm). Combined field (wet range) and laboratory (dry range) $\theta(\psi)$ data and field $K(\theta)$ data, with fitted VG function parameters.....	27
Figure 9b. Northwest Site water retention and hydraulic conductivity data (Depths 53 through 137 cm). Combined field (wet range) and laboratory (dry range) $\theta(\psi)$ data and field $K(\theta)$ data, with fitted VG function parameters.....	28
Figure 10a. Southeast Site water retention and hydraulic conductivity data (Depths 7 through 38 cm). Combined field (wet range) and laboratory (dry range) $\theta(\psi)$ data and field $K(\theta)$ data, with fitted VG function parameters. ....	32
Figure 10b. Southeast Site water retention and hydraulic conductivity data (Depths 53 through 137 cm). Combined field (wet range) and laboratory (dry range) $\theta(\psi)$ data and field $K(\theta)$ data, with fitted VG function parameters. ....	33

## LIST OF FIGURES

Page

Figure 11. SARE-ACE project site layout, including treatment and instrumentation plan.....	36
Figure 12. Sample site identification for the SARE-ACE experiment site. MWT indicates Carrington aquifer wells were drilled by Midwest Testing, using a hollow stem auger; SWC indicates Carrington aquifer wells were drilled by the State Water Commission using a forward-rotary drill rig.....	37
Figure 13. Mean water retention values for 107-cm, 122-cm and 152-cm depths.....	45
Figure 14. Upper and lower quartile water retention values for 107-cm, 122-cm and 152-cm depths.....	45
Figure 15. Tempe cell assembly used to measure $K_s$ and $K(\psi/\theta)$ .....	48
Figure 16. Acrylic disc used for $K_s$ and $K(\psi/\theta)$ measurements. Disc was overlain by a 0.11 mm thin porous membrane.....	48
Figure 17. Illustration of VG function use default for $K_s$ between the air entry / inflection $\theta(\psi)$ value near saturation and saturation moisture. <i>Note: <math>\psi</math> corresponding to <math>K(\theta)</math> on the graph is determined by first tracking vertically to the corresponding <math>\theta</math> curve, and then locating (horizontally) the <math>\psi</math> value corresponding to that <math>\theta</math> value.....</i>	55

### SARE-ACE VG Data and Figures by Site

Figure C3-1. Measured laboratory data and fitted VG functions for $\theta(\psi)$ and $K(\theta)$ (114 cm and 137-cm, Rep. 2) and $\theta(\psi)$ , $D(\theta)$ and $K(\theta)$ data for 137-cm Rep. 1. VG parameters are shown in the overlying boxes. <i>Note: <math>\psi</math> corresponding to <math>K(\theta)</math> on the graph is determined by first tracking vertically from <math>K(\theta)</math> (blue curve) to the corresponding <math>\theta(\psi)</math> curve (red), and then locating (horizontally right) the <math>\psi</math> value corresponding to that <math>\theta</math> and <math>K(\theta/\psi)</math> value.....</i>	59
Figure C3-2. Comparison of measured $\theta(\psi)$ (left) and $K(\theta)$ (right) data for C3-114 cm, C3-137-cm, Rep. 1, and C3-137-cm, Rep. 2. C3-137-cm, Rep. 1 uses fitted $K(\theta)$ values calculated from $D(\theta)$ data shown in the tables and figures above.....	60
Figure C4-1. Measured laboratory data and fitted VG functions for $\theta(\psi)$ and $K(\theta)$ (114 cm and 137-cm, Rep. 1 and Rep. 2). VG parameters are shown in the overlying boxes. <i>Note: <math>\psi</math> corresponding to <math>K(\theta)</math> on the graph is determined by first tracking vertically from <math>K(\theta)</math> (blue curve) to the corresponding <math>\theta(\psi)</math> curve (red), and then locating (horizontally right) the <math>\psi</math> value corresponding to that <math>\theta</math> and <math>K(\theta/\psi)</math> value.....</i>	62

## LIST OF FIGURES

	Page
Figure C4-2. Comparison of measured $\theta(\psi)$ (left) and $K(\theta)$ (right) data for C4-114 cm, C4-137-cm, Rep. 1, and C4-137-cm, Rep. 2.....	63
Figure C5-1. Measured laboratory data and fitted VG functions for $\theta(\psi)$ and $K(\theta)$ (114 cm and 137-cm, Rep. 1 and Rep. 2). VG parameters are shown in the overlying boxes. <i>Note: <math>\psi</math> corresponding to <math>K(\theta)</math> on the graph is determined by first tracking vertically from <math>K(\theta)</math> (blue curve) to the corresponding <math>\theta(\psi)</math> curve (red), and then locating (horizontally right) the <math>\psi</math> value corresponding to that <math>\theta</math> and <math>K(\theta/\psi)</math> value.....</i>	66
Figure C5-2. Comparison of measured $\theta(\psi)$ (left) and $K(\theta)$ (right) data for C5-114 cm, C5-137-cm, Rep. 1, and C5-137-cm, Rep. 2. Fitted function uses the mean of the three parameter set values.....	67
Figure C6-1. Measured laboratory data and fitted VG functions for $\theta(\psi)$ and $K(\theta)$ (114 cm and 137-cm, Rep. 1 and Rep. 2). VG parameters are shown in the overlying boxes. <i>Note: <math>\psi</math> corresponding to <math>K(\theta)</math> on the graph is determined by first tracking vertically from <math>K(\theta)</math> (blue curve) to the corresponding <math>\theta(\psi)</math> curve (red), and then locating (horizontally right) the <math>\psi</math> value corresponding to that <math>\theta</math> and <math>K(\theta/\psi)</math> value.....</i>	70
Figure C6-2. Comparison of measured $\theta(\psi)$ (left) and $K(\theta)$ (right) data for C6-114 cm, C6-137-cm, Rep. 1, and C6-137-cm, Rep. 2. Fitted function uses the mean of three parameter set values. In addition, the mean $\rho$ , best fit $\rho$ , and most common $\rho=0.0001$ .....	71
Figure C7-1. Measured laboratory data and fitted VG functions for $\theta(\psi)$ and $K(\theta)$ (114 cm, 137-cm Rep. 1 and 137-cm, Rep. 2). <i>Note: <math>\psi</math> corresponding to <math>K(\theta)</math> on the graph is determined by first tracking vertically from <math>K(\theta)</math> (blue curve) to the corresponding <math>\theta(\psi)</math> curve (red), and then locating (horizontally right) the <math>\psi</math> value corresponding to that <math>\theta</math> and <math>K(\theta/\psi)</math> value.....</i>	74
Figure C7-2. Comparison of measured $\psi(\theta)$ (left) and $K(\theta)$ (right) data for C7-114 cm, C7-137-cm, Rep. 1, and C7-137-cm, Rep. 2. This figure uses the mean water content, fits the mean suction using the mean of the VG parameters for the three samples. $K(\theta)$ is calculated using the mean fitted $K$ , and mean $\rho$ parameter for the three depths. Fitted $K(\theta)$ are also calculated using the mean $\rho$ for 114 cm and 137-cm Rep. 1 samples, and the most common $\rho$ ( $\rho=0.0001$ ).....	75
Figure C8-1. Measured laboratory data and fitted VG functions for $\theta(\psi)$ and $K(\theta)$ (114 cm, 137-cm Rep. 1 and 137-cm, Rep. 2). Fits not obtained for 114 cm and 137 cm, Rep. 1 samples. <i>Note: <math>\psi</math> corresponding to <math>K(\theta)</math> on the graph is determined by first tracking vertically from <math>K(\theta)</math> (blue curve) to the corresponding <math>\theta(\psi)</math> curve (red), and then locating (horizontally right) the <math>\psi</math> value corresponding to that <math>\theta</math> and <math>K(\theta/\psi)</math> value.....</i>	78

## LIST OF FIGURES

Page

<p>Figure C8-2. Comparison of measured <math>\psi(\theta)</math> (left) and <math>K(\theta)</math> (right) data for C8-114 cm, C8-137-cm, Rep. 1, and C8-137-cm, Rep. 2 data; This figure uses the mean water content, fits the mean suction using the mean of the VG parameters for the three samples. VG <math>K(\theta)</math> is calculated using the mean fitted <math>K</math>, and <math>\rho = 0.0001</math>.....</p>	79
<p>Figure D6-1. Measured laboratory data and fitted VG functions for <math>\theta(\psi)</math> (137-cm, Rep. 1 and Rep. 2); and <math>D(\theta)</math>, and <math>K(\theta)</math> for 137 cm, Rep. 2. VG parameters are shown in the overlying boxes. <i>Note: <math>\psi</math> corresponding to <math>K(\theta)</math> on the graph is determined by first tracking vertically from <math>K(\theta)</math> (blue curve) to the corresponding <math>\theta(\psi)</math> curve (red), and then locating (horizontally right) the <math>\psi</math> value corresponding to that <math>\theta</math> and <math>K(\theta/\psi)</math> value</i>.....</p>	83
<p>Figure D6-2. Comparison of measured <math>\theta(\psi)</math>, D6-137-cm, Rep. 1, and D6-137-cm, Rep. 2.....</p>	84
<p>Figure D7-1. Measured laboratory data and fitted VG functions for <math>\theta(\psi)</math> and <math>K(\theta)</math> (114 cm, 137-cm, Rep. 1 and 137-cm, Rep. 2). <i>Note: <math>\psi</math> corresponding to <math>K(\theta)</math> on the graph is determined by first tracking vertically from <math>K(\theta)</math> (blue curve) to the corresponding <math>\theta(\psi)</math> curve (red), and then locating (horizontally right) the <math>\psi</math> value corresponding to that <math>\theta</math> and <math>K(\theta/\psi)</math> value</i>.....</p>	87
<p>Figure D7-2. Comparison of measured <math>\psi(\theta)</math> (left) and <math>K(\theta)</math> (right) data for D7-114 cm, D7-137-cm, Rep. 1, and D7-137-cm, Rep. 2. This figure uses the mean water content, fits the mean suction using the mean of the VG parameters for the three samples. <math>K(\theta)</math> is calculated using the mean fitted <math>K</math>, and mean <math>\rho</math> parameter for the three depths. Fitted <math>K(\theta)</math> are also calculated using the most common <math>\rho</math> (<math>\rho = 0.0001</math>).....</p>	88
<p>Figure D8-1. Measured laboratory data and fitted VG functions for <math>\theta(\psi)</math> and <math>K(\theta)</math> data (114 cm); and <math>\theta(\psi)</math> and <math>D(\theta)</math>, and fitted <math>K(\theta)</math> curves (137-cm Rep. 1 and 137-cm, Rep. 2). <i>Note: <math>\psi</math> corresponding to <math>K(\theta)</math> on the graph is determined by first tracking vertically from <math>K(\theta)</math> (blue curve) to the corresponding <math>\theta(\psi)</math> curve (red), and then locating (horizontally right) the <math>\psi</math> value corresponding to that <math>\theta</math> and <math>K(\theta/\psi)</math> value</i>.....</p>	92
<p>Figure D8-2. Comparison of measured <math>\psi(\theta)</math> (left) and <math>K(\theta)</math> (right) data for D8-114 cm, D8-137 cm, Rep. 1, and D8-137 cm, Rep. 2. This figure uses the mean water content, fits the mean suction using the mean of the VG parameters for the three samples. <math>K(\theta)</math> is calculated using the mean fitted <math>K</math>, and mean <math>\rho</math> parameter for the three depths. Fitted <math>K(\theta)</math> are also calculated using the most common <math>\rho</math> (<math>\rho = 0.0001</math>).....</p>	93
<p>Figure D9-1. Measured laboratory data and fitted VG functions for <math>\theta(\psi)</math> and <math>K(\theta)</math> (114 cm and 137-cm, Rep. 1 and Rep. 2). VG parameters are shown in the overlying boxes. <i>Note: <math>\psi</math> corresponding to <math>K(\theta)</math> on the graph is determined by first tracking vertically from <math>K(\theta)</math> (blue curve) to the corresponding <math>\theta(\psi)</math> curve (red), and then locating (horizontally right) the <math>\psi</math> value corresponding to that <math>\theta</math> and <math>K(\theta/\psi)</math> value</i>.....</p>	96

## LIST OF FIGURES

Page

Figure D9-2. Comparison of measured  $\theta(\psi)$  (left) and  $K(\theta)$  (right) data for D9-114 cm, D9-137-cm, Rep. 1, and D9-137-cm, Rep. 2. Fitted function uses the mean of three parameter set values (including mean  $\rho = -0.883$ ), and the most common  $\rho$  value ( $\rho = 0.0001$ ).....97

Figure D10-1. Measured laboratory data and fitted VG functions for  $\theta(\psi)$  and  $K(\theta)$ . *Note:  $\psi$  corresponding to  $K(\theta)$  on the graph is determined by first tracking vertically from  $K(\theta)$  (blue curve) to the corresponding  $\theta(\psi)$  curve (red), and then locating (horizontally right) the  $\psi$  value corresponding to that  $\theta$  and  $K(\theta/\psi)$  value.....99*

Figure D10-2. Comparison of measured  $\theta(\psi)$  (left): measured  $K(\theta)$  for D10-114 cm, D10-137-cm, Rep. 1, and D10-137-cm, Rep. 2, and fitted VG functions determined using the mean of the VG parameters for the three samples.  $K(\theta)$  is calculated using the mean fitted  $K$ , and mean  $\rho$  ( $\rho = -2.1$ ) parameter for the three depths. Fitted  $K(\theta)$  are also calculated using the most common  $\rho$  ( $\rho = 0.0001$ ).....100

Figure D11-1. Measured laboratory data and fitted VG functions for  $\theta(\psi)$  and  $K(\theta)$ . *Note:  $\psi$  corresponding to  $K(\theta)$  on the graph is determined by first tracking vertically from  $K(\theta)$  (blue curve) to the corresponding  $\theta(\psi)$  curve (red), and then locating (horizontally right) the  $\psi$  value corresponding to that  $\theta$  and  $K(\theta/\psi)$  value.....103*

Figure D11-2. Comparison of measured  $\theta(\psi)$  (left): measured  $K(\theta)$  for D11-114 cm, D11-137-cm, Rep. 1, and D11-137-cm, Rep. 2, and fitted VG functions determined using the mean of the VG parameters for the three samples.  $K(\theta)$  is calculated using the mean fitted  $K$ , and mean  $\rho$  parameter for the three depths. Fitted  $K(\theta)$  are also calculated using the most common  $\rho$  ( $\rho = 0.0001$ ).....104

### End SARE-ACE VG Data and Figures by Site

Figure 18.  $^{15}\text{N}$  and  $^{18}\text{N}$  isotope vs. nitrate-N by depth.....113

Figure 19.  $^{15}\text{N}$  and  $^{18}\text{O}$  vs. depth by individual treatment site. ....114

Figure 20.  $^{15}\text{N}$  and  $^{18}\text{O}$  vs nitrate-N by Treatment. ....115



## LIST OF TABLES

	Page
Table 1. Infiltration rate (i) and cumulative infiltration (I) for the SE Site.....	10
Table 2. Infiltration rate (i) and cumulative infiltration (I) for the NW Site.....	11
Table 3. Infiltration rate (i) and cumulative infiltration (I) for the SE Site.....	12
Table 4. Northeast Site Bulk Density and Laboratory Moisture-Retention Data.....	13
Table 5. Northwest Site Bulk Density and Laboratory Moisture-Retention Data.....	13
Table 6. Southeast Site Bulk Density and Laboratory Moisture-Retention Data.....	14
Table 7a. Field hydraulic properties for the Northeast Site of the Carrington RECHARGE experiment (depths 7 through 38 cm).....	19
Table 7b. Field hydraulic properties for the Northeast Site of the Carrington RECHARGE experiment (depths 53 through 83 cm).....	20
Table 7c. Field hydraulic properties for the Northeast Site of the Carrington RECHARGE experiment (depths 99 through 137 cm). ....	21
Table 8a. Field hydraulic properties for the Northwest Site of the Carrington RECHARGE experiment (depths 7 through 38 cm).....	24
Table 8b. for the Northwest Site of the Carrington RECHARGE experiment (depths 53 through 83 cm).....	25
Table 8c. Field hydraulic properties for the Northwest Site of the Carrington RECHARGE experiment (depths 99 through 137 cm). ....	26
Table 9a. Field hydraulic properties for the Southeast Site of the Carrington RECHARGE experiment (depths 7 through 38 cm).....	29
Table 9b. Field hydraulic properties for the Southeast Site of the Carrington RECHARGE experiment (depths 53 through 83 cm).....	30
Table 9c. Field hydraulic properties for the Southeast Site of the Carrington RECHARGE experiment (depths 99 through 137 cm).....	31

## LIST OF TABLES

	Page
Table 10. Measured dry bulk density values for all samples, by depth.....	41
Table 11. Statistical distribution of bulk density values for all samples with depth.....	42
Table 12. Analysis of variance (ANOVA) for BD vs. Depth.....	42
Table 13. Post-hoc Bonferroni test difference between sample depths.....	54
Table 14. Probabilities for Bonferroni Significant Difference due to factors, Sample, subsample, depth, and Site using a sequential linear model. Green color highlights significance at $p < 0.05$ . Yellow color highlights significance at $p < 0.1$ .....	43
Table 15. Selected statistical parameters (mean, median, standard error, and upper and lower 25 <sup>th</sup> %tiles) by suction and depth. Color, and bold letters, indicate statistically inseparable means at BSD $p < 0.05$ .....	44
Table 16. Paired site comparisons having means separable using a Bonferroni significant difference criterion at $p < 0.05$ (green) and $p < 0.1$ (yellow) .....	46
Table 17. Membrane K (Km) statistics.....	47
Table 18. Effect of an 0.11 mm base membrane having a K of 0.05 cm/h on error in the computation of K in a 6-cm core sample.....	49
Table 19. Lab measured (K <sub>meas</sub> ) and final (K <sub>s</sub> ) K values adjusted for resistance of a 0.0011mm thick membrane having K values (Km) listed. Where Km was not measured the average value (Km=0.05 cm/h) was used, indicated by *.....	50
Table 20. Anova for 107—122 depth samples vs. 130-145 samples.....	51
Table 21. Summary statistics for depth increment K <sub>s</sub> values.....	51
Table 22. Summary statistics for material group increment K <sub>s</sub> values. 1= gravely till characteristic material distribution, 2=loamy characteristic material distribution.....	51

## LIST OF TABLES

### SARE-ACE VG Data Tables by Site

Table C3-1. Measured $\theta(\psi)$ , $K(\theta)$ , $D(\theta)$ , determined from laboratory data.....	57
Table C3-2. Measured $\theta(\psi)$ and $D(\theta)$ , determined from laboratory data, and fitted $K(\theta)$ calculated from $\theta(\psi)$ and $D(\theta)$ data input in the VG model.....	58
Table C4-1. Measured $\theta(\psi)$ and $K(\theta)$ determined from laboratory data.....	61
Table C5-1. Measured $\theta(\psi)$ and $K(\theta)$ determined from laboratory data.....	65
Table C6-1. Measured $\theta(\psi)$ and $K(\theta)$ determined from laboratory data.....	69
Table C7-1. Measured $\theta(\psi)$ and $K(\theta)$ determined from laboratory data.....	73
Table C8-1. Measured $\theta(\psi)$ and $K(\theta)$ determined from laboratory data.....	77
Table D6-1. Measured $\theta(\psi)$ and $D(\theta)$ , determined from laboratory data.....	81
Table D6-2. Fitted $\theta(\psi)$ and $K(\theta)$ , determined from laboratory $\theta(\psi)$ data and data shown in Table D6-1.....	82
Table D7-1. Measured $\theta(\psi)$ and $K(\theta)$ determined from laboratory data.....	86
Table D8-1. Measured $\theta(\psi)$ and $K(\theta)$ (114 cm) and $D(\theta)$ (137 cm, Rep. 1 and Rep. 2) determined from laboratory data.....	90
Table D8-2. Fitted $\theta(\psi)$ and $K(\theta)$ (137 cm, Rep. 1 and Rep. 2) determined from laboratory $D(\theta)$ and $\theta(\psi)$ data shown in Table D8-1.....	91
Table D9-1. Measured $\theta(\psi)$ and $K(\theta)$ determined from laboratory data.....	95
Table D10-1. Measured $\theta(\psi)$ and $K(\theta)$ determined from laboratory data.....	98
Table D11-1. Measured $\theta(\psi)$ and $K(\theta)$ determined from laboratory data.....	102

### End SARE-ACE VG Data Tables by Site







## INTRODUCTION

Two experiments were conducted on the lands of the North Dakota State University Carrington Research Extension Center (CREC) between 1988 and 1996, for the purpose of exploring the relationship between groundwater recharge, nitrate and other solute movement, and agricultural systems effects.

The first experiment, conducted from 1988 through 1990, was called the Carrington RECHARGE experiment. The primary objective was to measure, in situ, the movement of groundwater through the root zone to the water table and into the underlying aquifer throughout the growing season, for three years. The second objective was to determine the effect of groundwater flow characteristics on solute transport to each of the groundwater pools (vadose, saturated till, aquifer) beneath the solum within the stratigraphic column. The RECHARGE experiment involved a collaboration of the CREC (Ron Meyer), the North Dakota State Water Commission (William Schuh), and North Dakota State University (Mike Sweeney).

The second experiment, conducted from 1992 through 1996, was called the SARE-ACE experiment for the Station funding sources (North Central Region Sustainable Agriculture Research and Education - abbrev. SARE; and Agriculture in Concert with the Environment - abbrev. ACE). Its purpose was to determine the effects of three different agricultural management systems (labeled BIOLOGICAL, CONVENTIONAL, and INTEGRATED) on yield, deep drainage and recharge, and nitrate movement beneath the root zone. The experiment involved a collaboration of the CREC (Dr. David Klinkebiel and Dr. John Gardner), the North Dakota State Water Commission (William Schuh), and North Dakota State University Extension (Dr. Bruce Seelig). The North Dakota State Department of Health provided material assistance and laboratory assistance for both projects. Substantial field and laboratory soil hydraulic data were collected for both of the experiments, and may be of value for future modeling efforts or field experiments.

Locations of the two experiments are shown on Fig. 1. Soil series for the experiment sites are shown on Fig. 2.

**While some discussion and analysis of the data is provided, mainly for context, the purpose of this report is to assemble the hydraulic property data, and other ancillary unpublished data, in report form for future information, reference and use.**



Figure 1. Location of the RECHARGE and SARE-ACE project sites on the Carrington Station.

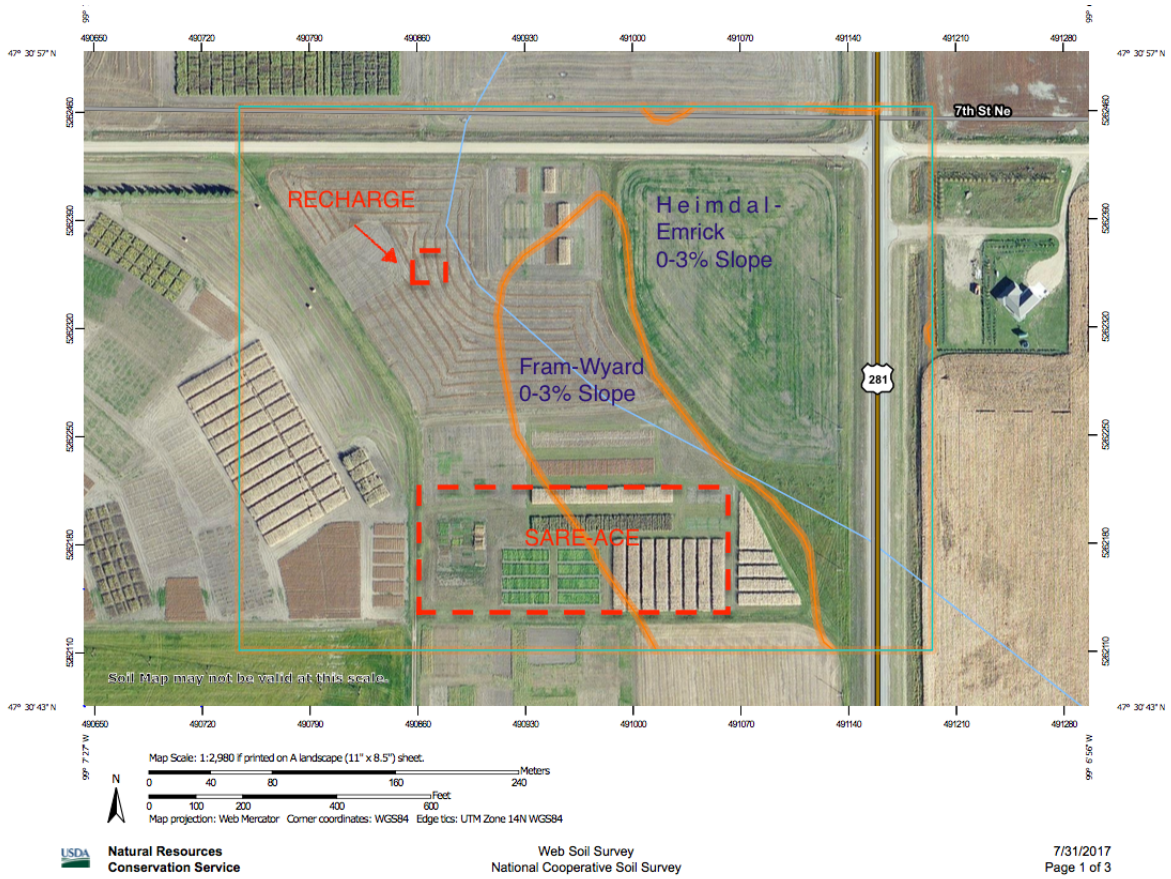


Figure 2. Soil Series map for the RECHARGE and SARE-ACE project sites.



## CARRINGTON RECHARGE: 1988-1990

The purpose of the RECHARGE experiment was to track the spatial variability and movement of water and tracers within the soil profile, to the underlying vadose zone; to the water table, seasonally varying at approx. 8 to 13 ft. (2.5 to 4 m), and to the underlying aquifer at 20 ft. (6 m) during the field season. The plot was located in the NE quarter of the NE quarter of Section 31, T 147 N, R 66 W. The approximate location is shown on Fig. 1. Detailed descriptions of the plot, rotation (wheat, sunflower and soybean), and methods used for hydrologic measurement, including theoretical development, hydrologic data measured, and results were described in Schuh et al. (1993a, 1993b). A general summary description is as follows.

### LAYOUT AND METHODS

The experiment plot consisted of a 100 ft. (30 m) square agronomic buffer perimeter, with an enclosed 40 ft. (12 m) square interior instrumented complex (Fig. 3). Each of four sides of the interior complex contained three monitoring wells placed in the Carrington aquifer at 22 to 23 ft. (6.8 to 7.07 m), the deep saturated till at 14 to 15 ft. (4.27 to 4.57 m), and the shallow seasonally saturated till at 11 to 12 ft. (3.29 to 3.60 m). Local soil series was Heimdal loam<sup>1</sup> (coarse-loamy mixed Udic Haploboroll). Within the interior complex, three sites (Northeast, Northwest, and Southeast) were instrumented with tensiometers at 6-inch (15.2 cm) increments, and a neutron probe access tube to 78 inches (2 m). In addition, 2-inch (5.1 cm) diameter x 9-inch (23-cm) diameter ceramic 1-bar vadose samplers, specially constructed by Soil Moisture Equipment Inc.<sup>TM</sup>, using only silicon glues, were placed at 1.5 m and 3 m below land surface on the west, north, and east sides of the instrumented complex. Samplers were accessed at the surface using 3.2 mm O.D. polytetrafluoroethylene (PTFE) tubing which was connected to the samplers in PTFE pressure fittings, and to stainless steel pressure couplings at the surface. Sampler suctions were applied using a hand vacuum pump, and water was evacuated using a Barnant Masterflex<sup>TM</sup> peristaltic pump.

### Measurement of In-Situ Hydraulic Properties

Field unsaturated hydraulic conductivity,  $K(\theta)$ , and water-retention,  $\theta(\psi)$ , properties were measured using the Instantaneous Profile Method (Rose et al., 1965; Hillel et al., 1972), using a field apparatus described by Schuh et al. (1991) for measurement of in-situ  $K(\theta)$  at Oakes, ND. The sites were diked and flooded until the bottom tensiometer readings were constant. During flooding, a 24-inch (61-cm) diameter infiltrometer ring was placed within diked perimeter and infiltration data were collected on each of the three monitoring sites. Neutron-probe and tensiometer measurements were collected throughout the drainage phase. After the soil profile

---

<sup>1</sup> Determined by Mike Sweeney, Soil Science Department, North Dakota State University.

was saturated, the site was covered and allowed to drain. Neutron probe and tensiometer readings were collected until changes in tensiometer readings were negligible. Neutron-probe moisture ( $\theta$ ) and tensiometric ( $\psi$ ) field data were plotted vs. time, and fitted with smooth curves. The data were then interpolated for calculation of  $K(\theta/\psi)$  using a finite-difference FORTRAN program (Code appended in Schuh et al. (SWC-WRI NO. 19, 1991).

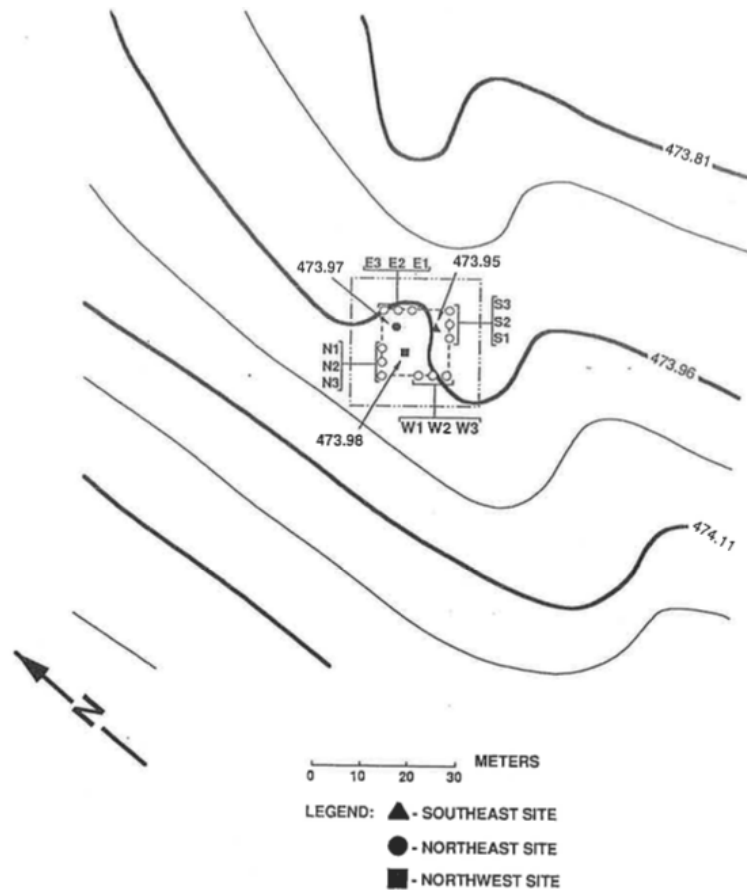


Figure 3. Carrington RECHARGE experiment Plot Layout. N, S, E, W labels are monitoring well nests. Southeast, Northeast, and Northwest symbols indicate measurement sites for soil hydraulic properties, including infiltration rates, unsaturated hydraulic-conductivity and water-retention data; and later used for monitoring ambient moisture conditions. Elevations are in meters.

### Soil Particle Size, Organic Carbon, and Specific Conductance

Particle-size distribution, organic carbon, and soil-water specific conductance (saturated paste extract) for 6-inch (15-cm) depth increments, using soil samples from the neutron-probe access tube placement on each of the three (NW, NE and SE) sites, were determined by the NDSU Soils Laboratory and are presented in Appendix A of this report.

### **Soil Bulk Density and Water Retention**

Core ring samples were collected using a Ulen-type sampling attachment designed for extracting cores using a 3-inch (7.62 cm) Giddings™ tube (Schuh, 1987). Samples were collected, sequentially, from the holes bored for placement of vadose samplers by hammering the Giddings probe to each desired depth, and then placing the sampling attachment to the end of the probe tube and gently tapping the anvil on the top of the tube to the depth desired to fill the core rings. Each sample removed consisted of two 3-cm length x 5.16-cm diameter cores samples in brass rings.

Samples in brass rings were each placed on pre-wetted 6-cm diameter 1-bar ceramic plates, covered with a plastic cap, and secured with a rubber band (Fig. 4).



Figure. 4. Sample-plate assembly used for measurement of soil water-retention curves.

Sample-ring assemblies were then placed in a pan with tap water to the near top of the sample and allowed to wet for 48 hours. The saturated sample and plate assemblies were weighed and then placed on pre-wetted 24-cm diameter 1-bar pressure plates with a wetted Whatman #2 paper filter between the plates to affect capillary continuity. Pressure plates and individual plate-sample assemblies were placed in Soil Moisture Equipment Inc. pressure pots, and subjected to applied pressure steps of 50, 100, 150, 200, 330, 500, and 800 cm pressure head. All pressures were controlled using a two-step regulator. Pressures to 150 cm were gaged using a water manometer. For 200 cm and above pressures were measured using the gage on the low-pressure regulator. Sample-plate assemblies were weighed after each step to determine water loss, and placed on a new wetted filter paper on the larger plate for the next sequential step. After the final (800-cm)

pressure step the sample and ring assemblies were removed from the plate assemblies and weighed in steel weighing cans, after weighing the cans. They were then dried at 105° C for 48 hours in a drying oven, and the oven dried samples were reweighed in their cans. Can weights and ring weights were subtracted from the oven-dried sample weight to obtain soil dry weight. The soil oven-dry weight was divided by the ring volume to determine dry bulk density. The wet weight, prior to drying, was used to measure the 800-cm suction gravimetric moisture content as  $g_{sw}/g_{sd}$ , where  $g_{sw}$  is wet soil weight and  $g_{sd}$  is dry soil weight. Volumetric water content at 800-cm suction was calculated by multiplying the gravimetric water content by the bulk density. Volumetric water content for each sequential lower pressure step was then determined by adding the weight loss from the preceding step, assuming one gram per cubic cm of water.

### **Field Measurements**

In situ water-retention and unsaturated hydraulic-conductivity functions, and laboratory soil water-retention data were fitted to closed-form parametric van Genuchten functions (van Genuchten, 1980) for use in modeling. Drainage through the root zone at 0.91 and 1.06 m was calculated using neutron-probe soil-water measurements collected at frequencies based on rainfall events; and corresponding in-situ and laboratory soil hydraulic-conductivity and water-retention data, to calculate hydraulic gradients and time-variant  $K(\theta)$  values at the target depths.

A tracer was placed on the plot in the spring of each year (bromide in 1988, chloride in 1989, and fluoride (which is non-conservative) in 1990. Sample frequencies, methods and results of the tracer experiments were described by Schuh et al. (1997).

Tensiometric data and neutron-probe volumetric water content measurements were collected at each 15.2-cm depth increment, and water levels were measured throughout the unfrozen period of the year. Water samples for tracer and nitrate measurements were collected from each of the monitoring wells, and from the vadose samplers placed beneath the root zone at 5 ft. (1.5 m) and 7 ft. (2.1 m) depths. Drainage through the root zone at 0.91, 1.06, and 1.83 m was calculated using neutron-probe soil water measurements and corresponding in-situ and laboratory measured soil hydraulic-conductivity and water-retention data.

### **SUMMARY OF PUBLISHED RESULTS**

The results indicated that root-zone drainage and the redistribution of water within the entire soil and vadose column was highly variable and complex, and governed mainly by the spatial distribution of surface elevations, rather than by soil property differences. On an artificially land-leveled field having surface elevation differences of less than one inch ( $< 0.03$  m, Fig. 3), root-zone drainage at 0.91 to 1.8 m varied from as high as 25 cm on the SE site, to 4 and 3 cm, on the NE and NW sites, respectively, in 1989; and 25 cm, 4 cm, and 0 cm, respectively, in 1990 (Schuh et. al., 1993). Surface water, following storms, would flow from microtopographic high areas to

microtopographic low areas; then pond, infiltrate, and drain locally. The resulting water table configuration would then consist of a localized hydraulic mound, which would then redistribute laterally until water-table conditions were uniform. The overall conceptual model of the water table within the till, resulting from these results, would be a topographical array of hydraulic mounds of varying height, shape, and size, ranging from "pimples" to large mounds more than a meter in height, forming following storms, and then coalescing (Schuh et. al., 1993a,b; Schuh and Klinkebiel, 2003). The local characteristic of the mound is governed by the size and geometry of the local runoff concentration zone, the size of the rainfall event, and soil and vadose properties. The locally formed hydraulic mounds would then cause what we labeled a local "hydraulic surge" of water from the till into the underlying aquifer. The lateral coalescence of the mound redistribution caused horizontal displacement of water, which then moved upward from the new locations back into the root zone at other locations where it was transpired or later re-drained as the water table dropped. The complex internal cycling of water was described by Schuh et al. (1993b). The hydraulic surge on water flux to the aquifer was modeled by Schuh and Klinkebiel (2003).

The solute movement effect of the complex cycling of water was that tracer and nitrate concentrations at equilibration after redistribution were characteristically distributed in discrete pools (vadose, saturated till, aquifer), with concentrations decreasing approximately logarithmically from the shallow vadose zone to the aquifer (Schuh et al. 1997). Following storms, each lower unit, near its surface, would temporarily reach the concentration of the overlying unit, indicating a displacement of water from the overlying unit to the underlying unit, and then gradually return to its characteristic background concentration as it mixed within the solute pool with more dilute water. The process of localized hydraulic-mound governed surges from the till to the aquifer (at 6 m), and consequent effects on nitrate concentrations, was modeled as described by Schuh et al. (2004). Modeling results were generally consistent with observed results, except that dissipation of nitrate was faster than expected. We hypothesized that denitrification was occurring. Later isotope samples confirmed that denitrification was occurring in the saturated till and in the upper aquifer (see isotope data and discussion in SARE-ACE section of this report).

## RECHARGE EXPERIMENT DATA

### Infiltration

Infiltration was measured at each of the three (Northeast, Northwest and Southeast) monitoring sites during the sorption phase of the field hydraulic property measurements. Methods and fitted equations from Phillip (1966), depth-specific sorption-phase suctions and water contents; and saturated hydraulic conductivities are described and provided in Schuh et al. (2005).

#### Northeast Site Infiltration Data

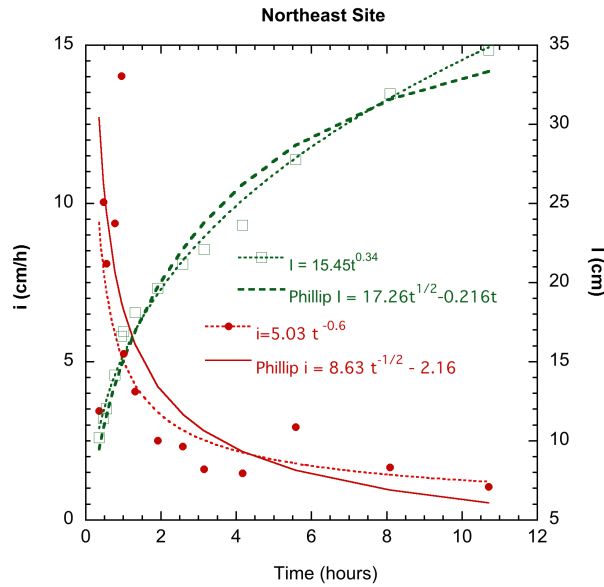


Figure 5. Infiltration rate ( $i$ ) and cumulative infiltration ( $I$ ) for the NE Site with fitted Phillip (1966) functions.

Table 1. Infiltration rate ( $i$ ) and cumulative infiltration ( $I$ ) for the NE Site.

T	I	t	i
hours	cm	hours	cm/hour
0.353	10.21	0.177	-
0.475	11.43	0.414	10.05
0.55	12.04	0.512	8.10
0.778	14.17	0.664	9.37
0.952	16.61	0.865	14.03
1.01	16.92	0.981	5.25
1.31	18.14	1.16	4.06
1.917	19.66	1.613	2.51
2.573	21.19	2.245	2.32
3.143	22.10	2.858	1.61
4.169	23.63	3.656	1.49
5.581	27.78	4.875	2.94
8.081	31.93	6.831	1.66
10.711	34.70	9.396	1.05

Northwest Site Infiltration Data

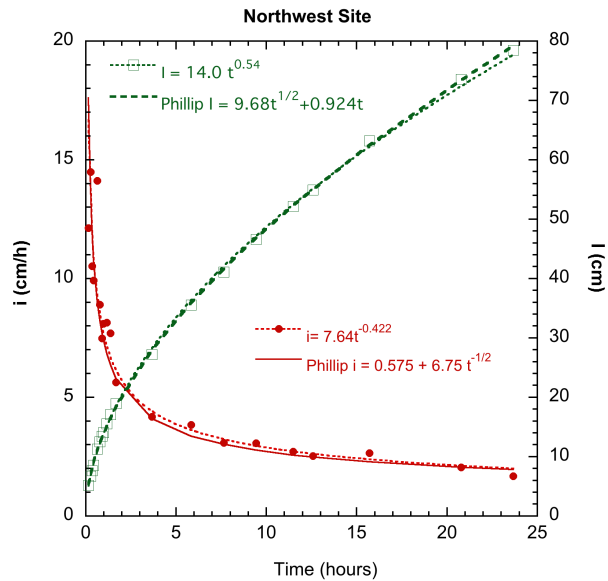


Figure 6. Infiltration rate (i) and cumulative infiltration (I) for the NW Site, with fitted Phillip (1966) functions.

Table 2. Infiltration rate (i) and cumulative infiltration (I) for the NW Site.

T	I	t	i
hours	cm	hours	cm/hour
0.157	5.20	0.079	12.12
0.262	6.72	0.21	14.49
0.349	7.64	0.306	10.52
0.442	8.55	0.396	9.92
0.636	11.30	0.539	14.12
0.773	12.52	0.705	8.91
0.895	13.43	0.834	7.49
0.971	14.04	0.933	8.10
1.158	15.57	1.064	8.15
1.356	17.09	1.257	7.70
1.68	18.92	1.518	5.64
3.669	27.23	2.675	4.18
5.836	35.54	4.753	3.83
7.629	41.07	6.733	3.09
9.436	46.61	8.533	3.06
11.477	52.15	10.457	2.71
12.569	54.92	12.023	2.54
15.701	63.23	14.135	2.65
20.771	73.61	18.236	2.05
23.651	78.46	22.211	1.68

Southeast Site Infiltration Data

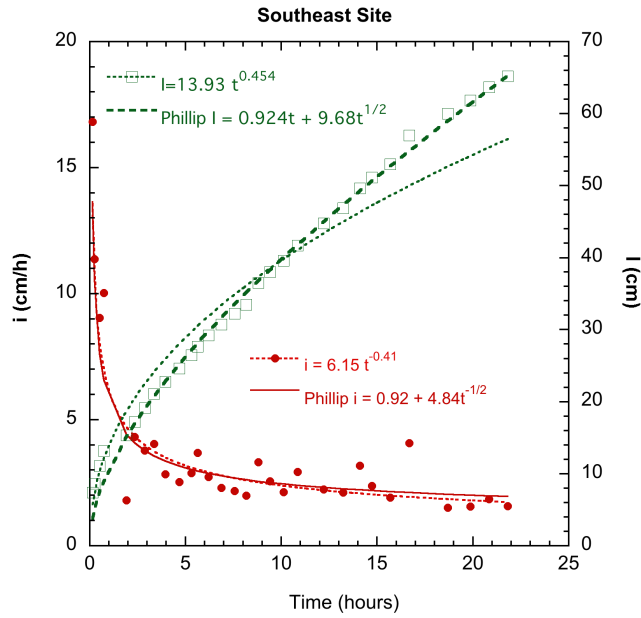


Figure 7. Infiltration rate (*i*) and cumulative infiltration (*I*) for the SE Site, with fitted Phillip (1966) functions.

Table 3. Infiltration rate (*i*) and cumulative infiltration (*I*) for the SE Site.

T	I	t	i
hours	cm	hours	cm/hour
2.342	17.15	2.13	4.31
2.867	19.14	2.605	3.77
3.357	21.12	3.112	4.05
3.949	22.80	3.653	2.84
4.674	24.63	4.311	2.52
5.308	26.46	4.991	2.89
5.639	27.68	5.474	3.69
6.198	29.20	5.918	2.73
6.862	30.73	6.53	2.30
7.561	32.25	7.211	2.18
8.175	33.47	7.868	1.99
9.406	38.05	9.108	2.56
10.123	39.57	9.764	2.13
10.853	41.71	10.488	2.93
12.218	44.76	11.535	2.23
13.231	46.89	12.724	2.11
14.737	51.16	14.416	2.38
15.695	52.99	15.216	1.91
18.681	60.01	17.676	1.52
19.861	61.84	19.271	1.55
20.847	63.67	20.354	1.86
21.815	65.19	21.331	1.58

**Laboratory Soil-Water Retention and Bulk Density**

Laboratory soil-water retention and bulk density for the RECHARGE experiment sites are provided on the following tables. Additional 15-bar gravimetric moisture determinations by the NDSU soils laboratory are provided in Appendix A of this report.

Table 4. Northeast Site bulk density and laboratory moisture-retention data.

Notes*:	A-Black	B-Brown	B-Brown	Coarse	-	-	-	
BD** g/cm <sup>3</sup>	1.38	1.41	1.35	1.45	1.64	1.58	1.78	
	$\theta$							
$\psi$ cm	Depth cm	30	47	61	68	114	153	202
50		0.423	0.385	0.3642	0.2666	0.2924	0.3686	0.3515
100		0.385	0.353	0.3284	0.2338	0.2511	0.3686	0.3415
150		0.369	0.3336	0.3098	0.2249	0.2341	0.3504	0.3347
200		0.366	0.3329	-	0.2189	0.2324	0.3366	-
330		0.3217	0.2666	0.2517	0.1832	0.1683	0.3351	0.3102
500		0.3135	0.2606	0.2465	0.1743	0.1546	0.2476	0.2983
800		0.2964	0.2338	0.2301	0.1638	0.1367	0.1962	0.277

\* Lab core sample description

\*\* Bulk Density determined using the water-retention lab core

Table 5. Northwest Site laboratory water-retention data.

Notes*:	A-Black	B-Brown	B-Brown	C	Loose Sand			
BD** g/cm <sup>3</sup>	1.47	1.48	1.34	1.32	1.48	1.61	1.71	
	$\theta$							
$\psi$ cm	Depth cm	26	44	52	81	113	155	206
50		0.4062	0.3731	0.4081	0.3758	0.3247	0.2707	0.3091
100		0.3727	0.3187	0.3634	0.3262	0.2875	0.2338	0.2919
150		0.3541	0.2949	0.3381	0.3024	0.2666	0.2141	0.283
200		0.3541	-	-	-	-	-	0.2543
330		0.3139	0.2495	0.283	0.2562	0.2189	0.156	0.2543
500		0.3098	0.245	0.28	0.2527	0.2145	0.1545	0.248
800		0.2923	0.2249	0.2592	0.2383	0.2041	0.1329	0.2346

\*Lab core sample description

\*\* Bulk Density determined using the water-retention lab core

Table 6. Southeast Site laboratory water-retention data.

Notes*:										
	A-Black	B-Brown	B-Brown	C	Brown Loose Carb.	Coarse	Coarse			
BD** g/cm <sup>3</sup>	1.46	1.37	1.41	1.42	1.63	1.64	1.67	1.78	1.72	
	$\theta$									
$\psi$ cm	Depth cm	22	40	46	76	93	102	168	198	219
50		0.3977	0.4096	0.3694	0.34	0.2522	0.3232	0.3191	0.3377	0.3307
100		0.3731	0.3761	0.3262	0.3016	0.2175	0.2361	0.2487	0.3128	0.3001
150		0.3532	0.353	0.2949	0.2755	0.1936	0.21	0.2305	0.305	0.2912
200		0.3604	0.3537	0.2767	-	-	-	-	-	-
330		0.3225	0.3016	0.2309	0.2294	0.1435	0.1653	0.1843	0.2841	0.2703
500		0.3165	0.3001	0.2309	0.2271	0.1395	0.1616	0.1798	0.2789	0.2644
800		0.3016	0.2793	0.2279	0.2126	0.1221	0.1393	0.1627	0.2666	0.2525

\*Lab core sample description

\*\* Bulk Density determined using the water-retention lab core

### Unsaturated Soil Hydraulic-Conductivity Values and Parameters

The use of soil hydraulic properties for modeling unsaturated soil processes, including moisture and solute transport, is greatly assisted by treatment of unsaturated hydraulic conductivity  $[K(\psi/\theta)]$  vs. suction head ( $\psi$ ) and moisture ( $\theta$ ) and water-retention curve  $[\psi(\theta)]$  relationships in functional format. The standard approach is to use a functional relationship between soil water-retention curves and the hydraulic-conductivity function, based on the distribution of flow in capillary pores of varying size. Put simply, flow in individual pores under conditions of laminar flow vary approximately logarithmically with the radius of the pore; soil water suction varies with pore radius; the total volume of pores corresponding to a given pore radius increment and flow rate is represented by the corresponding moisture increment, which can be determined from the soil water-retention curve. Therefore, the unsaturated flow rate at a given suction is related to the cumulative flow of all pores in all suctions at, or below that suction and corresponding moisture. Further theoretical adjustments have been developed to account for pore continuity, tortuosity, shape, and other complex factors. In practice, these are treated empirically. Some of these models and methods were discussed by Van Genuchten et al. (1980) and, van Genuchten et al. (1991).

All of the models are theoretically based on characterizing the dynamic flow characteristics of distributed pores of varying radii and other characteristics within the matrix, using the water-retention curve as a base. A wide variety of different theoretical platforms have been developed over the years in what may be described as a developmental process (ex. Burdine, 1953; Marshall, 1958; Millington and Quirk, 1962; Brooks and Corey, 1964). Two of the most commonly used model platforms are those of Burdine (1953) and Mualem (1976), which employ different methods for treating the stochastic element. Burdine and Brooks and Corey both used a parameterized power function relationship between  $\psi$  and  $\theta$ . The power function methods require a two-step application: a linear relationship between saturation and an air entry value, which represents the suction corresponding to the maximum pore radius of the soil; and a parameterized power function fit in the drier range at suctions higher than the air entry value. Van Genuchten has provided a closed-form parametric application for both Burdine and Mualem theoretical approaches. All of the models employ a dry-range minimum moisture (residual moisture). In earlier-model applications the transition between the two functions in power function applications caused some model instabilities. The closed-form Van Genuchten function is generally the easiest to use and has gained wide acceptance in modeling applications. We apply only the Mualem theoretical platform in calculating van Genuchten parameters combined field and laboratory data.

The van Genuchten parametric form for  $\psi(\theta)$  is:

$$\theta_{\psi} = [1 + (a\psi)^n]^{-m} \quad (1)$$

where  $\Theta_\psi$  is the relative moisture content corresponding to suction  $\psi$ , defined as:

$$\Theta_\psi = \frac{(\theta_\psi - \theta_r)}{(\theta_s - \theta_r)} \quad (2)$$

and where  $\theta_\psi$  is the volumetric-moisture content corresponding to  $\psi$ ;  $\theta_r$  is the residual-moisture content, an empirical parameter defining the low moisture boundary for the function; and  $\theta_s$  is the saturation-moisture content. Parameters  $\alpha$ ,  $m$  and  $n$  are empirical. Parameters  $m$  and  $n$  may be fitted separately in the optimizing algorithm, or simplified using the relation:  $m=1-1/n$  (van Genuchten et al. 1991). Separate fitting of  $m$  and  $n$  always provides the best fit. However, the functional form for  $K(\psi/\theta)$  is considerably simplified for model use employing the  $m(n)$  relationship. Use of the simplified relationship allows use of the following functions for  $K(\psi/\theta)$ ;

$$K(\Theta_\psi) = K_r K_e \quad (3)$$

where  $K_e$  is a measured matching  $K(\psi/\theta)$  in the wet range, and  $K_r$  is the ratio of any  $K(\psi/\theta)$  value to the matching value. If saturation  $K$  ( $K_s$ ) is used for  $K_e$ , which is commonly the case,

$$K(\Theta_\psi) = K_r K_s \quad (4)$$

The  $K(\psi)$  function is calculated as:

$$K_r = \frac{\{1 - (\alpha\psi)^{mn} [1 + (\alpha\psi)^n]^{-m}\}^2}{[1 + (\alpha\psi)^n]^{\rho m}} \quad (5)$$

where  $\rho$  is a pore-interaction factor. The exponential  $\rho$  parameter is theoretically developed to account for stochastic elements (ex. tortuosity, shape, non-continuity of pores, etc.). It is, however, empirically determined. Mualem (1976) empirically determined a value of  $\rho=0.5$  using predominantly coarse soils. Schuh and Cline (1991) found that the  $\rho=0.5$  was robust for sandy loam and loamy sand soils, but varied widely for finer soils.

The price of using the simplified ( $m=1-1/n$ ) relationship is described by Van Genuchten et al. (1991) as:

*“One drawback of imposing the restriction  $m=1-1/n$  is that the shape and curvature of the retention curve near saturation is now forced to have a unique relation with the shape and slope of the curve in the dry range when  $\alpha\psi > 1$ . Similarly, the position and slope of the  $K$ -curve near saturation will*

*be fixed for a given slope of the curve at the dry end of the conductivity curve.”*

VG functions were all fitted using a multi-parameter least-squares parameter optimization program (RETC) published by Van Genuchten et al. (1991). The FORTRAN code for computations is contained in the publication cited. Rather than optimizing fits for all data simultaneously,  $\psi(\theta)$  functions were first fitted to  $\alpha$  and  $n$  parameters ( $m$  constrained by  $n$ ).  $K(\psi/\theta)$  data were then optimized for constrained  $\alpha$ ,  $m$  and  $n$ , varying  $K_s$  and  $\rho$ . The pore-interaction factors ( $\rho$ ) from the Carrington RECHARGE experiment were previously examined in relation to those measured at Oakes, ND (Schuh et al. 1993)

The Carrington RECHARGE data were fitted using the simplified  $m(n)$  relationship. Van Genuchten's caveat resulting from the constraint of  $K(\psi/\theta)$  in the wet range is clearly encountered with near-saturation application using the Carrington data. Treating  $K_s$  as a parameter will be seen, in most cases, to result in values different from, and usually larger than measured  $K_s$  values, as predicted by van Genuchten et al (1991). This means that the use of the calculated  $K(\psi/\theta)$  function is usually limited to the unsaturated range, and that approaching saturation it must be truncated and constrained to the measured  $K_s$  value, thereby requiring a two-phase application similar to the Brooks and Corey power-function approach if near-saturation applications are desired. This drawback, however, was avoided in the application intended.

The intended use was modeling water movement just beneath the root zone (1-2 m), and about 1 to 2 m above the water table, so that neither wet-range capillary effects nor root-zone drying governed the moisture values. In addition, surface infiltration effects were attenuated by crop interception and by dry soil capture, so that moisture was always maintained within a relatively narrow range approximately between 70 and 300 cm suction. Limitation of the cycling range also limited hysteretic effect. The applied modeling range, approximately between 70 cm and 300 cm suction, must be kept in mind. For other purposes, particularly for applications near saturation, refits for and properly weighted for the intended range should be implemented. The measured data used are provided with each parameter set in the following tables. If users of the data wish to modify the parametric application of the data, the RETC code can be transcribed from van Genuchten (1991) and compiled for reapplication.

#### *K( $\theta$ ) and $\theta(\psi)$ data*

The smoothed interpolated data used to fit the VG functions, used for modeling root-zone drainage in the RECHARGE experiment, are provided for each site on the Table 7 (NE Site), Table 8 (NW Site), and Table 9 (SE Site) below. The original field data sheets have been lost. However, the outcomes of the FORTRAN computations and the smoothed data used for VG computations are still in record and are provided in the following tables.

*Van Genuchten Functions and Visual Fits to Data*

The interpolated data and fitted VG functions are shown on Fig. 7 (NE Site), Fig. 8 (NW Site), and Fig. 9 (SE Site) below.<sup>2</sup> VG function parameters are in the tables within the K( $\theta$ ) figures. These can be used for modeling soil-water redistribution in the wet range (above field capacity).

---

<sup>2</sup> *Note:* In some of the moisture-retention curve figures additional "dummy" replicates of the data were added near the 800 cm suction values to achieve better wet range fits, and prevent over-leveraging of the curve to the dry range by effect of the 15,300 cm suction value. The visual fits show the conformation of the curves to the data from best fits. These "dummy" replicates are not included on the tables.

In Situ Soil Hydraulic Data and VG Parameters for the NE Site

Table 7a. Field hydraulic properties for the Northeast Site of the Carrington RECHARGE experiment (depths 7 through 38 cm).

7 cm			22 cm			38 cm		
$\psi$ cm	$\theta$	K( $\theta$ ) cm/h	$\psi$ cm	$\theta$	K( $\theta$ ) cm/h	$\psi$ cm	$\theta$	K( $\theta$ ) cm/h
4	0.3958	0.0210						
12	0.3928	0.0180	4	0.3989	0.059	3	0.405	0.250
19	0.3903	0.0170	12	0.3966	0.050	7	0.4031	0.180
24	0.3881	0.0110	19	0.3947	0.047	15	0.4015	0.140
26	0.3863	0.0079	26	0.393	0.031	23	0.4002	0.140
30	0.3846	0.0073	31	0.3916	0.022	31	0.399	0.160
33	0.3831	0.0068	34	0.3903	0.020	33	0.3979	0.140
35	0.3817	0.0065	36	0.3891	0.019	35	0.397	0.130
39	0.3799	0.0061	39	0.3881	0.018	37	0.3961	0.120
43	0.3778	0.0057	42	0.3867	0.017	40	0.395	0.100
48	0.3759	0.0055	46	0.385	0.016	43	0.3936	0.090
54	0.3743	0.0056	50	0.3835	0.015	46	0.3925	0.080
58	0.3728	0.0057	54	0.3823		49	0.3914	0.072
62	0.3714	0.0060	58	0.3811		52	0.3905	0.066
70	0.3691	0.0071	61	0.38		54	0.3896	0.060
88	0.3644		67	0.3783		58	0.3881	0.052
114	0.3586		80	0.3746		67	0.3852	0.039
140	0.3539		98	0.3702		79	0.3815	0.028
160	0.3507		116	0.3665		90	0.3785	0.022
178	0.3481		129	0.364		98	0.3765	0.019
197	0.3456		141	0.362		105	0.3748	0.017
215	0.3434		153	0.3601		112	0.3733	0.016
232	0.3416		164	0.3584		118	0.3719	0.015
249	0.3399		174	0.357		124	0.3707	0.014
275	0.3374		183	0.3557		129	0.3697	0.014
309	0.3344		198	0.3538		136	0.3681	0.013
			218	0.3514		146	0.3662	
						155	0.3646	
						163	0.3632	
						170	0.3621	
						176	0.361	
						182	0.3601	
						188	0.3592	
						193	0.3584	
						198	0.3577	

Table 7b. Field hydraulic properties for the Northeast Site of the Carrington RECHARGE experiment (depths 53 through 83 cm).

53 cm			68 cm			83 cm		
$\psi$ cm	$\theta$	K( $\theta$ ) cm/h	$\psi$ cm	$\theta$	K( $\theta$ ) cm/h	$\psi$ cm	$\theta$	K( $\theta$ ) cm/h
5	0.4147	5.000	5	0.4042	1.500	3	0.3548	0.670
7	0.4126	3.600	7	0.4021	1.300	6	0.3526	0.590
17	0.4107	2.800	5	0.4002	1.200	6	0.3506	0.520
20	0.4091	2.400	8	0.3985	1.000	10	0.3488	0.470
22	0.4076	2.100	12	0.3962	0.920	13	0.3471	0.430
24	0.4063	1.900	15	0.3935	0.790	17	0.3443	0.370
27	0.4045	1.600	18	0.3911	0.690	26	0.3387	0.270
30	0.4024	1.300	22	0.389	0.610	39	0.3318	0.180
33	0.4006	1.100	24	0.3871	0.550	50	0.326	0.130
36	0.3989	0.960	27	0.3854	0.500	58	0.3222	0.110
39	0.3975	0.850	31	0.3825	0.420	65	0.3191	0.095
41	0.3961	0.750	40	0.3765	0.300	71	0.3161	0.081
45	0.3939	0.610	52	0.3692	0.200	77	0.3135	0.072
54	0.3893	0.400	63	0.3632	0.150	83	0.3112	0.065
67	0.3836	0.240	71	0.3592	0.120	88	0.3092	0.059
78	0.379	0.160	78	0.3559	0.099	95	0.3063	0.052
85	0.3758	0.120	85	0.3527	0.084	105	0.3027	0.044
92	0.3733	0.095	91	0.35	0.073	114	0.2996	0.040
99	0.3708	0.076	96	0.3477	0.065	121	0.297	0.036
105	0.3687	0.063	101	0.3455	0.058	128	0.2948	0.033
110	0.3669	0.053	109	0.3424	0.050	134	0.2928	0.031
115	0.3653	0.046	119	0.3386	0.042	140	0.291	0.030
123	0.3629	0.037	127	0.3354	0.036	145	0.2894	0.029
133	0.3599	0.028	135	0.3327	0.032	150	0.2879	0.028
141	0.3574	0.023	142	0.3303	0.028	155	0.2865	0.027
149	0.3553	0.019	148	0.3282	0.026			
155	0.3535	0.016	154	0.3263	0.024			
162	0.3519	0.014	159	0.3246	0.022			
167	0.3504	0.012	164	0.323	0.021			
173	0.3491	0.011	169	0.3216	0.020			
178	0.3478	0.010						
183	0.3467	0.009						

Table 7c. Field hydraulic properties for the Northeast Site of the Carrington RECHARGE experiment (depths 99 through 137 cm).

99 cm			114 cm			137 cm		
$\psi$	$\theta$	$K(\theta)$	$\psi$	$\theta$	$K(\theta)$	$\psi$	$\theta$	$K(\theta)$
cm		cm/h	cm		cm/h	cm		cm/h
1	0.3376	0.790	12	0.3308	1.200	1	0.3412	0.0340
5	0.3348	0.620	20	0.3253	0.500	23	0.3382	0.0160
9	0.3292	0.380	29	0.3215	0.300	31	0.3353	0.0091
25	0.3222	0.220	36	0.3185	0.210	46	0.3325	0.0065
37	0.3165	0.140	43	0.3155	0.150	58	0.3297	0.0048
45	0.3126	0.100	49	0.313	0.110	70	0.327	0.0036
52	0.3096	0.078	55	0.3108	0.087	82	0.3247	0.0028
58	0.3065	0.061	60	0.3089	0.071	92	0.3227	0.0023
65	0.304	0.050	67	0.306	0.053	101	0.3209	0.0019
70	0.3017	0.042	77	0.3024	0.037	115	0.3182	0.0014
75	0.2997	0.035	86	0.2995	0.028	135	0.3149	0.0010
83	0.2967	0.028	93	0.297	0.022	151	0.3122	0.0008
93	0.2931	0.021	100	0.2948	0.018	167	0.3099	0.0006
101	0.2901	0.017	107	0.2928	0.015	181	0.3078	0.0005
109	0.2875	0.014	112	0.2911	0.013	194	0.306	0.0004
116	0.2853	0.011	118	0.2895	0.011	206	0.3044	0.0004
122	0.2833	0.010	123	0.288	0.010	217	0.3029	0.0003
128	0.2815	0.008	128	0.2866	0.008	228	0.3016	0.0003
133	0.2798	0.007				238	0.3003	0.0002
138	0.2783	0.007						
143	0.2769	0.006						

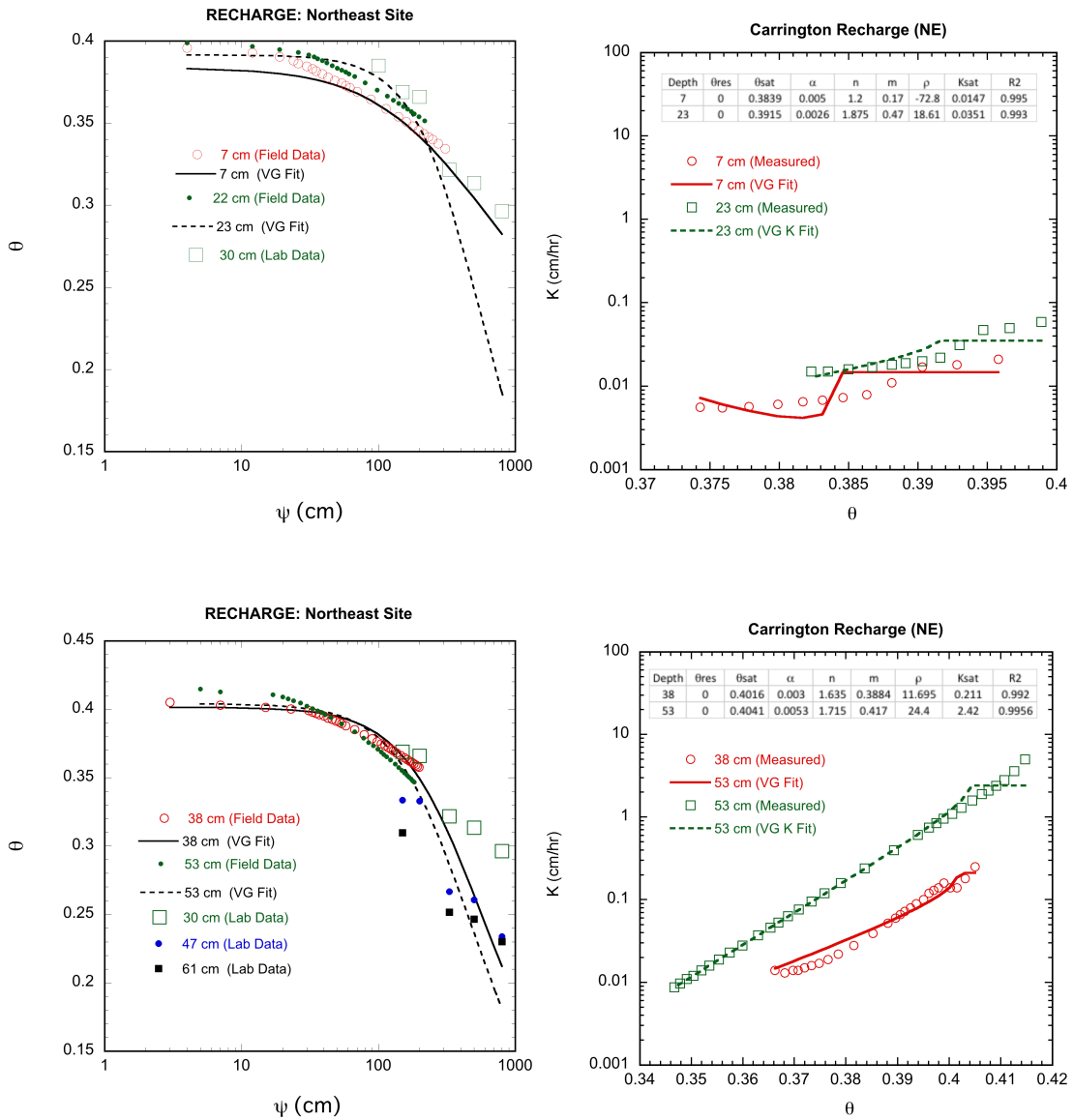


Figure 8a. Northeast Site water-retention and hydraulic-conductivity data (Depths 7 through 38 cm). Combined field (wet range) and laboratory (dry range)  $\theta(\psi)$  data and field  $K(\theta)$  data, with fitted VG function parameters.

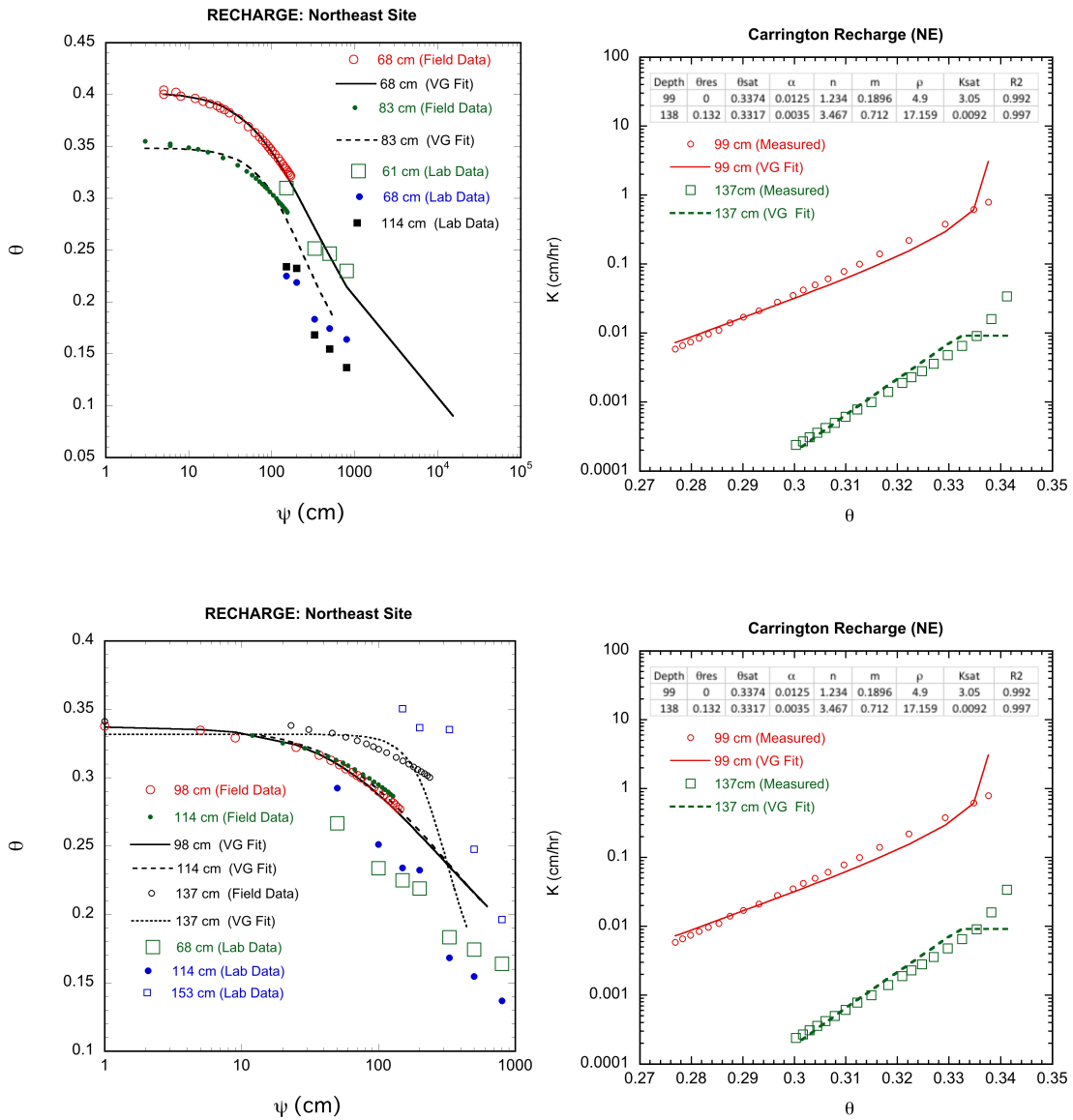


Figure 8b. Northeast Site water-retention and hydraulic-conductivity data (Depths 53 through 137 cm). Combined field (wet range) and laboratory (dry range)  $\theta(\psi)$  data and field  $K(\theta)$  data, with fitted VG function parameters.

In Situ Soil Hydraulic Data and VG Parameters for the NW Site

Table 8a. Field hydraulic properties for the Northwest Site of the Carrington RECHARGE experiment (depths 7 through 38 cm).

7 cm			22 cm			38 cm		
$\psi$ cm	$\theta$	K( $\theta$ ) cm/h	$\psi$ cm	$\theta$	K( $\theta$ ) cm/h	$\psi$ cm	$\theta$	K( $\theta$ ) cm/h
2	0.4002	-	2	0.3953		0.7	0.3981	0.229
7	0.3987	-	8	0.3937	0.388	6	0.3973	0.22
13	0.3955	0.155	13	0.3919	0.258	14	0.3942	0.177
18	0.3926	0.0919	20	0.3893	0.158	23	0.3903	0.118
25	0.3896	0.0538	28	0.3865	0.0935	30	0.3874	0.0885
31	0.3867	0.0318	34	0.3845	0.064	37	0.3851	0.07
37	0.3845	0.0218	40	0.3829	0.0468	43	0.3832	0.0527
42	0.3828	0.016	45	0.3816	0.0365	48	0.3816	0.044
46	0.3814	0.0125	49	0.3804	0.0293	52	0.3802	-
50	0.3802	0.00999	53	0.3794	0.0243	56	0.3789	-
54	0.3791	0.00829	56	0.3785	0.0143	59	0.3778	-
55	0.3755	0.00265	57	0.3778	0.00982	61	0.3768	-
58	0.3743	0.00225	59	0.377	0.00888	64	0.3754	-
60	0.3732	0.00196	61	0.3761	0.00776	67	0.3738	-
63	0.3723	0.00173	64	0.3749	0.00659	70	0.3724	0.0404
65	0.3714	0.00155	67	0.3739	0.00576	73	0.3711	0.0362
67	0.3706	0.00141	69	0.3731	0.00506	75	0.37	0.0333
71	0.3693	0.00118	72	0.3723	0.00456	77	0.369	0.0307
78	0.3667	0.000834	74	0.3715	0.00413	81	0.3672	0.0267
89	0.3634	0.000547	78	0.3703	0.00346	89	0.3637	0.0204
98	0.3607	0.000391	86	0.3678	0.00245	101	0.3593	0.015
104	0.3589	0.00031	96	0.3648	0.0016	110	0.3557	0.0119
110	0.3574	0.000257	106	0.3623	0.00115	117	0.3533	0.0103
116	0.356	0.000216	113	0.3606	0.000909	123	0.3514	0.00925
121	0.3548	0.000185	119	0.3592	0.000753	129	0.3495	0.00847
125	0.3537	0.000162	125	0.3579	0.000633	134	0.3479	0.00791
130	0.3528	0.000144	130	0.3567	0.000542	139	0.3465	0.00757
136	0.3514	0.000121	135	0.3557	0.000476	143	0.3452	0.00729
144	0.3496	9.84E-05	139	0.3548	0.000421	150	0.3433	0.00713
151	0.3482	8.27E-05	146	0.3535	0.000355			
158	0.347	7.10E-05	154	0.3519	0.000289			
164	0.3459	6.27E-05	161	0.3506	0.000243			
169	0.345	5.57E-05	168	0.3495	0.000208			
174	0.3441	5.06E-05	174	0.3485	0.000184			
178	0.3434	4.62E-05	179	0.3476	0.000164			
183	0.3426	4.25E-05	184	0.3468	0.000148			
187	0.342	3.87E-05	189	0.3461	0.000136			
			193	0.3454	0.000125			
			197	0.3448	0.000114			

Table 8b. Field hydraulic properties for the Northwest Site of the Carrington RECHARGE experiment (depths 53 through 83 cm).

53 cm			68 cm			83 cm		
$\psi$ cm	$\theta$	$K(\theta)$ cm/h	$\psi$ cm	$\theta$	$K(\theta)$ cm/h	$\psi$ cm	$\theta$	$K(\theta)$ cm/h
1	0.3988	-	6	0.3761	-	1	0.3553	2.47
10	0.3929	-	12	0.3726	-	6	0.3528	0.651
13	0.3884	-	17	0.3696	-	9	0.3507	0.404
22	0.3848	-	21	0.3671	-	12	0.3489	0.347
29	0.3818	-	25	0.365	-	15	0.3473	0.306
36	0.3792	-	29	0.363	1.77	18	0.3459	0.272
40	0.377	-	31	0.3613	-	20	0.3446	0.246
44	0.375	-	33	0.3597	1.56	22	0.3435	0.223
47	0.3732	-	36	0.3576	1.2	25	0.342	0.198
49	0.3716	-	39	0.3551	0.892	28	0.3402	0.171
51	0.3695	-	42	0.3529	0.698	31	0.3386	0.151
54	0.3669	-	45	0.351	0.561	34	0.3373	0.134
57	0.3647	-	48	0.3492	0.468	37	0.336	0.122
60	0.3627	-	50	0.3477	0.396	39	0.3349	0.111
63	0.3609	-	54	0.345	0.299	43	0.3329	0.0949
65	0.3593	-	63	0.3395	0.173	52	0.329	0.0694
69	0.3566	-	74	0.3328	0.0923	64	0.3242	0.0477
77	0.351	-	84	0.3273	0.0562	74	0.3202	0.0355
88	0.3441	-	92	0.3235	0.0404	81	0.3175	0.029
98	0.3385	1.06	98	0.3205	0.0311	87	0.3154	0.0248
105	0.3346	0.306	104	0.3176	0.0241	93	0.3133	0.0213
110	0.3316	0.165	109	0.3151	0.0195	99	0.3115	0.0188
116	0.3286	0.102	114	0.3129	0.0162	104	0.3099	0.0169
121	0.326	0.0709	118	0.311	0.0137	108	0.3085	0.0153
126	0.3238	0.0532	125	0.3081	0.0108	115	0.3065	0.0133
130	0.3218	0.0415	133	0.3046	0.00804	123	0.3039	0.0113
136	0.3189	0.0295	140	0.3017	0.00632	131	0.3018	0.00992
144	0.3153	0.0199	147	0.2992	0.00514	137	0.3	0.0089
151	0.3123	0.0146	153	0.297	0.00429	143	0.2985	0.00811
158	0.3098	0.0112	158	0.2951	0.00367	148	0.2971	0.00751
163	0.3075	0.00901	163	0.2933	0.00319	153	0.2958	0.00705
	0.3056	0.00746	167	0.2918	0.0028	158	0.2947	0.00663
173	0.3038	0.0063	171	0.2903	0.00249	162	0.2937	0.0063
177	0.3022	0.00541	175	0.289	0.00223	166	0.2927	0.00601
181	0.3007	0.00471	188	0.2763	-			
184	0.2993	0.00413						

Table 8c. Field hydraulic properties for the Northwest Site of the Carrington RECHARGE experiment (depths 99 through 137 cm).

99 cm			114 cm			137 cm		
$\psi$	$\theta$	K( $\theta$ )	$\psi$	$\theta$	K( $\theta$ )	$\psi$	$\theta$	K( $\theta$ )
cm		cm/h	cm		cm/h	cm		cm/h
1	0.3434	7.65	~0	0.3423	2.02	~0	0.3451	2.86
4	0.3421	6.46	-	0.3413	1.81	-	0.3445	1.54
6	0.341	5.52	-	0.3405	1.65	-	0.3439	1.38
3	0.3399	4.82	-	0.3397	1.52	-	0.3434	1.25
8	0.339	4.25	-	0.3387	1.36	-	0.3429	1.14
11	0.3377	3.61	2	0.3374	1.2	-	0.3423	1.01
15	0.3363	2.96	5	0.3363	1.07	-	0.3416	0.874
19	0.335	2.5	8	0.3354	0.97	-	0.3409	0.773
22	0.3338	2.15	7	0.3345	0.892	-	0.3403	0.693
24	0.3328	1.88	11	0.3337	0.824	-	0.3398	0.63
27	0.3318	1.66	15	0.3324	0.722	-	0.3393	0.576
31	0.3302	1.34	24	0.3297	0.559	-	0.3385	0.495
40	0.327	0.877	36	0.3264	0.419	5	0.3369	0.366
51	0.323	0.524	47	0.3237	0.341	17	0.3349	0.256
62	0.3197	0.345	54	0.3218	0.301	22	0.3333	0.193
69	0.3175	0.26	60	0.3203	0.277	31	0.3322	0.16
75	0.3157	0.207	67	0.3189	0.259	37	0.3313	0.138
81	0.314	0.166	72	0.3176	0.249	44	0.3304	0.12
87	0.3125	0.137	77	0.3166	0.245	49	0.3297	0.106
92	0.3112	0.116				54	0.329	0.0965
96	0.31	0.101				59	0.3284	0.0884
103	0.3083	0.0809				65	0.3276	0.0781
111	0.3063	0.0621				74	0.3265	0.0677
-	0.3045	0.0499				81	0.3257	0.0606
125	0.303	0.0414				87	0.3249	0.0554
-	0.3017	0.0351				93	0.3243	0.0515
136	0.3006	0.0304				98	0.3237	0.0487
141	0.2996	0.0267				103	0.3232	0.0466
146	0.2986	0.0237				108	0.3227	0.0447
150	0.2977	0.0212				112	0.3223	0.0434
154	0.297	0.0192				116	0.3219	0.0424

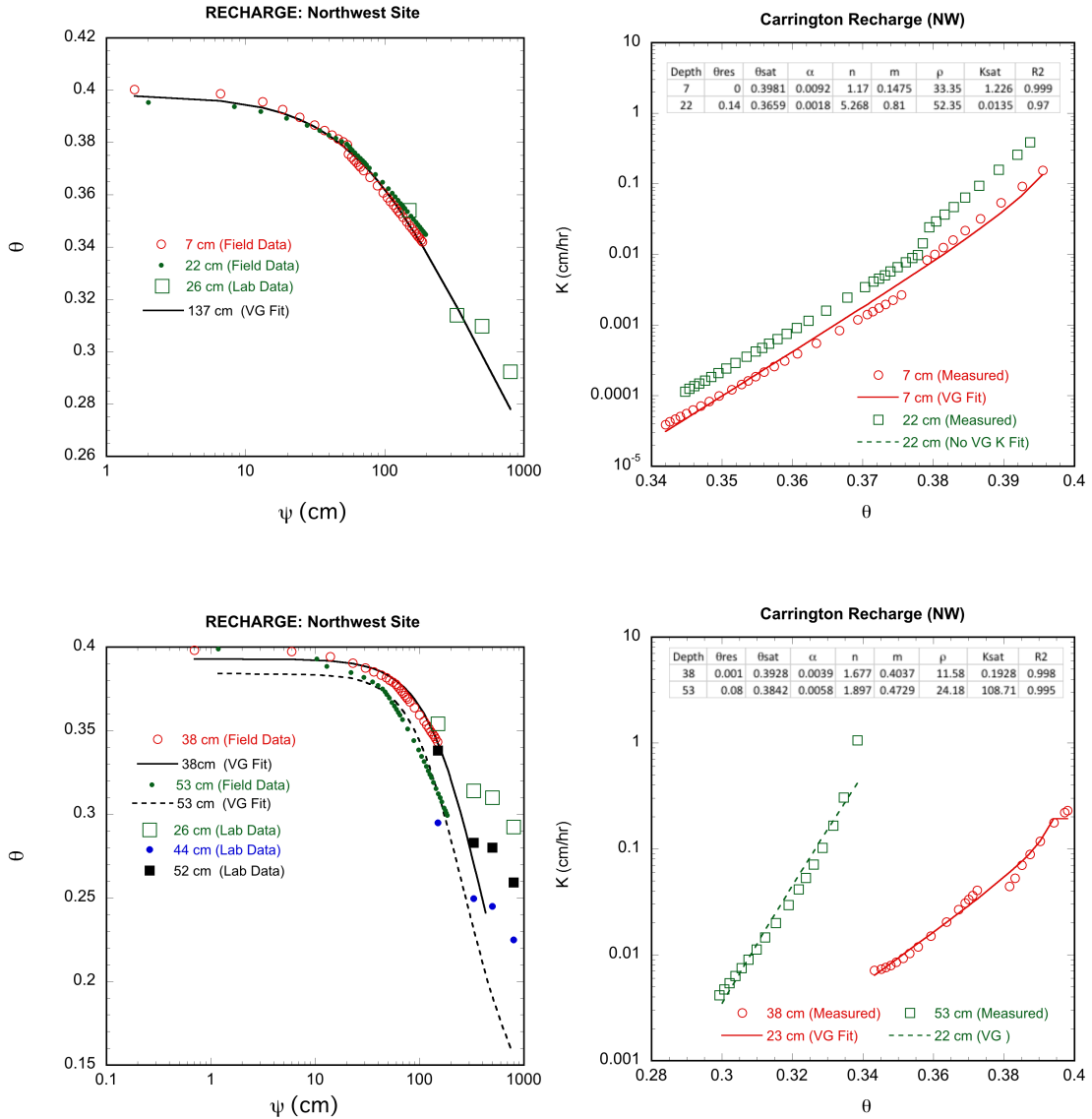


Figure 9a. Northwest Site water-retention and hydraulic-conductivity data (Depths 7 through 38 cm). Combined field (wet range) and laboratory (dry range)  $\theta(\psi)$  data and field  $K(\theta)$  data, with fitted VG function parameters.

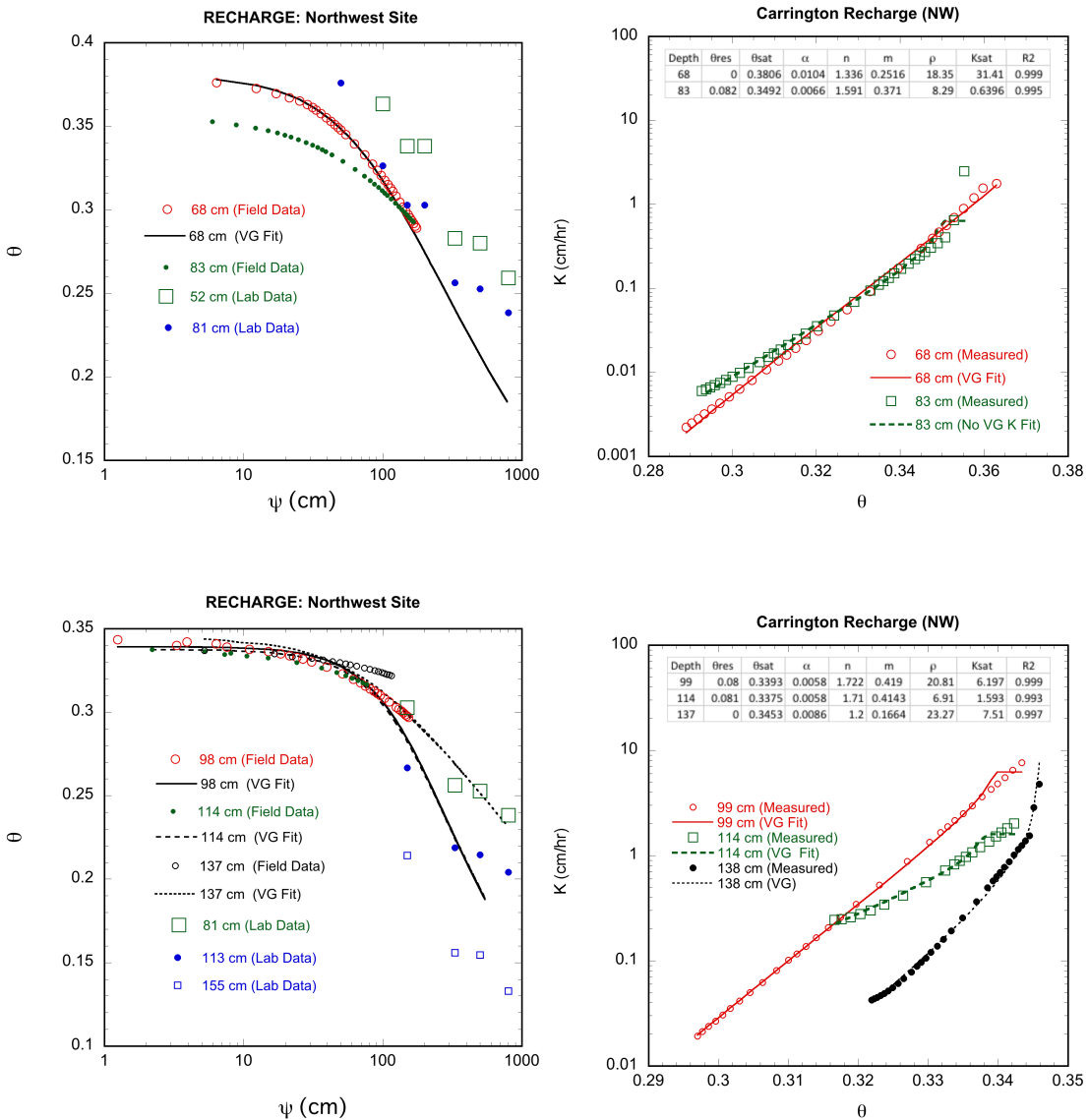


Figure 9b. Northwest Site water-retention and hydraulic-conductivity data (Depths 53 through 137 cm). Combined field (wet range) and laboratory (dry range)  $\theta(\psi)$  data and field  $K(\theta)$  data, with fitted VG function parameters.

In Situ Soil Hydraulic Data and VG Parameters for the SE Site

Table 9a. Field hydraulic properties for the Southeast Site of the Carrington RECHARGE experiment (depths 7 through 38 cm).

7 cm			22 cm			38 cm		
$\psi$	$\theta$	K( $\theta$ )	$\psi$	$\theta$	K( $\theta$ )	$\psi$	$\theta$	K( $\theta$ )
cm		cm/h	cm		cm/h	cm		cm/h
48	0.3714	0.00092	55	0.3788	0.00270	5	0.3956	0.0100
58	0.3669	0.00086	67	0.3751	0.00240	12	0.3942	0.0083
67	0.3624	0.00058	77	0.3716	0.00160	17	0.393	0.0070
73	0.3593	0.00044	85	0.3693	0.00120	22	0.3921	0.0060
79	0.3568	0.00036	91	0.3674	0.00098	26	0.3913	0.0050
85	0.3544	0.00029	98	0.3656	0.00079	29	0.3905	0.0040
90	0.3524	0.00024	104	0.3641	0.00066	32	0.3899	0.0034
95	0.3506	0.00021	109	0.3627	0.00057	34	0.3894	0.0030
99	0.349	0.00018	114	0.3615	0.00049	36	0.3888	0.0028
106	0.3466	0.00014	122	0.3597	0.00040	39	0.3882	0.0025
115	0.3437	0.00011	132	0.3575	0.00031	42	0.3874	0.0022
123	0.3413	9.0E-05	141	0.3557	0.00025	45	0.3866	0.0019
130	0.3393	7.6E-05	149	0.3541	0.00021	48	0.386	0.0017
136	0.3375	6.4E-05	157	0.3528	0.00018	50	0.3855	0.0016
142	0.3359	5.6E-05	164	0.3516	1.5E-04	53	0.3849	0.0014
148	0.3345	4.9E-05	170	0.3505	1.4E-04	57	0.3841	0.0012
153	0.3332	4.4E-05	176	0.3495	1.2E-04	66	0.3816	0.0072
158	0.332	4.0E-05	181	0.3486	1.1E-04	78	0.378	0.0069
163	0.3309	3.6E-05	187	0.3478	9.9E-05	90	0.375	0.0055
						98	0.373	0.0048
						105	0.3714	0.0044
						112	0.3698	0.0041
						118	0.3685	0.0039
						124	0.3673	0.0039
						129	0.3663	0.0039
						137	0.3647	0.0041
						147	0.3628	0.0050
						156	0.3613	0.0077
						164	0.3599	

Table 9b. Field hydraulic properties for the Southeast Site of the Carrington RECHARGE experiment (depths 53 through 83 cm).

7 cm			22 cm			38 cm		
$\psi$ cm	$\theta$	K( $\theta$ ) cm/h	$\psi$ cm	$\theta$	K( $\theta$ ) cm/h	$\psi$ cm	$\theta$	K( $\theta$ ) cm/h
2	0.3994	0.300	5	0.3679	0.290	1	0.3556	0.490
8	0.3955	0.170	8	0.3647	0.220	4	0.3527	0.420
13	0.3923	0.110	10	0.362		8	0.3493	0.350
18	0.3897	0.079	8	0.3596	0.200	8	0.3462	0.300
22	0.3875	0.074	11	0.3574	0.180	12	0.3435	0.260
25	0.3856	0.110	14	0.3554	0.170	15	0.3411	0.230
28	0.3838	0.180	17	0.3527	0.160	18	0.3389	0.200
30	0.3823	0.160	21	0.3496	0.150	22	0.3352	0.170
32	0.3809	0.150	24	0.3468	0.140	32	0.3276	0.160
35	0.379	0.130	27	0.3444	0.130	45	0.3182	0.110
38	0.3768	0.110	30	0.3422	0.120	56	0.3105	0.071
41	0.3748	0.099	33	0.3402	0.120	65	0.3053	0.054
44	0.3731	0.089	37	0.3368	0.120	72	0.3012	0.044
46	0.3716	0.080	46	0.3299	0.210	79	0.2971	0.035
49	0.3702	0.073	58	0.3214	0.440	85	0.2936	0.030
53	0.3678	0.062	69	0.3145	0.450	91	0.2906	0.025
61	0.3629	0.120	77	0.3098	0.130	96	0.2879	0.022
73	0.3569	0.098	84	0.306	0.068	104	0.2839	0.018
84	0.352	0.073	91	0.3023	0.042	114	0.279	0.014
91	0.3487	0.060	97	0.2992	0.029	123	0.275	0.011
97	0.346	0.051	102	0.2964	0.021	131	0.2715	0.009
104	0.3434	0.044	107	0.294	0.017	139	0.2685	0.008
109	0.3412	0.039	114	0.2904	0.012	145	0.2658	0.007
114	0.3392	0.035	124	0.2859	0.008	151	0.2634	0.006
119	0.3375	0.032	132	0.2822	0.006	157	0.2612	0.006
126	0.335	0.028	140	0.2791	0.004	162	0.2591	0.005
135	0.3318	0.024	146	0.2763	0.004	167	0.2573	0.005
143	0.3292	0.022	152	0.2739	0.003			
150	0.327	0.020	158	0.2717	0.002			
156	0.325	0.018	163	0.2697	0.002			
161	0.3233	0.017	168	0.2679	0.002			
167	0.3218	0.017	173	0.2662	0.002			
172	0.3204	0.016						
176	0.3191	0.015						
180	0.3179	0.015						

Table 9c. Field hydraulic properties for the Southeast Site of the Carrington RECHARGE experiment (depths 99 through 137 cm).

99 cm			114 cm			137 cm		
$\psi$	$\theta$	K( $\theta$ )	$\psi$	$\theta$	K( $\theta$ )	$\psi$	$\theta$	K( $\theta$ )
cm		cm/h	cm		cm/h	cm		cm/h
1	0.353	0.300	6	0.3383	0.590	8	0.3391	0.3200
4	0.3518	0.280	15	0.3342	0.530	15	0.3361	0.2800
7	0.3507	0.270	27	0.3279	0.470	16	0.3337	0.2500
8	0.3488	0.260	36	0.3222	0.440	24	0.3314	0.2200
18	0.3437	0.330	42	0.3176	0.420	30	0.3295	0.2100
31	0.3352	0.470	49	0.3132	0.430	36	0.3278	0.2000
43	0.3271	-	55	0.3094	0.450	41	0.3262	0.1900
51	0.3216	-	60	0.3061	0.500	48	0.324	0.1800
58	0.3172	0.210	65	0.3032	0.590	57	0.3212	-
65	0.3129	0.110	72	0.2988	-	66	0.3189	-
71	0.3093	0.074	81	0.2935	-	73	0.3169	-
77	0.3061	0.053	89	0.2891	0.4-50	79	0.3152	-
82	0.3032	0.040	96	0.2853	0.230	85	0.3137	-
89	0.2991	0.028	103	0.282	0.140	90	0.3123	-
99	0.2939	0.018	109	0.279	0.100	95	0.3111	-
108	0.2896	0.013	114	0.2764	0.077	99	0.3099	-
115	0.2859	0.010	119	0.274	0.061	104	0.3089	-
122	0.2827	0.008	124	0.2718	0.050			
128	0.2799	0.006	128	0.2697	0.042			
134	0.2773	0.005						
140	0.275	0.005						
145	0.2729	0.004						
149	0.2709	0.003						

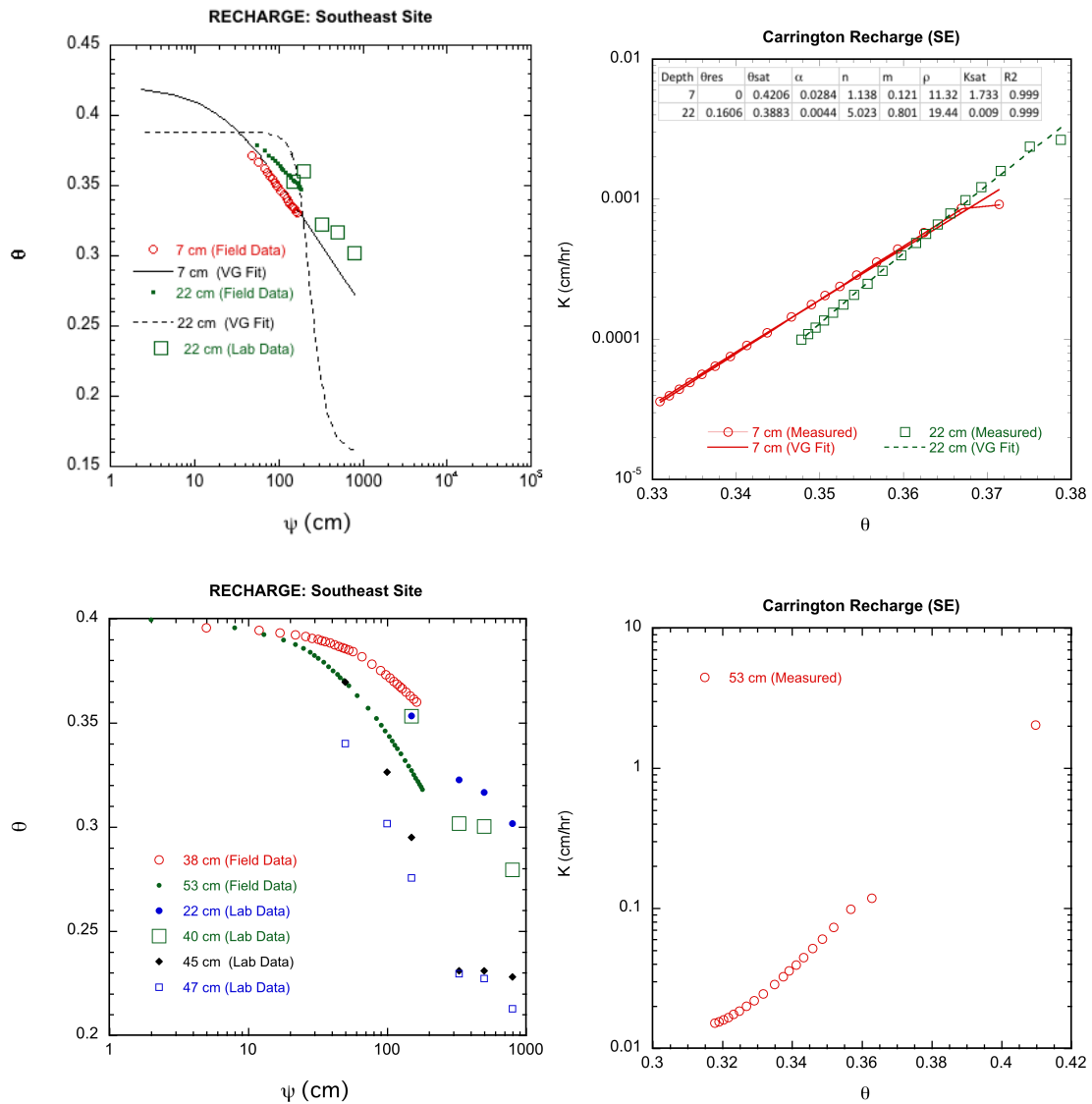


Figure 10a. Southeast Site water-retention and hydraulic-conductivity data (Depths 7 through 38 cm). Combined field (wet range) and laboratory (dry range)  $\theta(\psi)$  data and field  $K(\theta)$  data, with fitted VG function parameters.

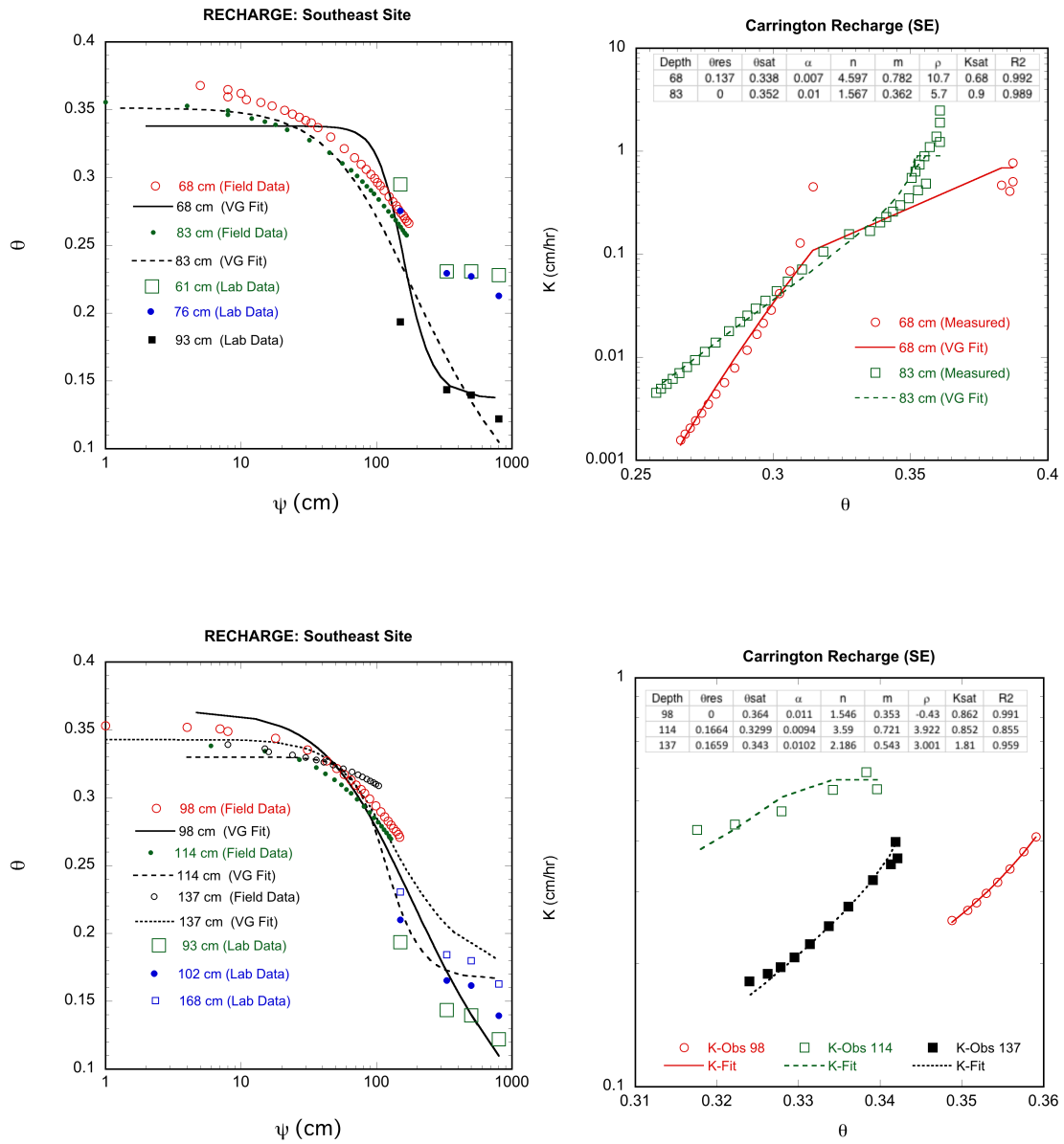


Figure 10b. Southeast Site water-retention and hydraulic-conductivity data (Depths 53 through 137 cm). Combined field (wet range) and laboratory (dry range)  $\theta(\psi)$  data and field  $K(\theta)$  data, with fitted VG function parameters.



## CARRINGTON SARE-ACE EXPERIMENT: 1992-1996

In 1992 a project was initiated by the Carrington Research Extension Center near Carrington, ND, to study the effects of three different cropping systems on production, economic cost and benefits, soil, and environmental integrity (pesticide and nitrate contamination) in a shallow confined aquifer. The project was sponsored by the North Central Region Sustainable Agriculture Research and Education Program (SARE) and Agriculture in Concert with the Environment (ACE).<sup>3</sup> The study was conducted by the CREC in cooperation with the Appropriation Division of the North Dakota State Water Commission, which provided the piezometer, sample well, neutron probe, and vadose sampler placements, as well as the hydrologic analysis portion of the experiment, and North Dakota State University Extension.

### FIELD DESIGN, LAYOUT AND SAMPLING PLAN

The SARE-ACE experiment was located in the NW  $\frac{1}{4}$  of the NW  $\frac{1}{4}$  of Section 31, T 147 N, R 66 W, on the lands of the Carrington Research Extension Center. General location of the SARE-ACE experiment is shown on Fig. 1. Soil series are identified on Fig. 2. The field design, plot layout, experiment treatment and instrumentation plan is shown on Fig. 11. Soil sample location identification for data in this report is shown on Fig. 12. Soil series trended from Heimdal-Emrick (Heimdal: Coarse-loamy, mixed, superactive, frigid Calcic Hapludoll; Emrick: Coarse-loamy, mixed, superactive, frigid Pachic Hapludoll), to Fram-Wyard (Fram: Coarse-loamy, mixed, superactive, frigid Aeric Calciaquoll; Wyard: Fine-loamy, mixed, superactive, frigid Typic Endoaquoll) from west to east. Experiment design was a randomized-block from west to east due to soil trends.

### Instrumentation

Instrumentation on each plot (Fig. 11) consisted of (1) a monitoring-sampling well placed in the upper Carrington aquifer at about 6 m below land surface with a 1.5 m screened interval; (2) a neutron probe tube placed to 1.5 m; (3) a vadose sampler placed at 2.1 m in the unsaturated till; and (4) a vadose sampler placed at 4 m, in the saturated till beneath the water table. Vadose samplers were custom-built<sup>4</sup> 2-inch (5.1 cm) diameter x 9-inch (23 cm) length enclosed 1-bar ceramic cups, with two PTFE pressure fittings. Samplers were accessed from the surface for suction applications and evacuation by two 1/8<sup>th</sup> inch (3.2 mm O.D.) PTFE spaghetti tubes with stainless steel pressure fittings on the active end, and clamped rubber tubes on the air-inlet end.

---

<sup>3</sup> Introduction redacted from: "Klinkebiel, D.L., W.M. Schuh, and B.D. Seelig. 1994 Report of the Carrington SARE-ACE experiment, 1992-1993: I. Influence of agricultural management practices on agronomic parameters. Carrington Research Extension Center Report. Carrington, ND.

<sup>4</sup> Soil Moisture Equipment Inc.

Extraction of water was performed by applying suction using a peristaltic pump, and then opening the inlet to allow movement of the extracted water to a receiving flask on the surface.

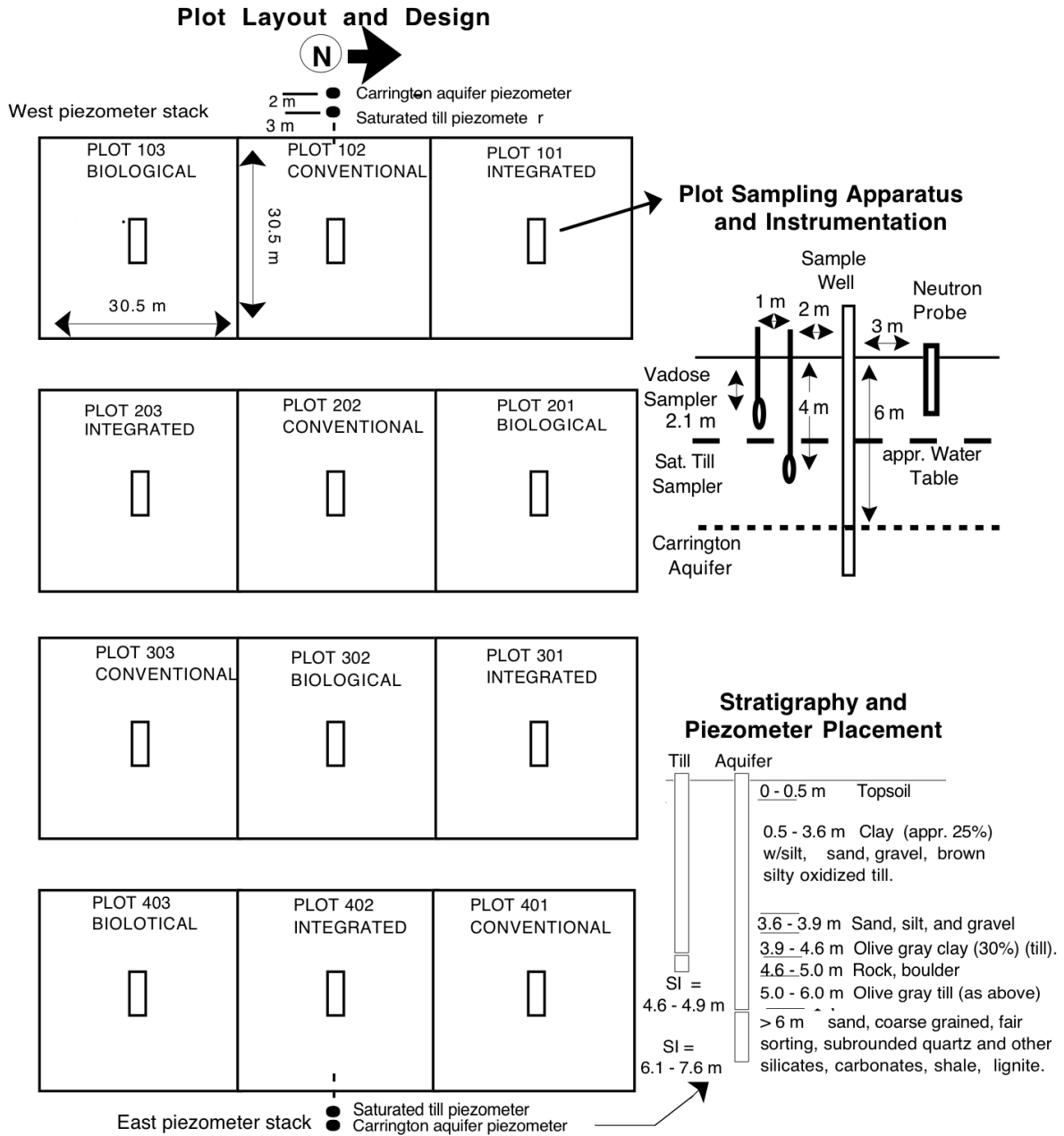


Figure 11. SARE-ACE project site layout, including treatment and instrumentation plan.

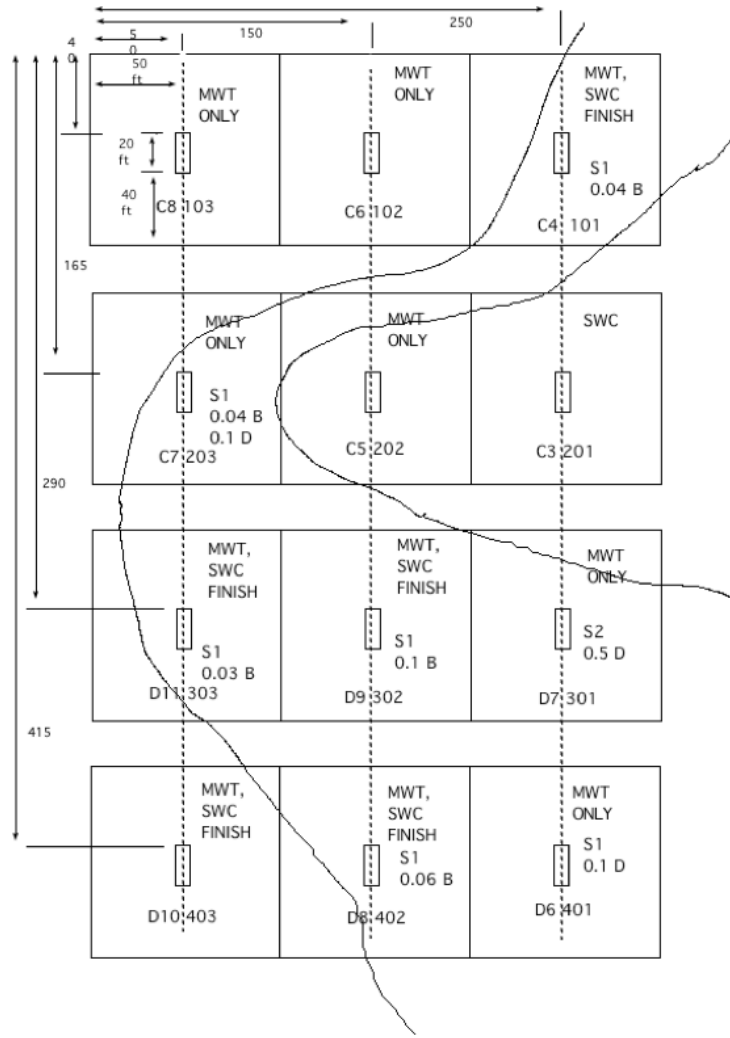


Figure 12. Sample site identification for the SARE-ACE experiment site. MWT indicates Carrington aquifer wells were drilled by Midwest Testing, using a hollow stem auger; SWC indicates Carrington aquifer wells were drilled by the State Water Commission using a forward-rotary drill rig. All units in feet.

### **Water Sample Collection and Measurement**

Detailed descriptions of field sampling schedules and methods were described in Schuh et al. (1994) and Schuh et al. (2004). In general, three water samples per year were collected for determination of pesticide residues from the sample well and suction samples in 1992 and 1993. Samples were collected using clean-clean procedures. Water samples for measurement of nitrate and ammonium-N were collected monthly from May through October, from 1992 through 1996, and analyzed as described by Schuh and Klinkebiel (2004).

### **Soil Hydraulic Characteristic Sample Collection**

Originally planned, but not completely used, was a part of the experiment in which soil hydraulic properties would be used to monitor deep drainage in a manner similar to the RECHARGE experiment. In the RECHARGE experiment, in-situ unsaturated hydraulic properties including moisture-characteristic curves and unsaturated soil hydraulic-conductivity functions were used with neutron-probe soil-moisture measurements in the deep profile at 1 m to calculate drainage from the root zone. Results of the RECHARGE experiment were reported by Schuh et al. (1993a), Schuh et al. (1993b), and Schuh et al. (2004).

For soil hydrologic analysis, undisturbed soil core samples in brass rings were collected within each treatment site using a Ulen-type sampler designed to fit to the end of a 3-inch (7.6 cm) diameter Giddings probe tube (Schuh, 1987). Two replicate 6-cm length x 5.1-cm diameter undisturbed core samples were collected from each experiment plot at the 114-cm and 136-cm depths. Each hole was evacuated using the Giddings probe to the desired depth (1 m). From each of two holes on each plot, single 6-cm length by 6-cm diameter core samples were collected at 114-cm and at 137-cm depths for laboratory measurement of saturated hydraulic conductivity ( $K_s$ ), unsaturated hydraulic diffusivity [ $D(\theta)$ ], and unsaturated hydraulic-conductivity [ $K(\psi/\theta)$ ] properties (for soil-water suction  $\psi$  and volumetric-moisture content  $\theta$ ). Buffer soil was allowed on each end of the sample (to be trimmed in the laboratory) to minimize surface disturbance on the samples, and samples were wrapped in aluminum foil and then bagged. Soil samples were stored in a refrigerator at the SWC lab until use. Two additional 3-cm length by 5-cm diameter (two replicate samples per 6-cm length barrel) were collected above and below each  $K(\psi/\theta)$  core sample for measurement of laboratory soil water-retention curves.

### **Laboratory Hydraulic Property Measurements**

Laboratory methods and procedures for measuring soil hydraulic properties, are described with the presentation and discussion of the hydraulic properties in the following sections.

## SUMMARY OF PUBLISHED RESULTS

Yield components of the study were reported in Klinkebiel et al. (1994). Treatment effects on nitrate trends, and crop management induced effects on hydrologic components of drainage and chemical transport were reported by Schuh and Klinkebiel (2004). Generally, it was determined that the short-term and long-term entry, placement and movement of nitrate within the soil-vadose-saturated till-upper aquifer continuum differed substantially between the BIOLOGICAL, CONVENTIONAL, and INTEGRATED management systems. Differences were not limited to application amounts and methods or crop uptake patterns alone, but also varied because of indirect hydraulic effect that cropping systems have on surface hydrologic distribution, and the subsequent patterns of redistribution of water contributing to infiltration and drainage in each layer. This confirmed the hypothesis established by the previous nearby Carrington research (the RECHARGE experiment conducted from 1988 through 1990), in which it was found that drainage and solute movement through the root zone to the underlying till and aquifer was influenced by runoff characteristics, which concentrated water in microtopographic low areas (Schuh et al., 1993a; 1993b, and Schuh and Klinkebiel, 2003). Crop management effects on surface runoff were hypothesized to have a significant influence on deep drainage and nitrate transport to groundwater.

## SOIL HYDRAULIC DATA, PROPERTIES, AND PARAMETERS

The following sections describe the methods for determining soil physical and hydraulic properties, and present a compendium of the resulting data and parameters determined for their use. While some comparative analysis is provided, the main purpose of this report is the data itself for modeling or comparative use by others.

### **Soil Bulk Density and Water Retention**

Soil water-retention curves were determined for 115 3-cm length by 5.1-cm diameter core samples in brass rings. The distribution of samples by depth is shown in Table 10. Samples in brass rings were each placed on pre-wetted 6-cm diameter 1-bar ceramic plates, covered with a plastic cap, and secured with a rubber band (Fig. 4), and were placed on 1-bar pressure plates in Soil Moisture Equipment Inc. pressure pots for extraction at pressure head steps of 14, 30, 46, 64, 80, 100, 140, 200, 330, 500, and 800 cm. Methods for soil-moisture characteristic curve and bulk density determinations were the same as those described under the subsection **Bulk Density and Water Retention** (pp. 6-8) in the RECHARGE experiment section of this report.

### Bulk Density

Bulk density values for each of the 115 samples are presented in Appendix B following this discussion. Bulk Density values are shown by depth on Table 10. Statistical distribution at each depth is shown on Table 11. The mean, median, minimum and maximum values increase with depth. Table 12 indicates a difference by depth at  $p < 0.0003$ . Table 13 disaggregates the differences using a Bonferroni test. Mean bulk density for deepest (152-cm) samples differed from the shallowest (107-cm) at  $p < 0.0004$ . Intermediate samples (122 cm) differed from shallow samples at  $p < 0.04$ , but not from the deep samples. The physical interpretation of the trends and differences can be described as predominant lower density loamy subsoil materials at 101 cm, and the predominant higher density gravelly till substratum materials at 152 cm. Interim transitional samples included admixtures of the two characteristic material types due to spatial variability of the boundary between the fluvially reworked till and the underlying gravelly till. The deeper gravelly fine-loamy subsoil materials generally have higher densities than shallow loamy soil materials because of natural compression from overburden and lack of pedoturbation. The highest values for the underlying gravelly till can be interpreted as the influence of non-porous gravel content.

Table 10. Measured dry bulk density values for all samples, by depth.

Depth cm	Bulk Density g/cm <sup>3</sup>						
107	1.62	122	1.57	122	1.68	152	1.52
107	1.58	122	1.48	122	1.72	152	1.4
107	1.7	122	1.69	122	1.5	152	1.67
107	1.52	122	1.57	122	1.93	152	1.63
122	1.54	122	1.84	122	1.87	152	1.86
122	1.64	122	1.92	122	1.7	152	1.83
107	1.53	122	1.74	122	1.81	152	1.59
107	1.82	122	1.78	122	1.65	152	1.77
107	1.8	122	1.69	122	1.51	152	1.74
107	1.8	122	1.72	122	1.56	152	1.73
107	1.7	122	1.52			152	1.78
107	1.62	122	1.51			152	1.95
107	1.61	122	1.6			152	1.85
107	1.61	122	1.47			152	1.83
107	1.32	122	1.59			152	1.67
107	1.51	122	1.66			152	1.94
107	1.76	122	1.65			152	1.8
107	1.76	122	1.73			152	1.89
107	1.58	122	1.87			152	1.85
107	1.38	122	1.7			152	1.95
107	1.76	122	1.73			152	1.83
107	1.49	122	1.8			152	1.73
107	1.5	122	1.8			152	1.91
107	1.91	122	1.72			152	1.86
107	1.6	122	1.8			152	1.86
107	1.41	122	1.8			152	1.9
114	1.55	122	1.66			152	1.82
		122	1.76			152	1.64
		122	1.88			152	1.59
		122	1.61			152	1.98
		122	1.65			152	2
		122	1.86			152	1.61
		122	1.95			152	1.71
		122	1.76			152	1.77
		122	1.76			152	1.83
		122	1.71			152	1.52
		122	1.86			152	1.64
		122	1.81			152	1.63
		122	1.58			152	1.84

Table 11. Statistical distribution of dry bulk density values with depth.

Depth cm	Count	Mean g/cm <sup>3</sup>	Median g/cm <sup>3</sup>	StdDev g/cm <sup>3</sup>	Min g/cm <sup>3</sup>	Max g/cm <sup>3</sup>	StdErr g/cm <sup>3</sup>	Lower 25th %tile g/cm <sup>3</sup>	Upper 25th %tile g/cm <sup>3</sup>	Lower 10th %tile g/cm <sup>3</sup>	Upper 10th %tile g/cm <sup>3</sup>
107	26	1.62	1.61	0.145	1.32	1.91	0.0284	1.52	1.76	1.42	1.80
114	1	1.55	1.55	•	1.55	1.55	•	1.55	1.55	1.55	1.55
122	49	1.71	1.72	0.126	1.47	1.95	0.0180	1.61	1.8	1.51	1.87
152	39	1.77	1.8	0.141	1.4	2	0.0226	1.65	1.86	1.59	1.95

Table 12. Analysis of variance (ANOVA) for BD vs. Depth.

Source	df	Sums of Squares	Mean Square	F-ratio	Prob
Const	1	334.973	334.973	18220	≤ 0.0001
Dpth	3	0.371624	0.123875	6.7379	0.0003
Error	111	2.04072	0.018385		
Total	114	2.41234			

Table 13. Post-hoc BSD test for BD difference between sample depths.

Depth Comparison	Difference	std. err.	Prob
114 - 107	-0.0681	0.138	0.997
122 - 107	0.0907	0.033	0.040
122 - 114	0.1588	0.137	0.820
152 - 107	0.1491	0.034	0.0004
152 - 114	0.2172	0.137	0.525
152 - 122	0.0584	0.029	0.252

### Soil Water-Retention Curves

Soil water-retention curve values for each of the 115 samples are presented in Appendix B following this discussion.

Results of analysis of covariance using a sequential linear model treating all covariates as discrete and fixed are shown on Table 14. “Site” label is the sample treatment location shown on Fig. 12. “Depth(s)” are 107, 122 and 152 cm. “Sample(s)” designate replicate, but separate holes within the Site, corresponding to the two vadose sampler holes. “(Subsamples)” are paired replicates within the same core sample. In most cases at least two subsamples are provided for each depth because a single sample extraction included two 3-cm length rings (paired rings) within the 6-cm length sampler barrel. All references to “significance difference” are rejection of the null hypothesis of no difference based on a Bonferroni Significant Difference (BSD),  $p < 0.05$ , unless otherwise specified.

Table 14. BSD probabilities for differences in soil water content due to factors: Sample, Subsample, Depth, and Site using a sequential linear model. Green color highlights significance at  $p < 0.05$ . Yellow color highlights significance at  $p < 0.1$ .

$\psi \rightarrow$	0 cm	14 cm	30 cm	46 cm	64 cm	80 cm	100 cm	140 cm	200 cm	330 cm	500 cm	800 cm
Source ↓												
Sample	< 0.0001	< 0.0001	< 0.0001	0.87	0.80	0.55	0.58	0.90	0.56	0.36	0.28	< 0.0001
Subsample	0.96	0.98	0.99	0.63	0.45	0.57	0.67	0.72	0.89	0.95	0.97	0.96
Depth	0.17	0.029	0.002	0.35	0.22	0.033	0.011	0.005	0.005	0.001	0.0002	0.88
Site	0.001	0.002	< 0.0001	0.000	0.000	0.001	0.001	0.005	0.028	0.062	0.057	0.091

Subsamples do not vary significantly. Differences between samples (different holes, same site) vary only in the very wet range ( $\psi < 46$  cm) and the very dry range ( $\psi \rightarrow 800$  cm). Differences between depths (107 cm, 122 cm, 152 cm) are significant in the wet and dry ranges, except for a 46 to 64 cm interval, saturation, and 800 cm. Differences in moisture are highly to marginally significant between treatment sites at all  $\psi$  values, especially in the wet range ( $\psi < 200$  cm).

Disaggregation by Depth: Table 15 is a summary of mean, median, standard error, and lower and upper quartile  $\theta$  values for each  $\psi$  value between depths. Uniformly colored blocks, or bold letters, indicate depth groups having indistinguishable means (BSD  $p < 0.05$ ).

Mean moistures cannot be differentiated between the 122 cm and 152 cm depths anywhere within the measured suction range. Mean moistures at the 107-cm depth, with certain exceptions, are differentiated from 152 cm depth means from  $\psi = 14$  through 30 cm, and from  $\psi > 80$  cm, with a concordance zone between  $\psi = 30$  and 80 cm. The concordance is explained by a crossover of curves, shown on Fig. 13. Soils of the 107-cm depth are shown to have a higher wet range moisture and a lower dry range moisture than those of the 122 and 152 cm depths. This is consistent with observed material properties. Samples were collected at the boundary of a loamy subsoil overlying a gravelly clay-loam till. The loamy soil is shown to have, on average, more porosity in the wet range. Materials of the 122-cm depth conform mostly to the 152 -cm depth, but are inseparable from the 107 cm materials in the very wet range. Lack of separation near saturation occurs mainly because of the relatively large standard error of the 107 cm soils. Quartile ranges for all three depths (Fig. 14) show a wide variation in values within depths.

The conclusion is that gravelly till soils of the 122 cm and 152 cm depths have lower wet range and higher dry range porosity and water retention than those of the loamy soils of 107 cm depth, which have substantially more wet-range porosity, but also more variability near saturation.

Table 15. Selected statistical parameters (mean, median, standard error, and upper and lower 25<sup>th</sup> %tiles) by suction and depth. Color, and bold letters, indicate statistically inseparable means at BSD  $p < 0.05$ .

Depth cm	N*	$\psi$ cm											
		0	14	30	46	64	80	100	140	200	330	500	800
		Mean $\theta$											
107	18	0.4438	0.4037	0.3843	0.3226	0.2934	0.2698	0.254839	0.2349	0.2079	0.1794	0.1579	0.1417
122	52	0.3724	<b>0.3602</b>	0.3326	0.3133	0.3013	<b>0.2895</b>	0.2805	0.2654	0.2428	0.2217	0.2065	0.1938
152	36	0.3659	<b>0.3493</b>	0.3306	0.3217	0.3126	<b>0.3030</b>	0.2936	0.2788	0.2563	0.2394	0.2277	0.2117
		Median $\theta$											
107		0.4066	0.3902	0.3902	0.3292	0.2882	0.2636	0.2495	0.2287	0.2048	0.1817	0.1609	0.1378
122		0.3753	0.3560	0.3441	0.3232	0.3061	0.2994	0.2875	0.2704	0.2398	0.2130	0.2018	0.1996
152		0.3560	0.3374	0.3217	0.3172	0.3136	0.3061	0.2987	0.2868	0.2532	0.2391	0.2398	0.2234
		SE $\theta$											
107		0.0425	0.0241	0.0147	0.0083	0.0071	0.0082	0.0094	0.0101	0.0104	0.0116	0.0121	0.0122
122		0.0046	0.0042	0.0068	0.0065	0.0065	0.0064	0.0065	0.0065	0.0069	0.0074	0.0077	0.0080
152		0.0066	0.0057	0.0059	0.0064	0.0066	0.0066	0.0065	0.0066	0.0072	0.0077	0.0079	0.0085
		Lower 25 <sup>th</sup> %tile $\theta$											
107		0.3798	0.3452	0.3359	0.2889	0.2681	0.2458	0.2294	0.2011	0.1802	0.1519	0.1236	0.1102
122		0.3538	0.3470	0.3113	0.2923	0.2763	0.2614	0.2510	0.2331	0.2093	0.1817	0.1572	0.1430
152		0.3351	0.3292	0.3098	0.3002	0.2890	0.2823	0.2719	0.2540	0.2272	0.2115	0.1951	0.1720
		Lower 25 <sup>th</sup> %tile $\theta$											
107		0.4264	0.4119	0.4074	0.3485	0.3192	0.3083	0.3053	0.2837	0.2450	0.2100	0.1802	0.1564
122		0.3917	0.3764	0.3590	0.3396	0.3314	0.3232	0.3110	0.3046	0.2845	0.2674	0.2547	0.2458
152		0.3962	0.3672	0.3411	0.3337	0.3217	0.3151	0.3091	0.3024	0.2860	0.2756	0.2681	0.2570

\* Predominant N reported ( $\psi = 64$  to 800 cm). For 122 cm depth ( $\psi = 0$  to 45 cm) N = 51. For 107 cm depth ( $\psi = 0$  cm) N = 13; and ( $\psi = 14$  to 30 cm) N = 17.

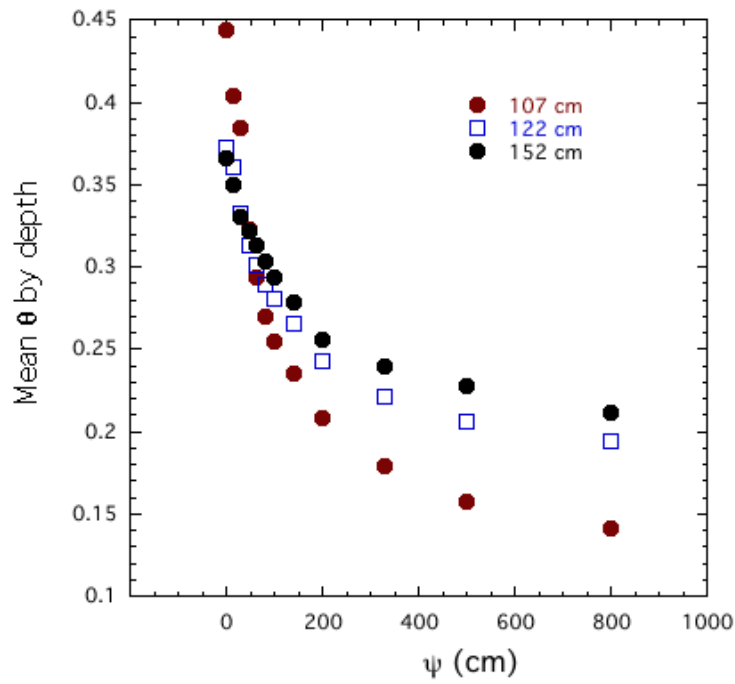


Figure 13. Mean water-retention values for 107-cm, 122-cm and 152-cm depths.

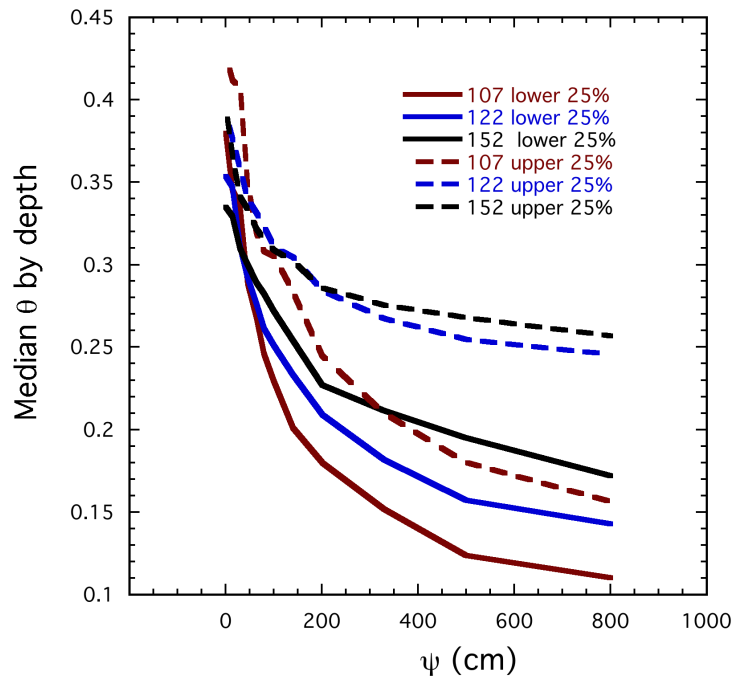


Figure 14. Upper and lower quartile water-retention values for 107-cm, 122-cm and 152-cm depths.

Disaggregation by Site: Of paired comparisons, 26 of the 27 having BSD  $p < 0.05$  (green) or BSD  $p < 0.1$  (yellow) are paired comparisons with D6 (Table 16). The only other paired comparison is D8 with C5 for the extreme wet range ( $\psi = 0$  to 14 cm). From Fig. 12 it can be seen that D6 is a corner plot, and likely non-characteristic of the rest of the field.

Without inclusion of D6, mean water retentions, adjusted for sample, subsample, and depth would not be discriminated between any of the sites over the  $\psi = 30$  to 800 cm range, and would only be discriminated between two sites, D8 and C5 above air entry, at  $\psi = 0$  and 14 cm.

Table 16. Paired site comparisons having means separable using a Bonferroni significant difference criterion at  $p < 0.05$  (green) and  $p < 0.1$  (yellow).

$\psi$ cm							
0		14		30		46	
Site	p	Site	p	Site	p	Site	p
D8 - C5	0.001	D8 - C5	0.005	D7 - D6	0.001	D6 - C8	0.060
D8 - D6	0.002	D8 - D6	0.002	D8 - D6	0.000	D7 - D6	0.016
		D11 - D6	0.043	D9 - D6	0.001	D8 - D6	0.000
				D10 - D6	0.068	D10 - D6	0.013
				D11 - D6	0.000	D11 - D6	0.010
$\psi$ cm							
64		80		100		140	
Site	p	Site	p	Site	p	Site	p
D7 - D6	0.006	D7 - D6	0.020	D7 - D6	0.023	D7 - D6	0.096
D9 - D6	0.015	D8 - D6	0.002	D8 - D6	0.010	D8 - D6	0.066
D10 - D6	0.003	D10 - D6	0.006	D10 - D6	0.011	D10 - D6	0.035

Disaggregation by Sample Replicates: The sample effect is undefined in the sense that two sample holes on a site are not specifically identifiable as fixed effects (left-right, north-south, first-second, etc.) and therefore cannot be internally discriminated. However, variation due to sample is significant ( $p < 0.0001$ ) only near or below the air entry value, at  $\psi = 0$  cm through 30 cm, without even marginal discrimination between means below  $\psi = 30$  cm.

**Conclusion: Almost all discrimination between moisture means is either between depths, or in the very wet range (saturation to  $\psi = 30$  cm) range. Differences between mean  $\theta$  values drier than  $\psi = 30$  cm cannot be discriminated by subsample, sample, or Site. There is a wide variation in individual sample moisture variability within all covariates. However, the bulk moisture characteristics of the field do not vary spatially, only with depth. The areal population across the field is essentially the same population having indistinguishable mean values within depths.**

### Soil Saturated Hydraulic-Conductivity

Saturated hydraulic conductivity ( $K_s$ ) was measured using 6-cm (length) by 5.3 (diameter) undisturbed core samples in Tempe cell assemblies (Fig. 15). Cores were placed on top of a thin (0.0011mm) nylon membrane over a specially designed acrylic disc (Fig. 17). The discs contained multiple perforations connected by grooves to expedite movement of water. Tests indicated that disc ability to conduct water was not limiting. Membrane conductivity ( $K_m$ ) was measured for 22 of the 36 samples by filling an empty ring with water and measuring the outflow rate.  $K_m$  varied from a minimum of 0.0047 cm/h to 0.077 cm/h, although  $K_m$  for two of the membranes used for the sample site D8 samples (Table 17) were an order of magnitude below the others. Mean and median values were very close at about 0.05 cm/h, with a 95% confidence interval between 0.041 cm/h and 0.059 cm/h. Where  $K_m$  was not measured, the mean value was used to calculate actual  $K_s$ . Core samples in rings were placed in the Tempe cells, wetted from the bottom using tap water, and measured for  $K_m$  using the falling head method (Klute, 1965).

Table 17. Membrane K ( $K_m$ ) statistics

Parameter	cm/h
Minimum	0.0047
Maximum	0.077
Points	22
Mean	0.0502
Median	0.0557
Std Deviation	0.0209
Std Error	0.00445

Membrane hydraulic conductivity ( $K_m$ ) can affect the  $K$  measurement of the sample, depending on the relative  $K$  values of the membrane and the sample and their relative thickness. Membrane effect can be adjusted using a two-layered vertical impedance relationship as follows:

$$K_{meas} = \frac{(L_s + L_m)}{\left(\frac{L_s}{K_s} + \frac{L_m}{K_m}\right)} \quad (6)$$

where s indicates the soil core sample and m indicates the membrane. Rearranged, the adjusted  $K_s$  value is calculated as:

$$K_s = \frac{L_s}{\left(\frac{(L_s + L_m)}{K_{meas}} - \frac{L_m}{K_m}\right)} \quad (7)$$

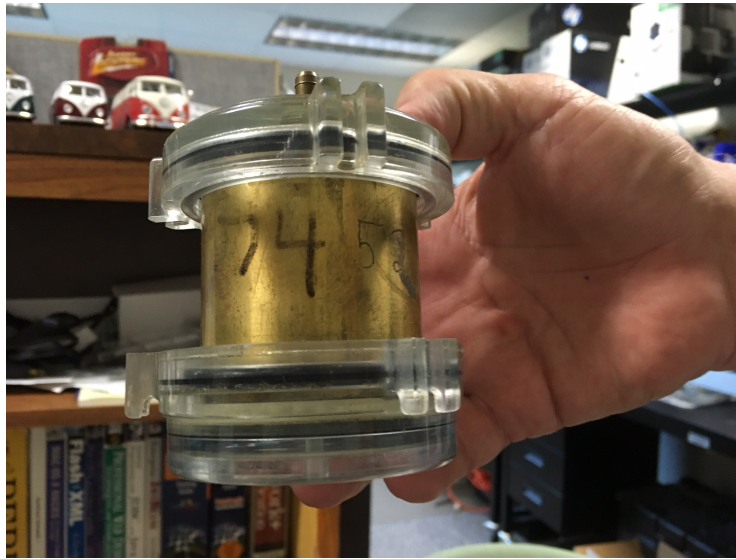


Figure 15. Tempe cell assembly used to measure  $K_s$  and  $K(\psi/\theta)$ .



Figure 16. Acrylic disc used for  $K_s$  and  $K(\psi/\theta)$  measurements. Disc was overlain by a 0.11 mm thin porous nylon membrane.

The effect of ignoring a 0.001 mm membrane having  $K_m = 0.05$  cm/h on a 6-cm length sample is shown on Table 18. Below  $K_s = 0.1$  cm/h membrane effect is negligible ( $< 0.18$  % error). At  $K_s = 1$  cm/h % error increases to 3.6%, still not large, but at 10 cm/h failure to account for the membrane would result in a 57% error. Above 20 cm/h the thin membrane dominates and the measurement is spurious. In the 22-sample set with membrane measurements, comparison of measured K for the soil and membrane assembly, and membrane-adjusted  $K_s$  indicated error ranging from 0.35% to 98 %, with a median of 4.96% and a mean of 13.38% error resulting from failure to account for the membrane. Substitution of the mean  $K_m = 0.05$  cm/h resulted in a mean error of  $-0.23\% \pm 1\%$  (95% confidence interval for the mean  $-1.23$  % to 0.77%). The 95% confidence interval for individual samples (Z test) is  $-4.23\%$  to 3.77%. The error potential for individual samples in a population can be limited to about 4% using the mean adjustment for samples without membrane measurements.

Table 18. Effect of an 0.11 mm base membrane having a K of 0.05 cm/h on error in the computation of K in a 6-cm core sample.

K(MEAS.) cm/h	K (ADJ.) cm/h	% ERROR
20	74.49	73
10	15.74	36
5	6.11	18
3	3.36	10.8
1	1.04	3.5
0.1	0.10	0.18
0.01	0.01	-0.15
1.00E-03	9.98E-04	-0.18
1.00E-04	9.98E-05	-0.18
1.00E-05	9.98E-06	-0.18
1.00E-06	9.98E-07	-0.18
1.00E-07	9.98E-08	-0.18
1.00E-08	9.98E-09	-0.18

Measured (no membrane adjustment) and membrane-adjusted  $K_s$  values are shown on Table 19. The two Site C-8 samples, having the  $K_m$  values an order of magnitude below the others, appear to be uncharacteristically high compared with the other samples. Adjustment for  $K_m = 0.05$  cm/h (shown on the table) results in values within the appropriate range, which indicates that the two anomalous membrane K values were likely inaccurate. The corrected values are likely more appropriate for use.

Table 19. Lab measured (Kmeas) and final (Ks) K values adjusted for resistance of a 0.0011mm thick membrane having K values (Km) listed. Where Km was not measured the average value (Km=0.05 cm/h) was used, indicated by \*.

Sample	Depth	Kmeas	Ks	Mem. Index	Km
Loc. Rep	cm	cm/h	cm/h	*=ave. value	cm/h
C3	130-145	0.57	<b>0.58</b>	*	0.05
C3	130-145	0.94	<b>0.97</b>	*	0.05
C3	107-122	2.96	<b>3.24</b>		0.0618
C4	130-145	1.01	<b>1.04</b>		0.067
C4	130-145	0.56	<b>0.58</b>		0.0424
C4	107-122	1.88	<b>2.00</b>		0.057
C5	130-145	0.53	<b>0.57</b>		0.0125
c5	130-145	0.23	<b>0.23</b>		0.077
C5	107-122	0.54	<b>0.54</b>		0.0726
C6	130-145	0.81	<b>0.84</b>	*	0.05
C6	130-145	0.91	<b>0.94</b>		0.0544
C6	107-122	1.37	<b>1.52</b>		0.0248
C7	130-145	1.41	<b>1.48</b>		0.053
C7	130-145	0.16	<b>0.16</b>	*	0.05
C7	107-122	1.12	<b>1.15</b>		0.0607
C8	130-145	1.60	<b>4.26 (1.48*)</b>		0.0047
C8	130-145	0.68	<b>0.69</b>	*	0.05
C8	107-122	1.95	<b>3.63 (1.16*)</b>		0.0077
D6	130-145	1.94	<b>2.09</b>	*	0.05
D6	130-145	0.01	<b>0.01</b>	*	0.05
D6	107-122	2.31	<b>2.47</b>		0.062
D7	130-145	0.04	<b>0.04</b>		0.037
D7	130-145	1.17	<b>1.22</b>	*	0.05
D7	107-122	1.76	<b>1.88</b>	*	0.05
D8	130-145	0.07	<b>0.07</b>	*	0.05
D8	130-145	0.39	<b>0.39</b>	*	0.05
D8	107-122	1.25	<b>1.29</b>		0.0637
D9	130-145	0.15	<b>0.15</b>	*	0.05
D9	130-145	2.86	<b>3.13</b>		0.06
D9	107-122	2.66	<b>2.86</b>		0.067
D10	130-145	0.64	<b>0.65</b>	*	0.05
d10	130-145	0.25	<b>0.25</b>		0.0513
D10	107-122	2.06	<b>2.17</b>		0.071
D11	130-145	0.55	<b>0.56</b>	*	0.05
D11	130-145	0.56	<b>0.58</b>		0.0452
D11	107-122	1.20	<b>1.25</b>		0.052

Ks values on Table 19 correspond to general observations of the sample textures. The two sample layers are at the boundary of the reworked loamy till comprising the soil profile and the underlying gravelly clay loam glacial till, the latter being of finer texture with gravel imbedded in the matrix, therefore occupying some of the volume with a non-porous component. A statistical comparison by depth indicates a significant difference between layers at  $p < 0.0006$  (Table 20). Summary statistics (Table 21) show that Ks for both layers has a similar distribution, indicated by the standard error. The shallower layer, however, has a mean Ks value more than double that of the deeper layer, with lowest 95<sup>th</sup> percentile values about an order of magnitude higher. Similarity of maximum values, however, indicates some probable cross-boundary overlap of the two materials from Site to Site.

Table 20. Anova for 107—122 depth samples vs. 130-145 samples.

Source	df	Sums of Squares	Mean Square	F-ratio	Prob
Const	1	44.6355	44.6355	78.297	$\leq 0.0001$
Dph	1	8.09837	8.09837	14.206	0.0006
Error	33	18.8126	0.570078		
Total	34	26.9109			

Table 21. Summary statistics for depth increment Ks values.

Group	Count	Mean	Median	Std. Dev.	Min	Max	Std. Err.	Lower 20th %tile	Upper 20th %tile
107-122	12	1.80	1.70	0.79	0.54	3.24	0.23	0.60	3.20
130-145	23	0.78	0.58	0.74	0.01	3.13	0.15	0.03	2.45

Using the Z test for depth class sample distributions, an approximate common boundary was found at the 80<sup>th</sup> percentile (lower boundary for 107-122 cm = 1.2 cm/h, upper boundary for 130-145 cm = 1.16 cm/h). Applying these boundaries, one sample of the shallow (loamy material) set was transferred to the deeper (gravelly till) set, and five samples of the deeper set were transferred to the shallow (loamy material) set. Analysis of variance indicated significant difference at  $p < 0.0001$ . Corresponding summary statistics by material group (1= loamy material, 2 = gravelly till material) are shown on Table 22. The change was not large.

Table 22. Summary statistics for material group increment Ks values: 1= loamy characteristic material distribution; 2 = gravelly till characteristic material distribution.

Group	Count	Mean	Median	Std. Dev.	Min.	Max.	Std. Err.	Lower 20th %tile	Upper 20th %tile
1	16	1.86	1.70	0.77	0.54	3.24	0.19	0.73	3.21
2	19	0.51	0.57	0.36	0.005	1.15	0.08	0.02	1.10

### Unsaturated Hydraulic Diffusivity and Conductivity

After measuring  $K_s$ , 500 cm of pressure was applied to the core sample-cell assembly, and the unsaturated diffusivity function,  $D(\theta)$ , was measured using the One-Step method (Doering, 1965). Using the One-Step method, a single pressure step is applied to a soil sample and volume outflow of water is measured as a function of time using a graduated cylinder until outflow ceases. After completion of outflow, the core sample is dried at 105° C to measure bulk density and final water content  $\theta_f$ . Stepwise volumetric water measurements  $\theta$  from the graduated cylinders are then added sequentially, and  $D(\theta)$  is then calculated from:

$$D(\theta) = \frac{4L^2}{\pi^2} \frac{d\theta}{dt} \frac{1}{(\theta - \theta_f)} \quad (8)$$

where  $L$  is the length of the sample, and  $\theta$  is the time-dependent content of the sample.

Laboratory  $K(\psi/\theta)$  was calculated from:

$$K(\theta) = D(\theta) \frac{d\theta}{d\psi} \quad (9)$$

where  $\frac{d\theta}{d\psi}$  is the soil specific-water retention, calculated from the slope of the laboratory soil-water-retention curve and  $D(\theta)$  is the soil-water diffusivity measured using the one-step outflow method of Doering (1965).

### Unsaturated Soil Hydraulic-Conductivity Parametric Form

Parametric form for use of unsaturated hydraulic properties in modeling was discussed in the Section titled: “**Unsaturated Soil Hydraulic-Conductivity Values and Parameters,**” in the earlier (RECHARGE) experiment description (pp. 15-18). To briefly review key points of this application, we use the Mualem (1976) theoretical pore-interaction model, applied using the closed-form parametric function of van Genuchten (1980); and the FORTRAN code (labeled RETC ) for a multi-variate least-squares optimization of parameters published by van Genuchten et al. (1991).

Van Genuchten (hereafter labeled VG) equations used are equations (1) through (5) in the RECHARGE section.<sup>5</sup> Parameters are, residual percent saturation ( $\Theta_r$ ), saturated moisture percent

---

<sup>5</sup> **IMPORTANT** One VG option is calculating  $K_r$  using present saturation ( $\Theta$ ) as  $K_r = \Theta^p [1 - (1 - \Theta^{1/m})^m]^2$ . Undoubtedly through a deficiency of understanding on our part, we, including my own applications and independent checks by other staff members have been unable to apply this equation successfully. We have checked several published sources. Readers may wish to do their own tests before using the parameters calculation of  $K_r$  using  $\Theta$  for their applications. We calculate  $\psi$  using  $\Theta$  (Eq. 1), and then  $K(\psi)$  using (Eq. 5) in our modeling applications.

( $\Theta_s$ ), saturated hydraulic conductivity ( $K_s$ ), fitting parameters  $\alpha$ ,  $m$ ,  $n$ , and pore interaction factor ( $\rho$ ). The fitting procedure uses both the soil-water characteristic curve data  $\psi(\theta)$ , and corresponding measured  $K(\theta)$  [or  $K(\psi)$ ] input data. Alternately, diffusivity [ $D(\theta)$ ] may be used in place of  $K(\psi/\theta)$  input data. In almost all cases  $K(\theta)$  were used. In some cases, by trial and error,  $D(\theta)$  input data gave better results. These are noted in the data and parameter presentations.

As in the RECHARGE experiment, VG  $\psi(\theta)$  parameters ( $\Theta_r$ ,  $\Theta_s$ ,  $\alpha$ ,  $m$ ,  $n$ ) were fitted first and separately, rather than simultaneously with the  $K(\theta)$  data (which is one RETC option). The  $\theta(\psi)$  data used are averaged for each site and replication from the raw laboratory data in Appendix B. Water-retention parameters were then held constant, and  $K_s$  and the pore interaction factor,  $\rho$ , were optimized for  $K(\theta)$  data. “ $\rho$ ” is an exponential parameter which adjusts for multiple deviations of soil porosity from tube flow. “ $\rho$ ” was developed to account theoretically for stochastic elements (ex. tortuosity, shape, non-continuity of pores, etc.). It is, however, empirically determined. Mualem (1976) empirically determined a value of  $\rho=0.5$  using predominantly coarse soils. Schuh and Cline (1991) found that the  $\rho=0.5$  was robust for sandy loam and loamy sand soils, but varied widely for finer soils. In most cases  $K(\theta)$  was determined separately from the lab data and applied in the RETC model. In a few cases, use of  $D(\theta)$  as the input data in the RETC program allowed for better calculations of  $K(\theta)$  by the RETC program. In a few cases, reasonable fits could not be achieved.

A forced identity of  $m=1-1/n$  (van Genuchten et al., 1980) ) was used because it greatly simplifies the use of the VG model in modeling application. As explained in the RECHARGE discussion, the price of this simplification is less precision of fits near saturation (van Genuchten et al., 1991). Van Genuchten’s caveat resulting from the constraint of  $K(\psi/\theta)$  in the wet range is clearly encountered with near-saturation application using the Carrington data.

Treating  $K_s$  as a parameter will be seen, in most cases, to result in values different from, and usually larger than measured  $K_s$  values, as predicted by van Genuchten et al (1991), and discussed above. This means that the use of the calculated  $K(\psi/\theta)$  function is limited to the unsaturated range, and that approaching saturation it must be truncated and constrained to the measured  $K_s$  value, thereby requiring a two-phase application similar to the Brooks and Corey approach if near-saturation applications are desired. This drawback, however, was not of concern for the planned application. The intended use was modeling water movement beneath the root zone. Near saturation limitations will be further explained in the next section and with the data presentation. The data used are provided with each parameter set so that parameters can be rerun suitable to other experimental objectives using RETC code from van Genuchten (1991) or other software if desired.

### **Unsaturated Soil Hydraulic-Conductivity Values and Parameters**

This section presents the combined water-retention data and hydraulic-conductivity data for each site, the determined VG parameters for each site and depth, an illustration of VG curve fits to the  $\theta(\psi)$  and  $K(\theta)$  data, and a subjective evaluation of the data quality and the usefulness of the parametric fits.

**Wet Range Bias:** As discussed by van Genuchten et al. (1991) use of the  $m(n)$  simplification caused less accurate fits in the sigmoid portion of the  $K(\theta)$  between the inflection or air entry value and saturation. This was not considered a problem for the location of the samples (deep profile) and the modeling objectives of the project, which involved deep drainage. Except for the case of saturation from a rising water table, or long-term (hours to days) constant infiltration into an isotropic and homogeneous profile, the deep soil profile is almost never fully saturated, or even nearly so. In the case of surface infiltration, air entrapment or restrictive layers almost always limit the final saturation level. In our experience, and as observed in the RECHARGE experiment, under normal field local conditions the deep soil profile moisture, beneath the root zone, almost always cycles between field capacity and about 75 cm suction on the wet end. This occurs because precipitation impact on deep drainage is mitigated by crop root-zone interception, sorption, and plant use; soil anisotropy, which augments desaturation under impeding layers; and by limitations in precipitation amounts to less than a few inches, which is diffused with depth. Water tables on the site generally varied from about 2.5 to 3 m below land surface on the site during the summer season, so that water-table capillary dominance of  $\theta(\psi)$  at 1 to 1.5 m (the experiment measurement zone) would cause a wet range minimum suction in the range of 100 cm to 200 cm, unless augmented periodically by deep root zone drainage.

**Near-Saturation Treatment:** For use of the VG functions near saturation, above the moisture curve inflection/or air entry value, it will be necessary to employ a two-phase function similar to the Brooks and Corey approach: i.e. when iterations within the model application reach or exceed the measured  $K_s$  value, the measured  $K_s$  value is used as the default value. While this somewhat limits the unique usefulness of the VG approach (i.e. the full sigmoid curve), it is not a problem in the application for which the VG fits used in this application for reasons explained above. The required application near saturation is illustrated on Fig. 17. The default  $K(\theta)$  value above the air entry / inflection value is  $K_s = 0.94$  cm/h.

Site C6 137 cm, Rep. 2

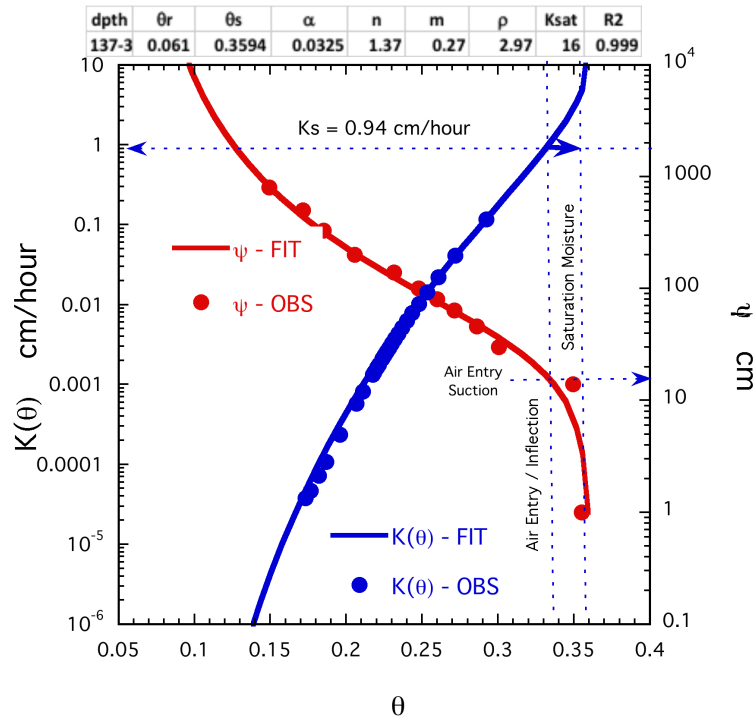


Figure 17. Illustration of VG function use default for  $K_s$  between the air entry / inflection  $\theta(\psi)$  value near saturation and saturation moisture. *Note:  $\psi$  corresponding to  $K(\theta)$  on the graph is determined by first tracking vertically from  $K(\theta)$  (blue curve) to the corresponding  $\theta(\psi)$  curve (red), and then locating (horizontally right) the  $\psi$  value corresponding to that  $\theta$  and  $K(\theta)$  value.*

Dry Range Bias: VG curve fits for  $K(\theta)$  vary in their fits, and not infrequently tend to diverge somewhat also in the drier ranges. This is not necessarily a serious problem in monitoring cumulative root-zone drainage, for the following reasons:

1. Because  $K(\theta)$  decreases logarithmically with decreasing moisture, drainage contributions from the drier range are exponentially smaller.
2. Errors in drainage (or other water movement) estimation from over or under estimation of  $K(\theta)$  are not proportional to the  $K(\theta)$  errors themselves, but are somewhat dampened by changes in hydraulic gradient and dynamic compensatory changes in  $K(\theta)$  within the soil profile during drainage.

**The following twelve subsections provide:**

- 1. Laboratory measured  $\psi(\theta)$  and  $K(\theta)$  data for each of the depths on each of the twelve site locations (C3, C4, C5, C6, C7, C8, D6, D7, D8, D9, D10, D11), identified on Fig. 12.**
- 2. VG function fits and parameters for each depth on each site.**
- 3. Subjective estimates of suitability for the purposes of the drainage estimation simulations.**

**All tables and figures in this subsection will be numbered by site (ex. C3-1, C3-2, etc.), separate from the overall numbering of this report. The report numbering sequence will be resumed in the discussion following the data and parameter presentation section.**

Site C3. Evaluation Comments, Hydraulic Data, and VG Functions

- All  $\theta(\psi)$  fits are excellent (Fig. C3-1).
- $K_s$  for the 114-cm depth corresponds to  $\theta_s \sim 0.39$ , very close to measured  $\theta_s=0.4$  and an air entry/inflection value at  $\psi \sim 8$  cm.  $K(\theta)$  fits are excellent at  $\psi =75$  cm to 100 cm, reasonably good to  $\psi =200$  cm.
- $K_s$  for the replicate 137-cm depth, Rep. 1 was calculated using  $D(\theta)$  input data in the VG model. VG  $D(\theta)$  fits are good over a limited range.  $K(\theta)$  corresponds to  $\theta_s \sim 0.365$ , and an air entry/inflection values at  $\psi \sim 16$  cm.
- $K_s$  for the replicate 137-cm depth, Rep. 2 corresponds to  $\theta_s \sim 0.37$ , and an air entry/inflection value at  $\psi \sim 40$  cm. VG function fits with  $K(\theta)$  are excellent throughout the measured range at  $\psi =50$  cm to 200 cm.
- All  $\theta(\psi)$  and  $K(\theta)$  values are closely concordant; variability is relatively small (Fig. C3-2).

Table C3-1. Measured  $\theta(\psi)$ ,  $K(\theta)$ ,  $D(\theta)$ , determined from laboratory data.

114 cm				137 cm Rep. 1				137 cm Rep. 2			
$K_s=3.24$ cm/h				$K_s=0.97$ cm/h				$K_s=0.58$ cm/h			
$\theta$	$\psi$	$\theta$	$K(\theta)$	$\theta$	$\psi$	$\theta$	$D(\theta)$	$\theta$	$\psi$	$\theta$	$K(\theta)$
	cm		cm/h		cm		cm <sup>2</sup> /h		cm		cm/h
0.3977	0.1	0.3977		0.4102	1	0.3341	82.67	0.3817	0	0.2956	0.067
0.3813	14	0.3215	0.94	0.3843	14	0.322	60.7	0.3683	14	0.2869	0.031
0.3691	30	0.3055	0.081	0.3378	30	0.3084	36.61	0.3429	30	0.2821	0.019
0.3118	46	0.2959	0.035	0.305	46	0.3016	27.56	0.3042	46	0.2789	0.014
0.2979	64	0.2891	0.021	0.2913	64	0.2971	3.824	0.2897	64	0.2765	0.011
0.2822	80	0.2839	0.014	0.2797	80	0.2939	4.894	0.277	80	0.2706	0.0056
0.2741	100	0.2797	0.0084	0.2735	100			0.2681	100	0.2671	0.0038
0.2597	140	0.2732	0.0057	0.2612	140			0.2554	0	0.2634	0.0024
0.2393	200	0.2682	0.0043	0.2472	200			0.2335	200	0.261	0.0018
0.216	330	0.2625	0.0030	0.2297	330			0.2115	330	0.2596	0.0015
0.1988	500	0.2581	0.0023	0.2163	500			0.1966	500	0.2579	0.0012
0.1842	800	0.2524	0.0016	0.2046	800			0.1802	800	0.2531	0.00064
		0.2497	0.0014							0.2489	0.00037
		0.246	0.0011							0.2441	0.00025
		0.2423	0.00087								
		0.2402	0.00076								
		0.2397	0.00074								
		0.2271	0.00034								
		0.2155	0.00019								
		0.2091	0.00015								

Table C3-2. Measured  $\theta(\psi)$  and  $D(\theta)$ , determined from laboratory data, and fitted  $K(\theta)$  calculated from  $\theta(\psi)$  and  $D(\theta)$  data input in the VG model.

137 cm Rep. 1			
$\theta$	$\psi$ cm	$K(\theta)$ cm/h	$D(\theta)$ cm <sup>2</sup> /h
0.413	0	26.98	
0.4101	2.282	12.69	6535
0.4071	3.625	9.55	4001
0.4013	5.856	6.19	2201
0.3954	7.866	4.30	1438
0.3896	9.805	3.07	1012
0.3837	11.74	2.23	741.8
0.3779	13.7	1.64	558
0.372	15.74	1.21	426.9
0.3662	17.86	0.89	330.3
0.3603	20.09	0.66	257.6
0.3544	22.46	0.48	201.9
0.3486	25	0.35	158.7
0.3427	27.73	0.26	124.8
0.3369	30.69	0.19	98.14
0.331	33.92	0.13	77.04
0.3252	37.46	0.095	60.3
0.3193	41.36	0.067	47
0.3135	45.7	0.047	36.44
0.3076	50.54	0.032	28.07
0.3018	55.99	0.022	21.46
0.2959	62.16	0.014	16.25
0.29	69.21	0.0094	12.18
0.2842	77.33	0.0061	9.02
0.2783	86.77	0.0038	6.59
0.2725	97.84	0.0023	4.74
0.2666	111	0.0014	3.34
0.2608	126.8	0.00078	2.31
0.2549	146	0.00043	1.55
0.2491	169.9	0.00022	1.02
0.2432	200	0.00011	0.64
0.2373	238.8	5.13E-05	0.39
0.2315	290.2	2.20E-05	0.22
0.2256	360.5	8.53E-06	0.12
0.2198	460.5	2.92E-06	0.060
0.2139	610.5	8.46E-07	0.027
0.2081	851.6	1.96E-07	0.010

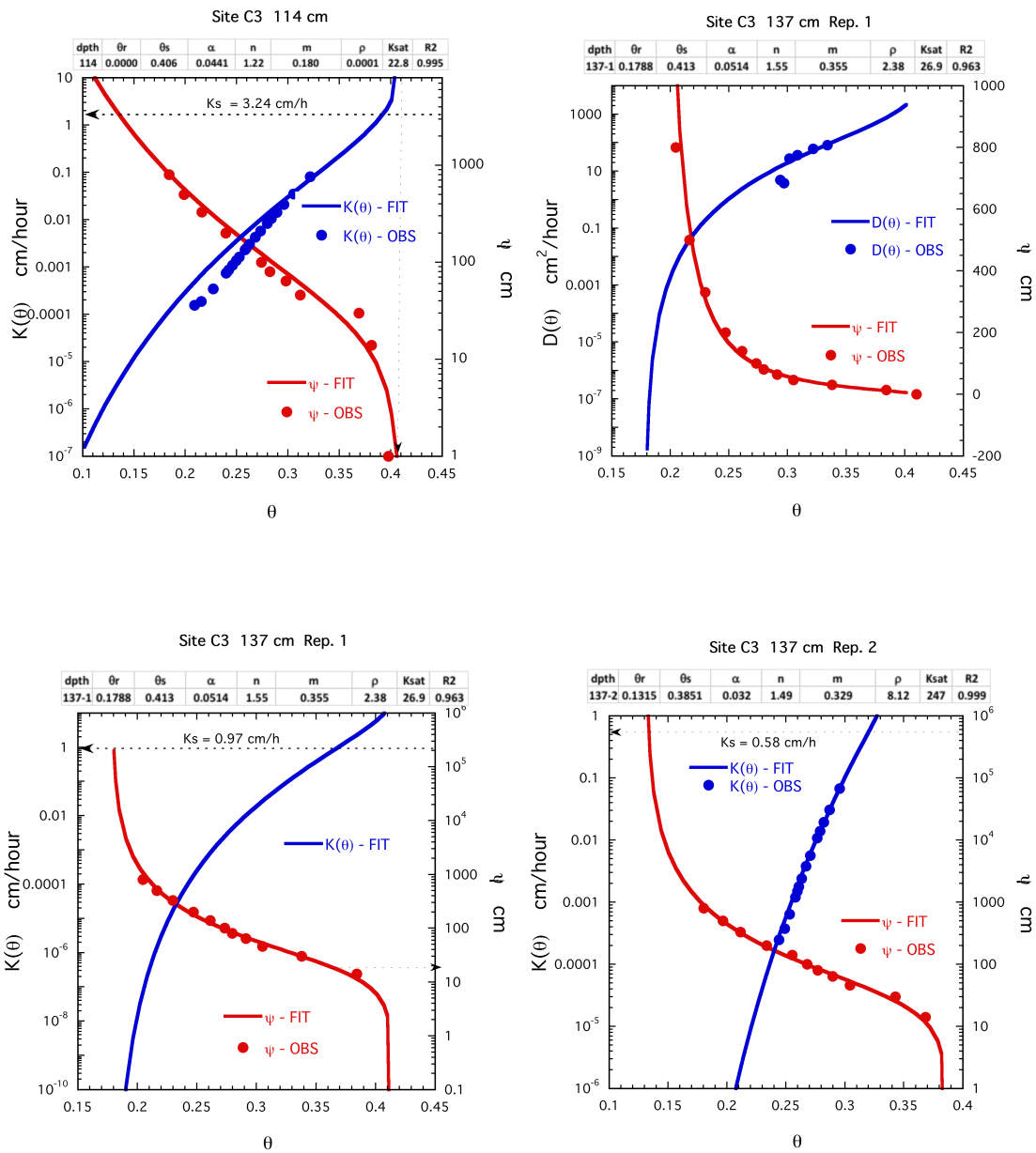


Figure C3-1. Measured laboratory data and fitted VG functions for  $\theta(\psi)$  and  $K(\theta)$  (114 cm and 137-cm, Rep. 2) and  $\theta(\psi)$ ,  $D(\theta)$  and  $K(\theta)$  data for 137-cm Rep. 1. VG parameters are shown in the overlying boxes. *Note:  $\psi$  corresponding to  $K(\theta)$  on the graph is determined by first tracking vertically from  $K(\theta)$  (blue curve) to the corresponding  $\theta(\psi)$  curve (red), and then locating (horizontally right) the  $\psi$  value corresponding to that  $\theta$  and  $K(\theta/\psi)$  value.*

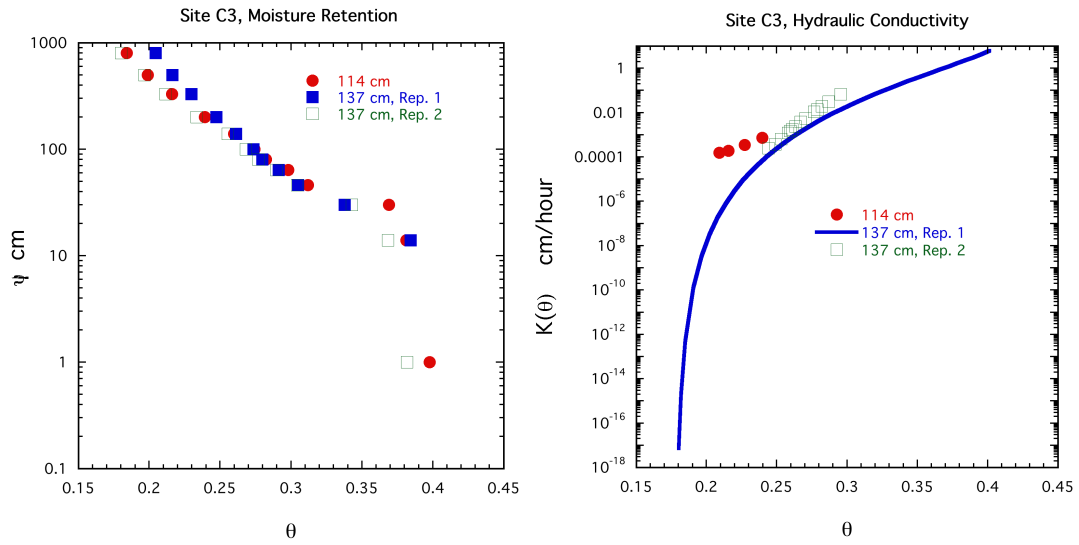


Figure C3-2. Comparison of measured  $\theta(\psi)$  (left) and  $K(\theta)$  (right) data for C3-114 cm, C3-137-cm, Rep. 1, and C3-137-cm, Rep. 2. C3-137-cm, Rep. 1 uses fitted  $K(\theta)$  values calculated from  $D(\theta)$  data shown in the tables and figures above.

Site C4. Evaluation Comments, Hydraulic Data, and VG Functions

- $\theta(\psi)$  VG fits are excellent for C4 at 114 cm and 137-cm Rep. 2. Fit for C4-137 Rep. 1 is poor (Fig. C4-1).
- $K_s$  for the replicate 114-cm depth corresponds to  $\theta_s \sim 0.355$ , and an air entry/inflection value at  $\psi \sim 13$  cm. Correspondence of  $K(\theta)$  for 114 cm with VG fit is good for wet range ( $\psi \sim 20$  top 80 cm) only.
- $K_s$  for the replicate 137- cm Rep. 1 sample corresponds to  $\theta_s \sim 0.345$ , and an air entry/inflection values at  $\psi \sim 25$  cm. Correspondence of  $K(\theta)$  for 137 cm Rep.1 with VG fit is good for wet range ( $\psi = 20$  top 80 cm ) only.
- Sample 137-cm Rep. 2: No reasonable VG fit was achieved.
- $\theta(\psi)$  data for 114 cm and 137-cm Rep. 1 samples are closely concordant in the wet range and then diverge.  $K(\theta)$  curves for 114 cm and 137-cm Rep. 1 are closely concordant. The 137-cm Rep. 2 curve is of similar slope, but lower values.

Table C4-1. Measured  $\theta(\psi)$  and  $K(\theta)$  determined from laboratory data.

114 cm				137 cm Rep. 1				137 cm Rep. 2			
$\theta$	$\psi$	$\theta$	$K(\theta)$	$\theta$	$\psi$	$\theta$	$K(\theta)$	$\theta$	$\psi$	$\theta$	$K(\theta)$
	cm		cm/h		cm		cm/h		cm		cm/h
$K_s=2$ cm/h				$K_s=0.58$ cm/h				$K_s=1.04$ cm/h			
0.372	0	0.35	1.78	0.3567	1	0.32	0.2	0.3567	0	0.3719	1
0.3532	14	0.35	1.59	0.3504	14	0.31	0.17	0.3504	14	0.3076	0.67
0.3467	30	0.34	1.34	0.3266	30	0.3	0.15	0.3266	30	0.2842	0.24
0.304	46	0.33	1.19	0.3225	46	0.3	0.14	0.3225	46	0.2703	0.13
0.2867	64	0.33	1.12	0.3143	64	0.28	0.068	0.3143	64	0.2606	0.08
0.2718	80	0.32	0.94	0.3076	80	0.28	0.04	0.3076	80	0.2532	0.055
0.2627	100	0.31	0.78	0.3001	100	0.27	0.027	0.3001	100	0.2472	0.04
0.2489	140	0.31	0.73	0.2882	140	0.26	0.015	0.2882	0	0.2423	0.031
0.2324	200	0.3	0.61	0.2677	200	0.25	0.0055	0.2677	200	0.2381	0.025
0.2102	330	0.29	0.47	0.2499	330	0.25	0.0049	0.2499	330	0.2345	0.02
0.1992	500	0.28	0.44	0.2364	500	0.23	0.0009	0.2364	500	0.2313	0.017
0.1832	800	0.26	0.12	0.2216	800	0.23	0.0006	0.2216	800	0.2284	0.014
		0.24	0.06							0.2235	0.01
		0.24	0.036							0.2194	0.008
		0.22	0.017								
		0.22	0.013								
		0.21	0.008								
		0.2	0.006								
		0.2	0.004								

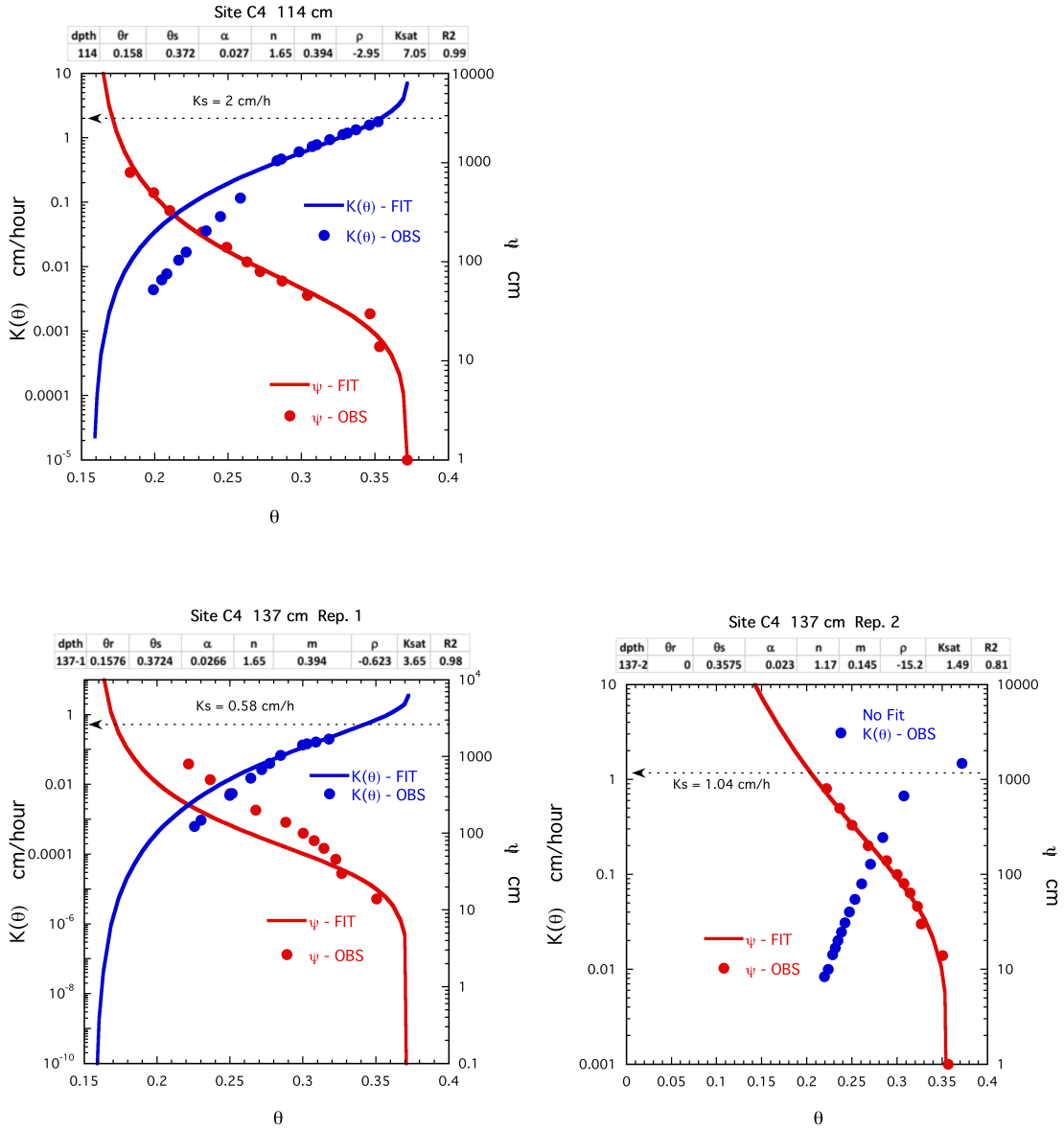


Figure C4-1. Measured laboratory data and fitted VG functions for  $\theta(\psi)$  and  $K(\theta)$  (114 cm and 137-cm, Rep. 1 and Rep. 2). VG parameters are shown in the overlying boxes. *Note:  $\psi$  corresponding to  $K(\theta)$  on the graph is determined by first tracking vertically from  $K(\theta)$  (blue curve) to the corresponding  $\theta(\psi)$  curve (red), and then locating (horizontally right) the  $\psi$  value corresponding to that  $\theta$  and  $K(\theta/\psi)$  value.*

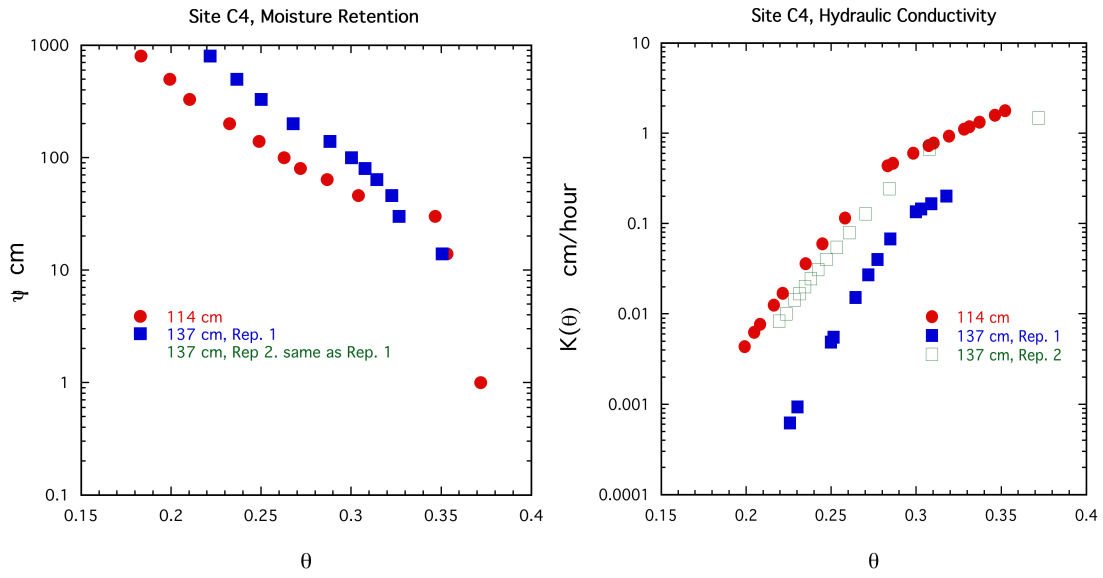


Figure C4-2. Comparison of measured  $\theta(\psi)$  (left) and  $K(\theta)$  (right) data for C4-114 cm, C4-137-cm, Rep. 1, and C4-137-cm, Rep. 2.

Site C5. Evaluation Comments, Hydraulic Data, and VG Functions

- All  $\theta(\psi)$  VG fits are excellent (Fig. C5-1).
- $K_s$  for the 114-cm depth corresponds to  $\theta_s \sim 0.34$ , air entry/inflection value at  $\psi \sim 30$  cm. VG fit with  $K(\theta)$  is excellent at  $\psi = 30$  cm to 100 cm, fair fit to  $\psi \sim 200$  cm.
- $K_s$  for the replicate 137-cm Rep. 1 sample corresponds to  $\theta_s \sim 0.33$ , air entry/inflection value at  $\psi \sim 30$  cm. VG fit with  $K(\theta)$  for 137-cm Rep.1 is good near saturation only.
- $K_s$  for the replicate 137-cm Rep. 2 sample corresponds to  $\theta_s \sim 0.33$ , and an air entry/inflection value at  $\psi \sim 30$  cm. VG fit with  $K(\theta)$  for 137 cm Rep.2 is excellent at  $\psi \sim 30$  cm to 100 cm, fair fit to  $\psi \sim 200$  cm.
- All of the  $\theta(\psi)$  curves are closely concordant.  $K(\theta)$  curves for 114 cm and 137-cm Rep. 2 are closely concordant; 137-cm Rep. 1 curve varies from the others and is lower. (Fig. C5-2).

Table C5-1. Measured  $\theta(\psi)$  and  $K(\theta)$  determined from laboratory data.

114 cm				137 cm Rep. 1				137 cm Rep. 2				
Ks = 0.54 cm/h				Ks = 0.23 cm/h				Ks = 0.57 cm				
$\theta$	$\psi$	$\theta$	K( $\theta$ )	$\theta$	$\psi$	$\theta$	K( $\theta$ )	$\theta$	$\psi$	$\theta$	K( $\theta$ )	
	cm		cm/h		cm		cm/h		cm		cm/h	
0.3724	0	0.3152	0.2265	0.3467	1	0.3183	0.1796	0.3542	0	0.3353	0.775	
0.3602	14	0.3084	0.1564	0.3432	14	0.3102	0.07305	0.3432	14	0.3199	0.4049	
0.3504	30	0.3031	0.116	0.3238	30	0.3084	0.05992	0.336	30	0.3097	0.2568	
0.3115	46	0.2986	0.09026	0.3158	46	0.3044	0.03798	0.3056	46	0.3022	0.1809	
0.3002	64	0.2949	0.07277	0.3068	64	0.3	0.02272	0.2925	64	0.2962	0.1362	
0.2875	80	0.2916	0.06024	0.3018	80	0.2969	0.01584	0.2788	80	0.2913	0.1072	
0.2792	100	0.2887	0.05092	0.2922	100	0.2931	0.009978	0.2696	100	0.2872	0.08729	
0.2641	140	0.2862	0.04377	0.2797	140	0.2901	0.006929	0.2532	0	0.2836	0.07286	
0.2415	200	0.2817	0.03362	0.2577	200	0.286	0.004187	0.2255	200	0.2805	0.06203	
0.2177	330	0.2798	0.02992	0.2437	330	0.2837	0.003137	0.2008	330	0.2777	0.05365	
0.2017	500	0.2707	0.01717	0.2318	500	0.2802	0.002012	0.1793	500	0.2689	0.03359	
0.1841	800	0.2633	0.01082		0.21	800	0.2779	0.001513	0.1597	800	0.26	0.02035
		0.2541	0.00596				0.2765	0.00126			0.2536	0.01406
		0.2494	0.0044				0.2743	0.00094			0.2495	0.01097
		0.2397	0.0023								0.2437	0.008
		0.2366	0.00186								0.2397	0.0059
		0.2327	0.0014								0.2349	0.0044
		0.2291	0.0011								0.2346	0.0043
		0.2228	0.00072								0.2311	0.0034
		0.2199	0.00059								0.229	0.0029
											0.2248	0.002197
											0.221	0.001676
											0.2191	0.001462
											0.2151	0.001092

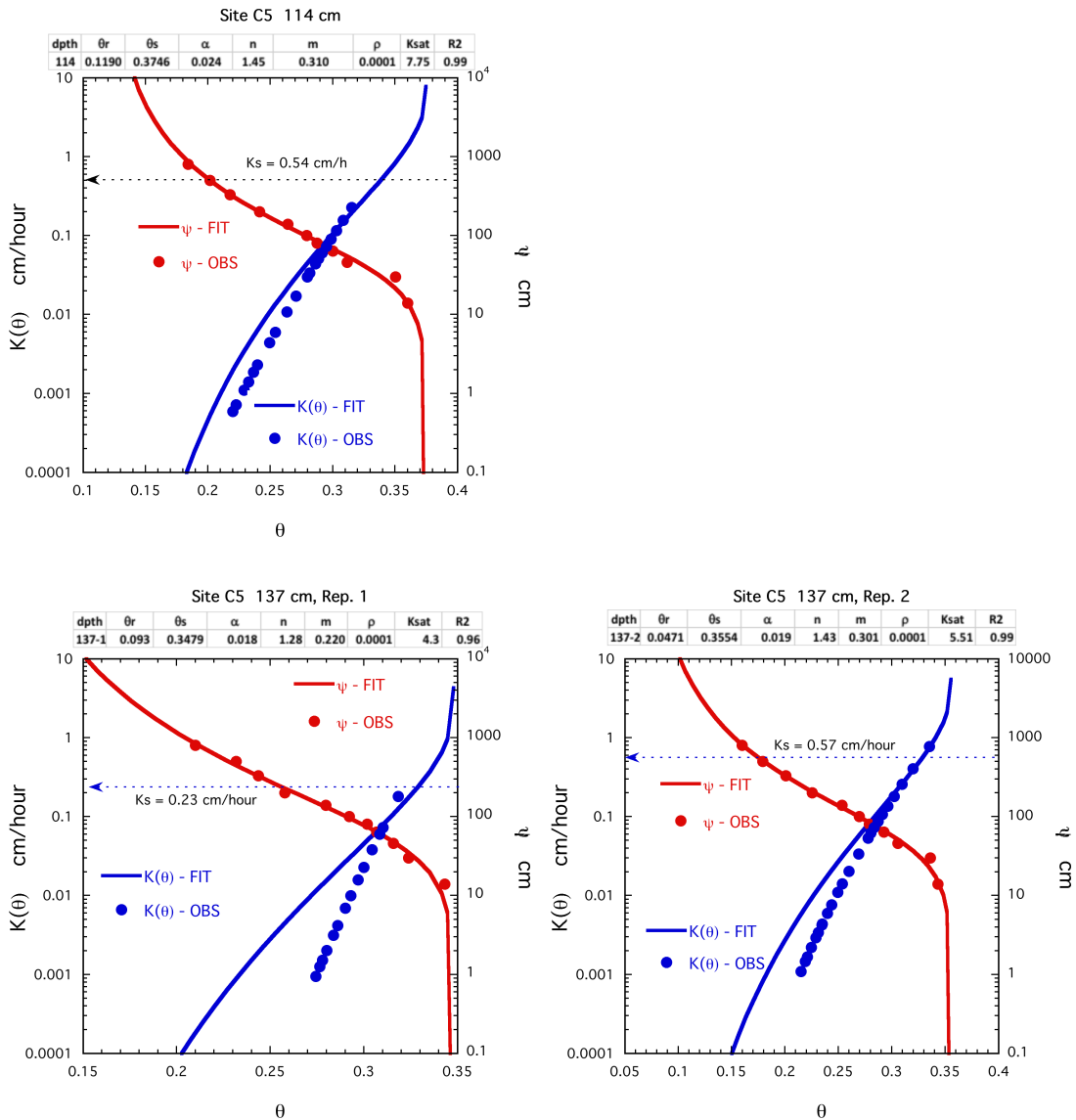


Figure C5-1. Measured laboratory data and fitted VG functions for  $\theta(\psi)$  and  $K(\theta)$  (114 cm and 137-cm, Rep. 1 and Rep. 2). VG parameters are shown in the overlying boxes. *Note:  $\psi$  corresponding to  $K(\theta)$  on the graph is determined by first tracking vertically from  $K(\theta)$  (blue curve) to the corresponding  $\theta(\psi)$  curve (red), and then locating (horizontally right) the  $\psi$  value corresponding to that  $\theta$  and  $K(\theta/\psi)$  value.*

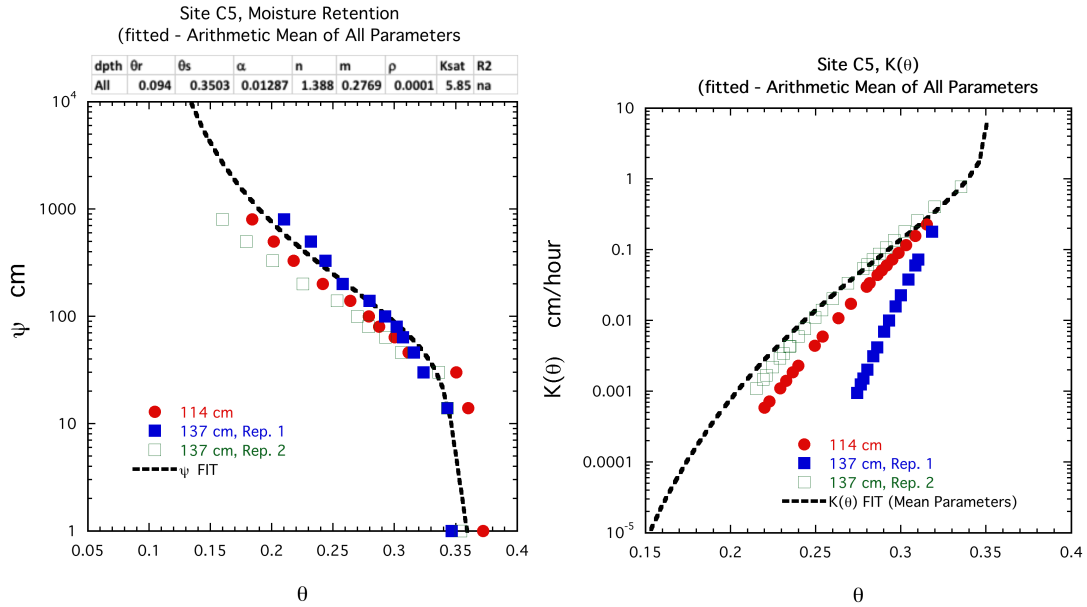


Figure C5-2. Comparison of measured  $\theta(\psi)$  (left) and  $K(\theta)$  (right) data for C5-114 cm, C5-137-cm, Rep. 1, and C5-137-cm, Rep. 2. Fitted function uses the mean of the three parameter set values.

Site C6. Evaluation Comments, Hydraulic Data, and VG Functions

- All  $\theta(\psi)$  fits are excellent (Fig. C6-1). The same water-retention data are used for both 137-cm samples.
- $K_s$  for the 114-cm depth corresponds to  $\theta_s \sim 0.385$ , air entry/inflection value at  $\psi \sim 1$  cm, almost exact fit at saturation moisture. Excellent fit with  $K(\theta)$  at  $\psi = 0$  cm to 70 cm.
- $K_s$  for the replicate 137-cm Rep. 1 sample corresponds to  $\theta_s \sim 0.33$ , air entry/inflection value at  $\psi \sim 20$  cm. Excellent fit to  $\psi \sim 200$ .
- $K_s$  for the replicate 137-cm Rep. 2 cm sample corresponds to  $\theta_s \sim 0.33$ , air entry/inflection value at  $\psi \sim 20$  cm. Excellent fit over the entire  $K(\theta)$  range.
- All of the  $\theta(\psi)$  curves are closely concordant.  $K(\theta)$  curves are all concordant within a reasonably tight range and pattern (Figure C6-2).

Table C6-1. Measured  $\theta(\psi)$  and  $K(\theta)$  determined from laboratory data.

114 cm				137 cm Rep. 1				137 cm Rep. 2			
$K_s=1.52$ cm/h				$K_s=0.84$ cm/h				$K_s=0.94$ cm/h			
$\theta$	$\psi$	$\theta$	$K(\theta)$	$\theta$	$\psi$	$\theta$	$K(\theta)$	$\theta$	$\psi$	$\theta$	$K(\theta)$
	cm		cm/h		cm		cm/h		cm		cm/h
0.3869	0	0.3609	0.41	0.355	0	0.2627	0.063	0.355	0	0.2924	0.117
0.3658	14	0.3579	0.38	0.3495	14	0.2458	0.023	0.3495	14	0.2718	0.041
0.338	30	0.3549	0.35	0.3006	30	0.2366	0.013	0.3006	30	0.2607	0.022
0.3057	46	0.3519	0.33	0.286	46	0.2304	0.0087	0.286	46	0.2533	0.014
0.2892	64	0.3489	0.30	0.2713	64	0.2258	0.0064	0.2713	64	0.2478	0.010
0.2717	80	0.3459	0.28	0.2599	80	0.2221	0.0050	0.2599	80	0.2435	0.0078
0.2588	100	0.3429	0.26	0.2477	100	0.2191	0.0040	0.2477	100	0.2399	0.0062
0.2414	140	0.3399	0.25	0.2316	140	0.2124	0.0025	0.2316	140	0.2369	0.0051
0.2192	200	0.3302	0.17	0.2055	200	0.2091	0.0020	0.2055	200	0.2344	0.0043
0.1985	330	0.3019	0.052	0.1852	330	0.2031	0.0013	0.1852	330	0.2321	0.0037
0.1848	500	0.2863	0.026	0.1715	500	0.2004	0.00103	0.1715	500	0.2301	0.0032
0.1661	800	0.2757	0.016	0.1492	800	0.1975	0.00082	0.1492	800	0.2283	0.0029
		0.2678	0.011			0.1925	0.00056			0.2267	0.0026
		0.2615	0.0081			0.1904	0.00048			0.2252	0.0023
		0.2563	0.0062			0.1897	0.00045			0.2238	0.0021
		0.2519	0.0050			0.1801	0.00022			0.2214	0.0018
		0.2481	0.0041			0.1716	0.00014			0.2203	0.0016
		0.2448	0.0034							0.2184	0.0014
		0.2418	0.0029							0.2175	0.0013
		0.2392	0.0025							0.2111	0.00081
		0.2305	0.0016							0.2068	0.00058
		0.2288	0.0014							0.1959	0.00024
		0.2241	0.0011							0.1868	0.00011
		0.2202	0.00088							0.182	7.18E-05
		0.214	0.00061							0.1766	4.66E-05
		0.2106	0.00050							0.1732	3.79E-05
		0.2083	0.00044								
		0.2056	0.00037								
		0.1888	0.00013								

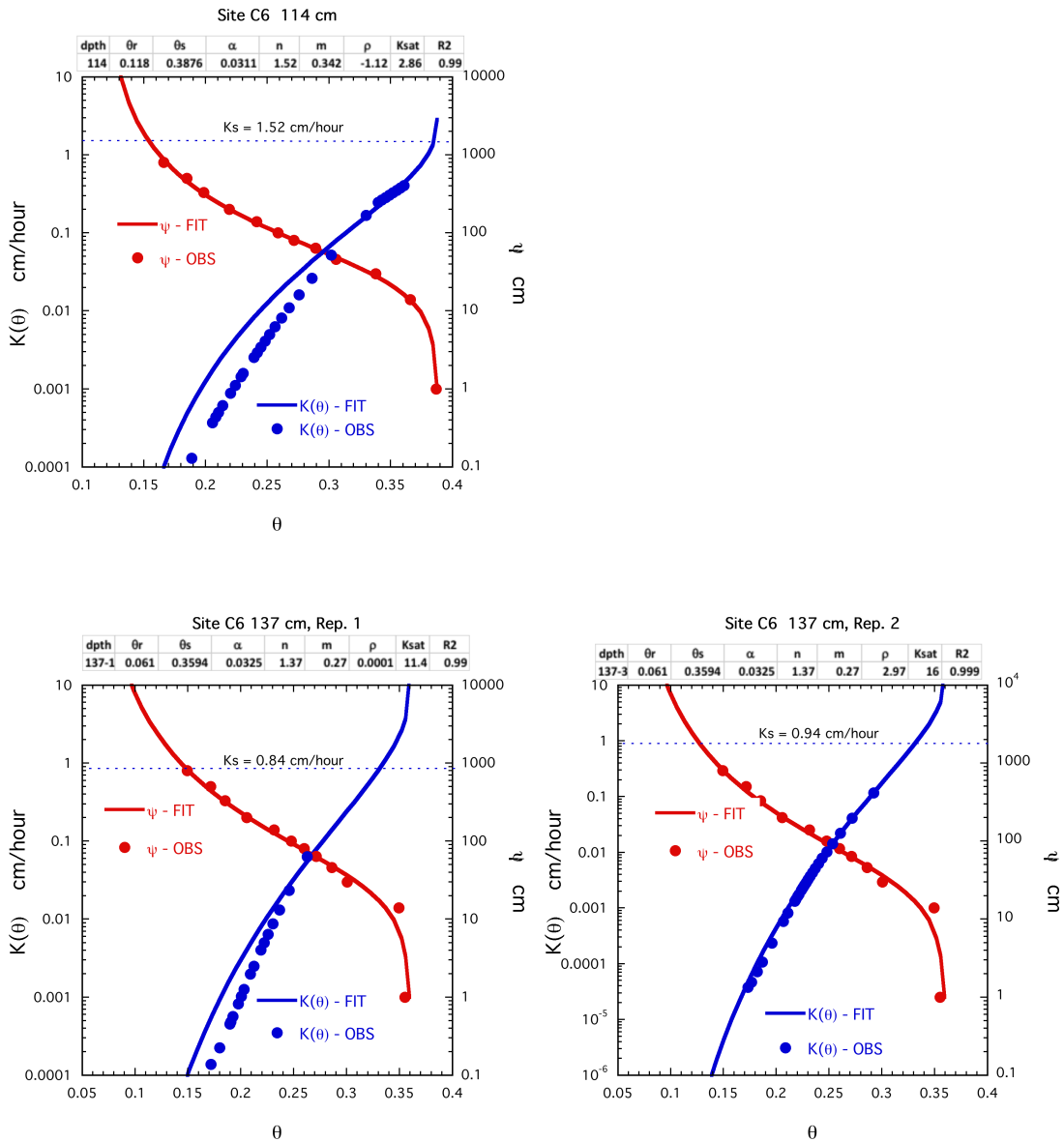


Figure C6-1. Measured laboratory data and fitted VG functions for  $\theta(\psi)$  and  $K(\theta)$  (114 cm and 137-cm, Rep. 1 and Rep. 2). VG parameters are shown in the overlying boxes. *Note:  $\psi$  corresponding to  $K(\theta)$  on the graph is determined by first tracking vertically from  $K(\theta)$  (blue curve) to the corresponding  $\theta(\psi)$  curve (red), and then locating (horizontally right) the  $\psi$  value corresponding to that  $\theta$  and  $K(\theta/\psi)$  value.*

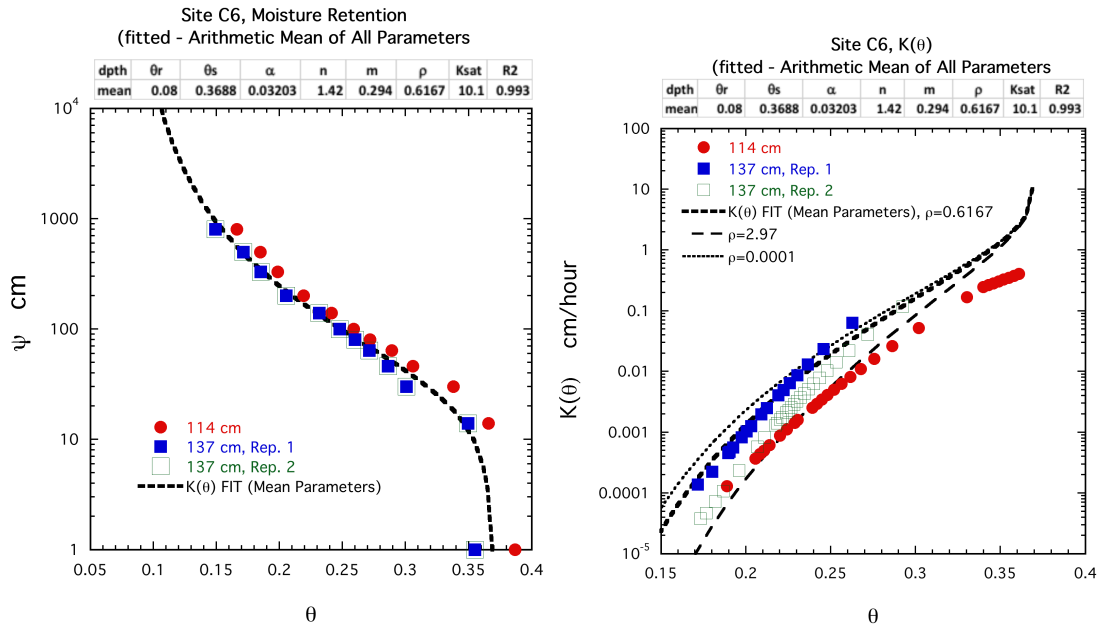


Figure C6-2. Comparison of measured  $\theta(\psi)$  (left) and  $K(\theta)$  (right) data for C6-114 cm, C6-137-cm, Rep. 1, and C6-137-cm, Rep. 2. Fitted function uses the mean of three parameter set values. In addition, the mean  $\rho$ , best fit  $\rho$ , and most common  $\rho=0.0001$ .

Site C7. Evaluation Comments, Hydraulic Data, and VG Functions

- All  $\theta(\psi)$  fits are excellent (Figure C7-1).
- $K_s$  for the 114-cm depth corresponds to  $\theta_s \sim 0.380$ , air entry/inflection values at  $\psi \sim 13$  cm. Excellent VG fit with  $K(\theta)$  over the measured range.
- $K_s$  for 137-cm Rep.1 sample corresponds to  $\theta_s \sim 0.33$ , and air entry/inflection value at  $\psi \sim 28$  cm. Excellent VG over the measured range.
- $K_s$  for 137-cm Rep.2 corresponds to  $\theta_s \sim 0.341$ , and air entry/inflection value at  $\psi \sim 13$  cm. VG fit is good only in the very wet range ( $\psi < 70$  cm)
- All of the  $\theta(\psi)$  data are closely concordant.  $K(\theta)$  curves vary in range and pattern (Fig. C7-2).

Table C7-1. Measured  $\theta(\psi)$  and  $K(\theta)$  determined from laboratory data.

114 cm				137 cm, Rep. 1				137 Rep. 2			
$K_s=1.15$ cm/h				$K_s=0.16$ cm/h				$K_s=1.48$ cm/h			
$\theta$	$\psi$	$\theta$	$K(\theta)$	$\theta$	$\psi$	$\theta$	$K(\theta)$	$\theta$	$\psi$	$\theta$	$K(\theta)$
	cm		cm/h		cm		cm/h		cm		cm/h
0.4076	0	0.3575	0.21	0.3791	0	0.334	0.17	0.356	0	0.3279	0.040
0.3801	14	0.3545	0.18	0.3467	14	0.3228	0.12	0.3415	14	0.3249	0.019
0.3565	30	0.3523	0.13	0.331	30	0.3181	0.099	0.3221	30	0.3219	0.012
0.3217	46	0.3356	0.060	0.3158	46	0.3139	0.083	0.3139	46	0.3189	0.008
0.3016	64	0.3256	0.037	0.3024	64	0.3101	0.070	0.305	64	0.3129	0.005
0.2813	80	0.3187	0.026	0.2893	80	0.3066	0.060	0.2979	80	0.3099	0.0036
0.2703	100	0.3133	0.020	0.2819	100	0.2826	0.020	0.2927	100	0.3017	0.0021
0.2532	140	0.309	0.016	0.2674	140	0.2686	0.0097	0.2826	140	0.3008	0.0020
0.2356	200	0.3023	0.011	0.2502	200	0.259	0.0057	0.2692	200	0.2975	0.0014
0.2117	330	0.2931	0.0065	0.2331	330	0.2519	0.0038	0.2569	330	0.2938	0.0010
0.1961	500	0.2897	0.0054	0.2212	500	0.2463	0.0027	0.2454	500	0.2909	0.00075
0.1807	800	0.2831	0.0037	0.207	800	0.2418	0.0021	0.2331	800	0.2885	0.00060
		0.2791	0.0029			0.2379	0.0016			0.2855	0.00045
		0.2737	0.0021			0.2347	0.0013			0.2836	0.00037
		0.2695	0.0016			0.2271	0.00080			0.276	0.00018
		0.2426	0.00033			0.2202	0.00049			0.268	0.00008
		0.236	0.00023							0.2597	0.00004
		0.2315	0.00019								
		0.2281	0.00017								
		0.2231	0.00017								

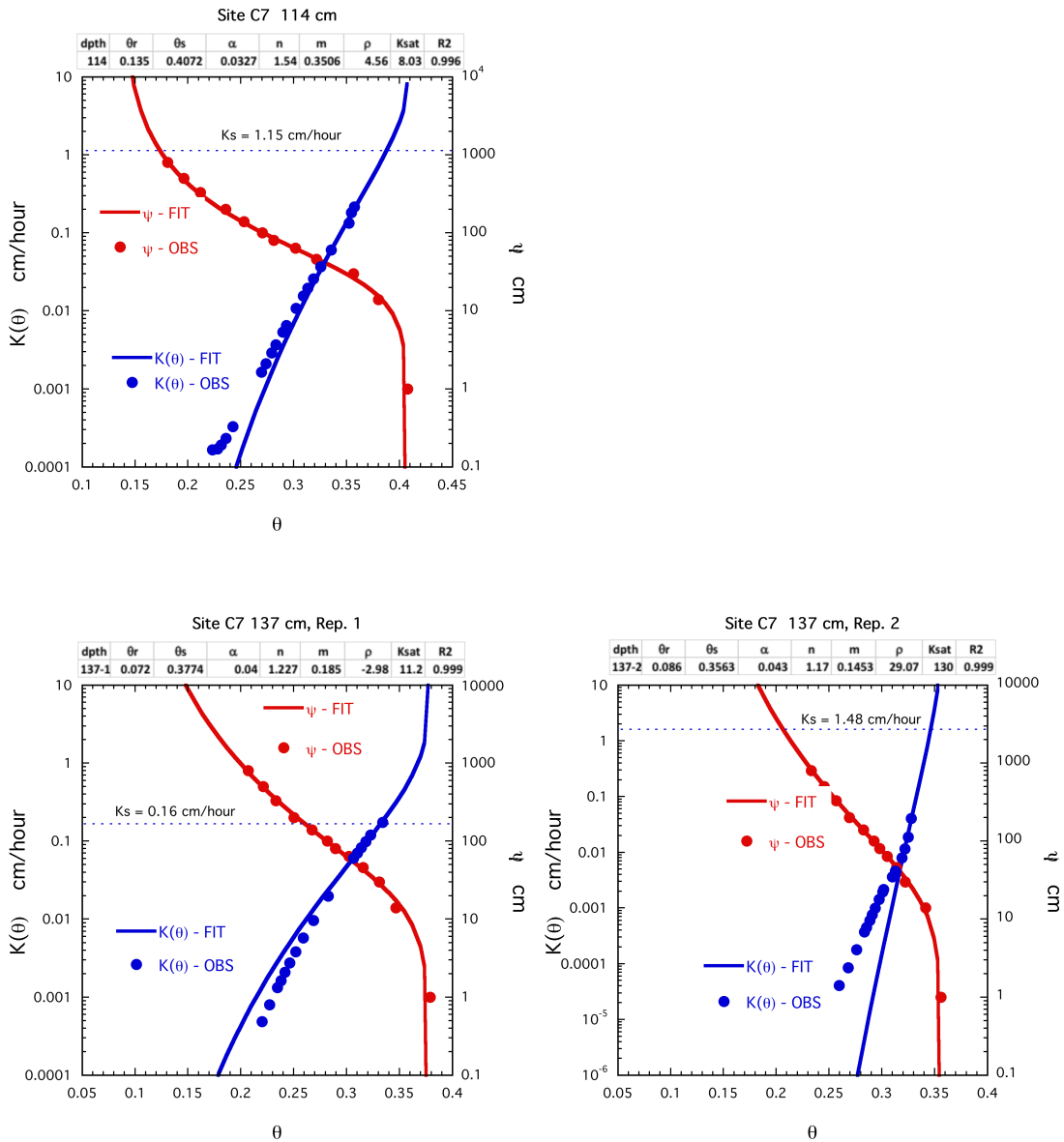


Figure C7-1. Measured laboratory data and fitted VG functions for  $\theta(\psi)$  and  $K(\theta)$  (114 cm, 137-cm Rep. 1 and 137-cm, Rep. 2). Note:  $\psi$  corresponding to  $K(\theta)$  on the graph is determined by first tracking vertically from  $K(\theta)$  (blue curve) to the corresponding  $\theta(\psi)$  curve (red), and then locating (horizontally right) the  $\psi$  value corresponding to that  $\theta$  and  $K(\theta/\psi)$  value.

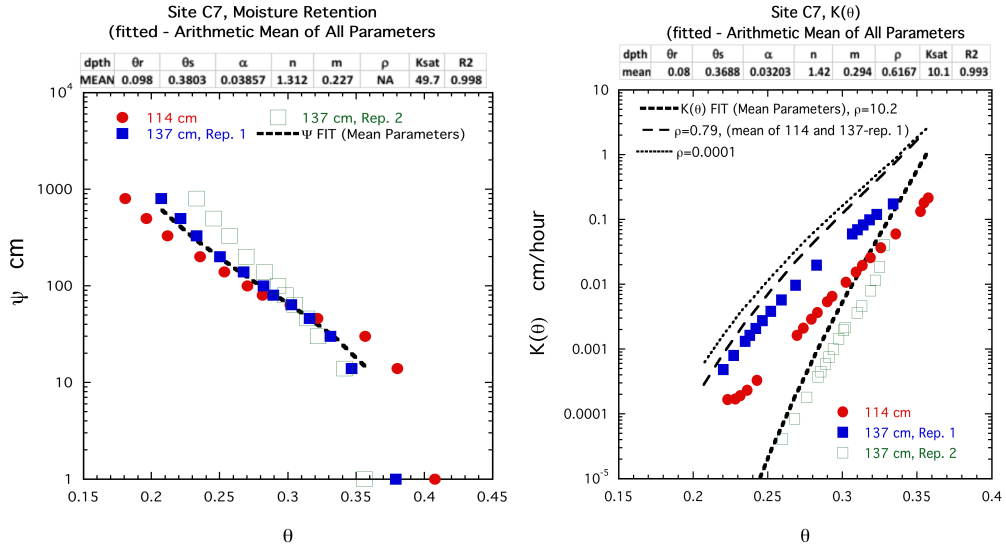


Figure C7-2. Comparison of measured  $\psi(\theta)$  (left) and  $K(\theta)$  (right) data for C7-114 cm, C7-137-cm, Rep. 1, and C7-137-cm, Rep. 2. This figure uses the mean water content, fits the mean suction using the mean of the VG parameters for the three samples.  $K(\theta)$  is calculated using the mean fitted  $K$ , and mean  $\rho$  parameter for the three depths. Fitted  $K(\theta)$  are also calculated using the mean  $\rho$  for 114 cm and 137-cm Rep. 1 samples, and the most common  $\rho$  ( $\rho=0.0001$ ).

### Site C8. Evaluation Comments, Hydraulic Data, and VG Functions

- All  $\theta(\psi)$  fits are excellent (Fig. C7-1).
- No reasonable fit was achieved for  $K(\theta)$  at the 114-cm depth.
- No reasonable fit was achieved for  $K(\theta)$  in the 137-cm Rep. 1 sample.
- Projected  $K_s$  for 137-cm Rep.2 corresponds to  $\theta_s \sim 0.42$  (saturation moisture), and air entry/inflection value at  $\psi \sim 0$  cm. Fit is good from saturation to  $\psi \sim 100$  cm, fair beyond that.
- All of the  $\theta(\psi)$  curves are reasonably closely concordant.  $K(\theta)$  for the three samples vary.  $K(\theta)$  for the 137-cm Rep. 1 sample is likely spurious as noted in the table.

Table C8-1. Measured  $\theta(\psi)$  and  $K(\theta)$  determined from laboratory data.

114 cm				137 cm, Rep. 1				137 cm, Rep. 2			
$K_s=1.16$ cm/h				$K_s=1.48$ cm/h				$K_s=0.69$ cm/h			
$\theta$	$\psi$	$\theta$	$K(\theta)$	$\theta$	$\psi$	$\theta$	$K(\theta)^*$	$\theta$	$\psi$	$\theta$	$K(\theta)$
	cm		cm/h		cm		cm/h		cm		cm/h
	0	0.4377	1.80	0.3418	0	0.3302	33.01	0.4029	0	0.3364	0.033
	14	0.3784	1.07	0.3366	14	0.3196	21.02	0.3798	14	0.3324	0.024
	30	0.3562	0.54	0.3053	30	0.3128	17.98	0.356	30	0.3294	0.018
0.377	46	0.3422	0.340	0.3016	46	0.306	13.51	0.3344	46	0.3271	0.015
0.3452	64	0.3321	0.240	0.2927	64	0.2984	1.634	0.3195	64	0.3252	0.012
0.3203	80	0.3243	0.182	0.2852	80	0.2939	1.021	0.3076	80	0.3235	0.0104
0.306	100	0.318	0.145	0.277	100	0.2912	0.4567	0.3016	100	0.3222	0.0091
0.2837	140	0.3127	0.119	0.2621	140	0.2859	0.02729	0.2889	140	0.3209	0.0081
0.245	200	0.3081	0.100	0.2316	200			0.2741	200	0.3199	0.0073
0.1951	330	0.3041	0.0859	0.207	330			0.2562	330	0.3189	0.0066
0.1654	500	0.3006	0.0749	0.1884	500			0.2443	500	0.318	0.0061
0.1342	800	0.2974	0.066	0.1586	800			0.2294	800	0.3172	0.0056
		0.2895	0.048							0.314	0.0040
		0.2815	0.035							0.311	0.0029
		0.2798	0.032							0.3096	0.0026
		0.2702	0.021							0.3083	0.0022
		0.2691	0.020							0.3015	0.0011
		0.2623	0.015							0.2967	0.00085
		0.2615	0.014								
		0.2569	0.012								
		0.2498	0.0084								
		0.2436	0.0062								
		0.2399	0.0052								
		0.2365	0.0044								
		0.231	0.0033								
		0.2287	0.0030								
		0.2247	0.0024								
		0.22	0.0019								
		0.2176	0.0016								

\* $K(\theta)$  data for 137-cm, Rep. 1 are implausibly large for any local soil materials, likely spurious, resulting from a lab or computational error.

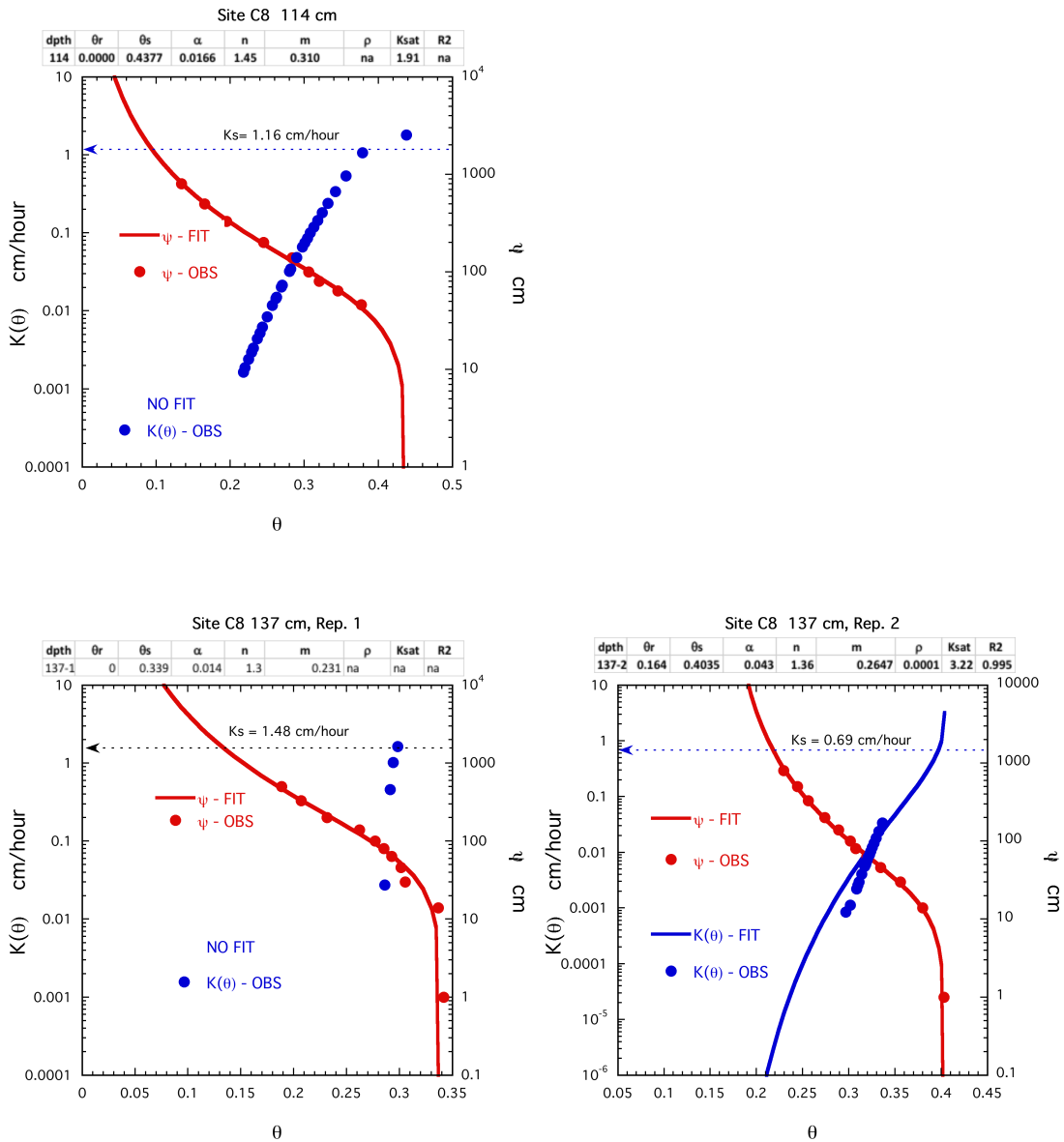


Figure C8-1. Measured laboratory data and fitted VG functions for  $\theta(\psi)$  and  $K(\theta)$  (114 cm, 137-cm Rep. 1 and 137-cm, Rep. 2). Fits not obtained for 114 cm and 137 cm, Rep. 1 samples. Note:  $\psi$  corresponding to  $K(\theta)$  on the graph is determined by first tracking vertically from  $K(\theta)$  (blue curve) to the corresponding  $\theta(\psi)$  curve (red), and then locating (horizontally right) the  $\psi$  value corresponding to that  $\theta$  and  $K(\theta/\psi)$  value.

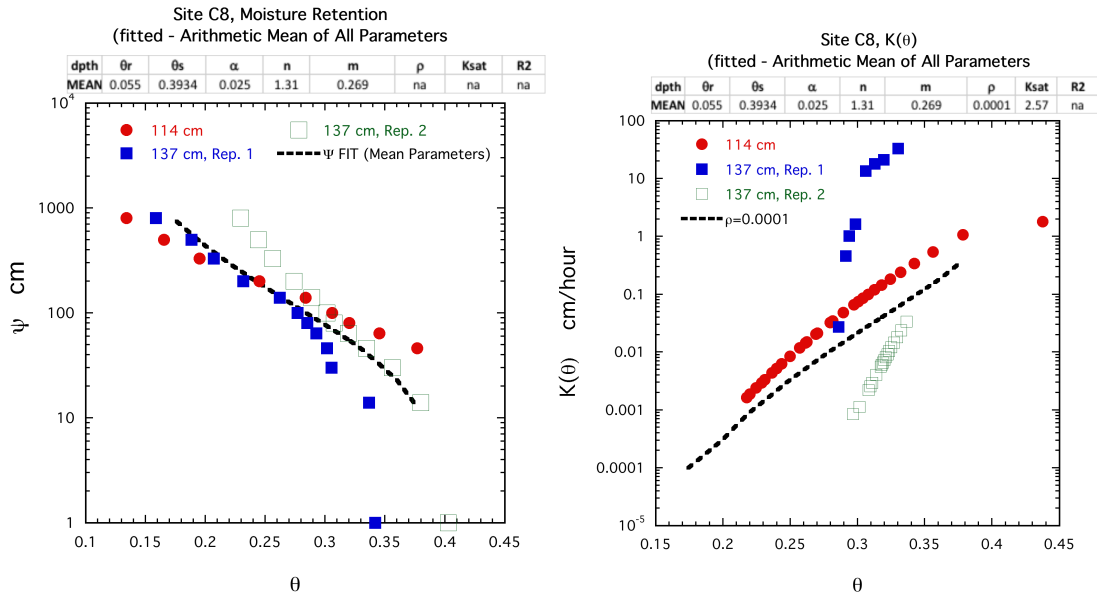


Figure C8-2. Comparison of measured  $\psi(\theta)$  (left) and  $K(\theta)$  (right) data for C8-114 cm, C8-137-cm, Rep. 1, and C8-137-cm, Rep. 2 data; This figure uses the mean water content, fits the mean suction using the mean of the VG parameters for the three samples. VG  $K(\theta)$  is calculated using the mean fitted  $K$ , and  $\rho = 0.0001$ .

Site D6. Evaluation Comments, Hydraulic Data, and VG Functions

- VG fits for 137-cm Rep. 1 and Rep. 2 samples are excellent (Fig. D6-1). No 114 cm  $\theta(\psi)$  data were measured.
- No reasonable  $K(\theta)$  was obtained for 114 cm or 137-cm Rep. 1.
- $K_s$  for the 137-cm Rep. 2 sample corresponds to  $\theta_s \sim 0.362$  (near saturation moisture), with air entry/inflection values at  $\psi \sim 1$  cm (Fig. D6-1). Function fits for  $D(\theta)$  are fair over the limited moisture range measured.  $K(\theta)$  fitted range seems reasonable, but accuracy is speculative based on the  $D(\theta)$  range and fit.
- $\theta(\psi)$  data for 137-cm Rep. 1 and Rep. 2 vary in range and pattern (Fig. D6-2).

Table D6-1. Measured  $\theta(\psi)$  and  $D(\theta)$ , determined from laboratory data.

137 cm Rep. 1				137 cm Rep. 2			
$\theta$	$\psi$	$\theta$	$D(\theta)$	$\theta$	$\psi$	$\theta$	$D(\theta)$
	cm		$\text{cm}^2/\text{h}$		cm		$\text{cm}^2/\text{h}$
-	0	-	-	-	0	0.3167	20.02
0.3191	14	-	-	0.3132	14	0.3138	14.87
0.2487	30	-	-	0.2796	30	0.3118	12.14
0.2417	46	-	-	0.2767	46	0.3102	10.44
0.2338	64	-	-	0.2714	64	0.3088	7.157
0.2294	80	-	-	0.2688	80	0.3079	6.406
0.2208	100	-	-	0.264	100	0.3072	5.832
0.2119	140	-	-	0.2554	140	0.3066	5.376
0.1929	200	-	-	0.242	200	0.306	5.004
0.1806	330	-	-	0.2316	330	0.3048	4.317
0.1717	500	-	-	0.223	500	0.3038	3.845
0.1609	800	-	-	0.213	800	0.303	3.499
		-	-			0.3023	3.236
		-	-			0.3017	3.028
		-	-			0.3011	2.861
		-	-			0.3006	2.723
		-	-			0.3002	2.609
		-	-			0.2998	2.512
		-	-			0.2994	2.43
		-	-			0.299	2.361
		-	-			0.2987	2.3
		-	-			0.2984	2.249
		-	-			0.298	2.204
		-	-			0.2978	2.173
		-	-			0.2975	2.132
		-	-			0.2965	2.043
		-	-			0.2951	2.008

Table D6-2. Fitted  $\theta(\psi)$  and  $K(\theta)$ , determined from laboratory  $\theta(\psi)$  data and data shown in Table D6-1.

137 cm Rep. 2		
Ks = 2.09 cm/h		
$\theta$	$\psi$	K( $\theta$ )
	cm	cm/h
0.395	0	-
0.3901	0	14.08
0.3851	0	6.909
0.3753	0	2.454
0.3654	1	1.038
0.3555	2	0.4702
0.3456	3	0.2193
0.3358	5	0.1034
0.3259	7	0.04869
0.316	11	0.02274
0.3061	16	0.01048
0.2963	23	0.00474
0.2864	34	0.002098
0.2765	50	0.0009057
0.2666	74	0.0003802
0.2568	113	0.0001547
0.2469	173	6.085e-05
0.237	270	2.306e-05
0.2271	430	8.389e-06
0.2173	698	2.919e-06
0.2074	1158	9.67e-07
0.1975	1969	3.036e-07
0.1876	3439	8.983e-08
0.1778	6190	2.489e-08

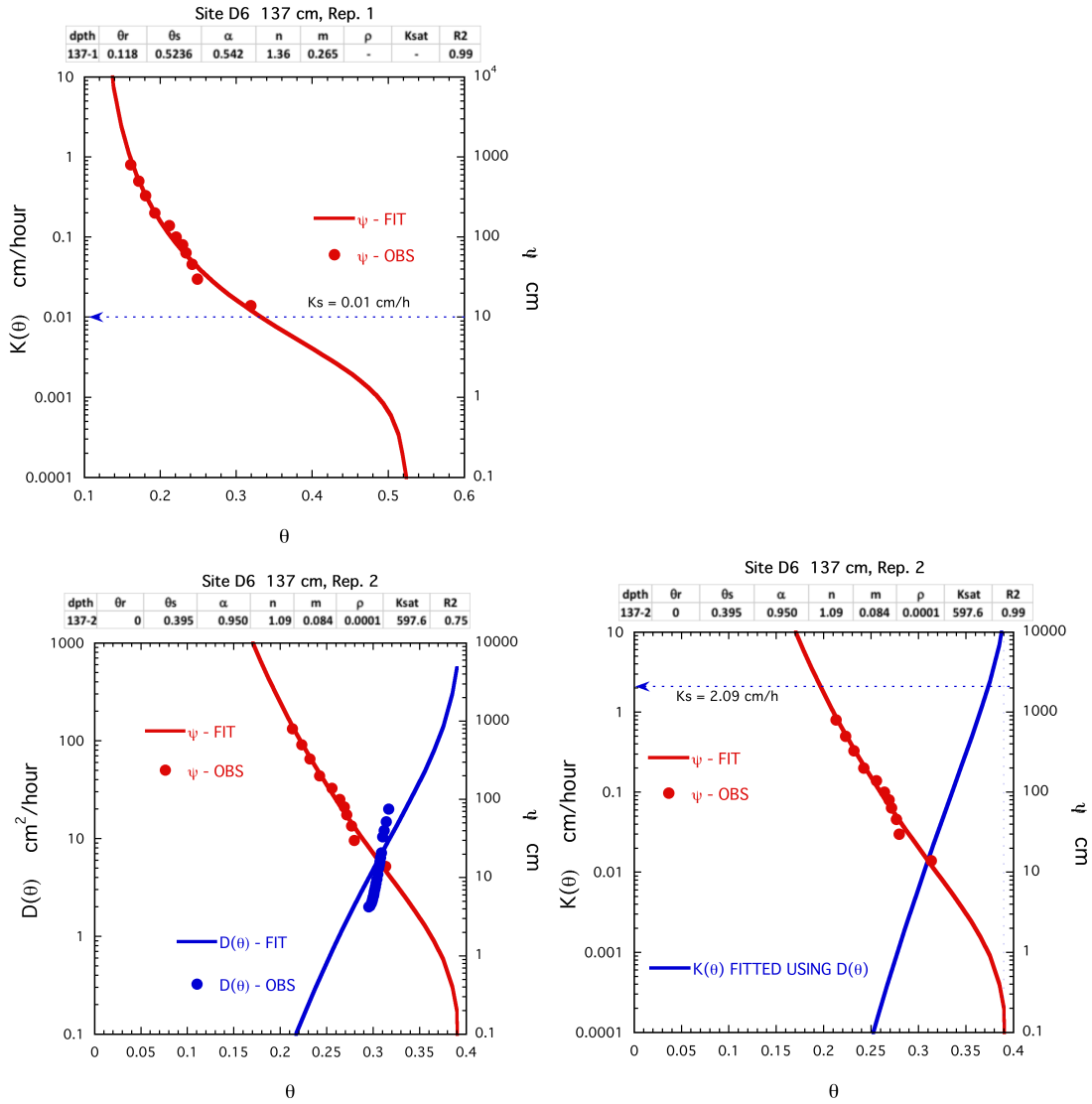


Figure D6-1. Measured laboratory data and fitted VG functions for  $\theta(\psi)$  (137-cm, Rep. 1 and Rep. 2); and  $D(\theta)$ , and  $K(\theta)$  for 137 cm, Rep. 2. VG parameters are shown in the overlying boxes. *Note:  $\psi$  corresponding to  $K(\theta)$  on the graph is determined by first tracking vertically from  $K(\theta)$  (blue curve) to the corresponding  $\theta(\psi)$  curve (red), and then locating (horizontally right) the  $\psi$  value corresponding to that  $\theta$  and  $K(\theta/\psi)$  value.*

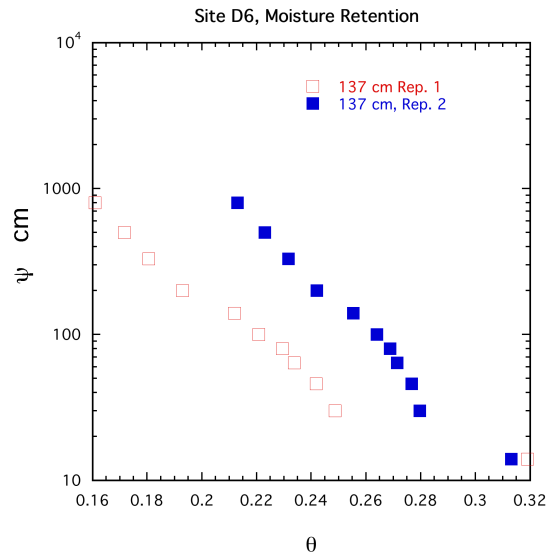


Figure D6-2. Comparison of measured  $\theta(\psi)$ , D6-137-cm, Rep. 1, and D6-137-cm, Rep. 2.

Site D7. Evaluation Comments, Hydraulic Data, and VG Functions

- All  $\theta(\psi)$  fits are excellent (Fig. D7-1).
- $K_s$  for the 114-cm depth fitted at saturation may fit well if extrapolated. VG  $K(\theta)$  function fits corresponded well to the data over the entire measured range.
- $K_s$  for the 137-cm Rep. 1 corresponds to  $\theta_s \sim 0.365$  (near saturation moisture), with air entry/inflection values at  $\psi \sim 0$  cm. Function fits corresponded well to the data over the entire measured range. Near saturation, however, while the fit corresponds closely with saturation moisture,  $K(\theta)$  is highly sensitive to small moisture changes near saturation. Caution is needed near saturation.
- $K_s$  for the 137-cm Rep. 2 corresponds to  $\theta_s \sim 0.299$  (near saturation moisture), with air entry/inflection values at  $\psi \sim 0$  cm. Function fits corresponded well to the data over the entire measured range. Near saturation, however, while the fit corresponds closely with saturation moisture,  $K(\theta)$  is highly sensitive to small moisture changes near saturation. Caution is needed near saturation.
- $\theta(\psi)$  data vary in range and form.  $K(\theta)$  curves exhibit a similar form and have strong concordance.  $K(\theta)$  fitted using mean parameters and the most common ( $\rho=0.0001$ ) value, fit the data poorly (Fig. D7-2).

Table D7-1. Measured  $\theta(\psi)$  and  $K(\theta)$  determined from laboratory data.

114 cm				137 cm Rep. 1				137 cm Rep. 2			
$K_s=1.88$ cm/h				$K_s=1.22$ cm/h				$K_s=0.04$ cm/h			
$\theta$	$\psi$	$\theta$	$K(q)$	$\theta$	$\psi$	$\theta$	$K(\theta)$	$\theta$	$\psi$	$\theta$	$K(q)$
	cm		cm/h		cm		cm/h		cm		cm/h
	0	0.3191	0.05	0.3709	0	0.33	0.11	0.2979	0	0.2397	0.00041
46	0.3113	0.3067	0.03	0.3521	14	0.3254	0.085	0.2875	14	0.2323	0.00031
64	0.3024	0.2988	0.02	0.3411	30	0.3202	0.067	0.2666	30	0.2299	0.00024
80	0.2875	0.2931	0.013	0.3308	46	0.3156	0.055	0.2547	46	0.2284	0.00021
100	0.2822	0.2886	0.010	0.3256	64	0.3115	0.045	0.2502	64	0.2214	0.00011
140	0.2644	0.2818	0.0063	0.3174	80	0.3014	0.028	0.2443	80	0.2146	0.000056
200	0.2435	0.2727	0.0036	0.31	100	0.2985	0.024	0.2428	100	0.2103	0.000038
330	0.2219	0.2693	0.0029	0.2949	140	0.2912	0.016960	0.2338	140	0.2071	0.000030
500	0.2093	0.2652	0.0022	0.2761	200	0.28	0.0095	0.2264	200	0.2046	0.000026
800	0.1966	0.2619	0.0018	0.2521	330	0.2718	0.0061	0.2145	330	0.2026	0.000024
		0.2609	0.0017	0.2364	500	0.2654	0.0042	0.2041	500	0.2009	0.000023
		0.2559	0.0012	0.2238	800	0.261	0.0033	0.1981	800		
		0.2532	0.0010			0.2565	0.0025				
		0.2508	0.00090			0.2527	0.0020				
		0.2488	0.00079			0.2494	0.0016				
		0.2478	0.00074			0.2455	0.0013				
		0.2355	0.00036			0.2426	0.0010				
		0.2239	0.00021			0.2387	0.00081				
						0.2384	0.00079				
						0.2326	0.00053				
						0.225	0.00030				

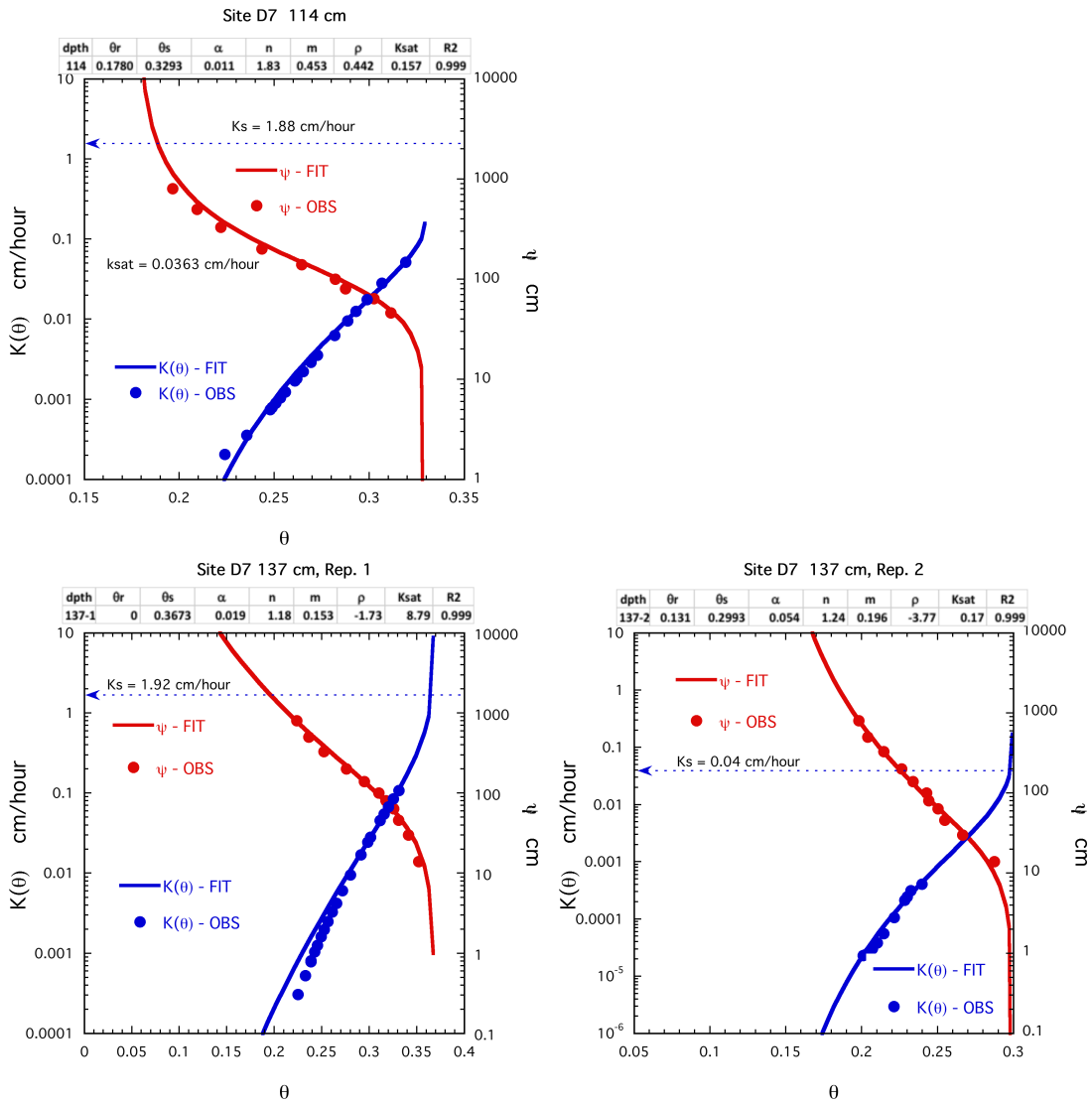


Figure D7-1. Measured laboratory data and fitted VG functions for  $\theta(\psi)$  and  $K(\theta)$  (114 cm, 137-cm, Rep. 1 and 137-cm, Rep. 2). Note:  $\psi$  corresponding to  $K(\theta)$  on the graph is determined by first tracking vertically from  $K(\theta)$  (blue curve) to the corresponding  $\theta(\psi)$  curve (red), and then locating (horizontally right) the  $\psi$  value corresponding to that  $\theta$  and  $K(\theta/\psi)$  value.

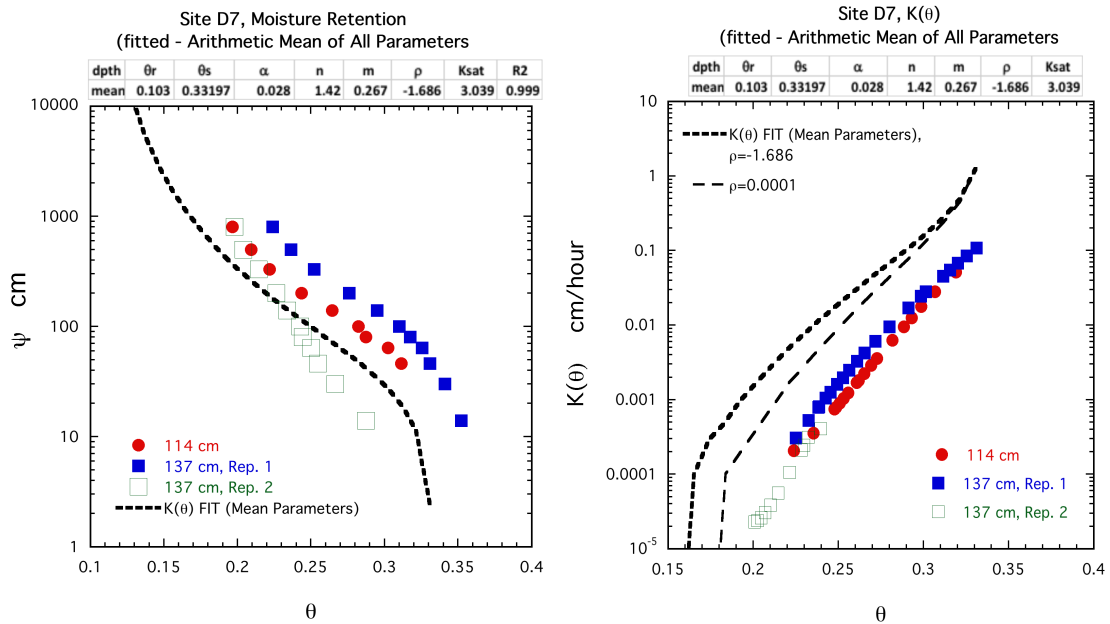


Figure D7-2. Comparison of measured  $\psi(\theta)$  (left) and  $K(\theta)$  (right) data for D7-114 cm, D7-137-cm, Rep. 1, and D7-137-cm, Rep. 2. This figure uses the mean water content, fits the mean suction using the mean of the VG parameters for the three samples.  $K(\theta)$  is calculated using the mean fitted K, and mean  $\rho$  parameter for the three depths. Fitted  $K(\theta)$  are also calculated using the most common  $\rho$  ( $\rho = 0.0001$ ).

Site D8. Evaluation Comments, Hydraulic Data, and VG Functions

- All  $\theta(\psi)$  fits are excellent.
- $K_s$  for 114 cm corresponds to  $\theta_s \sim 0.336$  (near saturation moisture), with air entry/inflection values at  $\psi \sim 40$  cm (Fig. D8-1). VG function fits to the data were excellent over the entire measured range. Near saturation, however, while the fit corresponds closely with saturation moisture,  $K(\theta)$  is highly sensitive to small moisture changes near saturation. Caution is needed near saturation.
- $K_s$  for the 137-cm Rep. 1 corresponds to  $\theta_s \sim 0.385$  (near saturation moisture); air entry/inflection values at  $\psi \sim 30$  cm.  $K(\theta)$  functions VG functions were fitted directly from  $D(\theta)$  and  $\theta(\psi)$  data.
- 
- $K_s$  for the 137-cm Rep. 2 corresponds to  $\theta_s \sim 0.354$  air entry/inflection values at  $\psi \sim 35$  cm.  $K(\theta)$  functions VG functions were fitted directly from  $D(\theta)$  and  $\theta(\psi)$  data.
- $\theta(\psi)$  data are closely concordant in range and pattern.  $K(\theta)$  curves vary, with lower range for deeper samples.  $K(\theta)$  fitted using mean parameters and the most common ( $\rho=0.0001$ ) value are within the range of curve parameters (Fig. D8-2).

Table D8-1. Measured  $\theta(\psi)$  and  $K(\theta)$  (114 cm) and  $D(\theta)$  (137 cm, Rep. 1 and Rep. 2) determined from laboratory data.

114 cm				137 cm Rep. 1				137 cm Rep. 2			
$K_s=1.29$ cm/h				$K_s=0.39$ cm/h				$K_s=0.07$ cm/h			
$\theta$	$\psi$	$\theta$	$K(\theta)$	$\theta$	$\psi$	$\theta$	$D(\theta)$	$\theta$	$\psi$	$\theta$	$D(\theta)$
	cm		cm/h		cm		cm <sup>2</sup> /h		cm		cm <sup>2</sup> /h
	0	0.2974	0.25		0	0.327	46.0		0	0.3118	27.0
0.326	46.5	0.2952	0.22	0.3947	14	0.3179	36.0	0.3638	14	0.31	12.0
0.317	64	0.28	0.11	0.3738	30	0.3066	26.0	0.3578	30	0.3071	11.0
0.302	80	0.27	0.065	0.3716	46	0.3027	22.0	0.3388	46	0.3058	10.0
0.293	100	0.26	0.039	0.363	64	0.2969	18.0	0.328	64	0.3036	9.2
0.279	140	0.25	0.0226	0.3508	80	0.2947	16.0	0.3158	80	0.3026	8.8
0.259	200	0.24	0.0129	0.3318	100	0.2911	14.0	0.3098	100	0.3008	8.1
0.237	330	0.23	0.0072	0.3098	140	0.2896	13.0	0.2979	140	0.3	7.8
0.222	500	0.22	0.0039	0.2647	200	0.2871	11.0	0.2837	200	0.2985	7.3
0.206	800	0.2104	0.0021	0.2472	330	0.286	11.0	0.2647	330	0.2979	7.1
		0.1996	0.0010	0.2476	500	0.2841	9.6	0.2499	500	0.2966	6.7
				0.2141	800	0.2825	8.7	0.2316	800	0.2955	6.3
						0.2818	8.3			0.295	6.1
						0.2805	7.7			0.294	5.8
						0.2799	7.4			0.2936	5.7
						0.2788	6.9			0.2927	5.4
						0.2783	6.7			0.2923	5.3
						0.2774	6.2			0.2916	5.1
						0.277	6.1			0.2912	5.0
						0.2763	5.7			0.2905	4.8
						0.2759	5.6			0.2902	4.7
						0.2752	5.3			0.2896	4.6
						0.2749	5.2			0.2893	4.5
						0.2743	4.9			0.2888	4.4
						0.2733	4.5			0.2878	4.1
						0.2674	2.6			0.2873	4.0
						0.2634	1.5			0.2814	2.8
						0.2616	1.2			0.2764	2.1
						0.2605	1.1				
						0.2598	1.0				
						0.2592	1.0				

Table D8-2. Fitted  $\theta(\psi)$  and  $K(\theta)$  (137 cm, Rep. 1 and Rep. 2) determined from laboratory  $D(\theta)$  and  $\theta(\psi)$  data shown in Table D8-1.

137 cm Rep. 1			137 cm Rep. 2		
$\theta$	$\psi$	$K(\theta)$	$\theta$	$\psi$	$K(\theta)$
	cm	cm/h		cm	cm/h
0.388	0	0.63	0.3788	0	1.34
0.3858	19	0.49	0.3755	4	0.28
0.3836	26	0.42	0.3723	8	0.19
0.3792	36	0.34	0.3657	14	0.10
0.3748	43	0.28	0.3592	21	0.066
0.3704	50	0.23	0.3527	29	0.044
0.3659	56	0.19	0.3461	37	0.030
0.3615	62	0.16	0.3396	46	0.021
0.3571	67	0.13	0.3331	56	0.015
0.3527	72	0.11	0.3265	67	0.010
0.3483	78	0.094	0.32	80	0.0072
0.3439	83	0.078	0.3135	95	0.0051
0.3395	88	0.065	0.3069	112	0.0036
0.3351	94	0.054	0.3004	132	0.0025
0.3306	99	0.045	0.2938	156	0.0017
0.3262	105	0.037	0.2873	183	0.0012
0.3218	111	0.030	0.2808	216	0.00080
0.3174	117	0.025	0.2742	256	0.00053
0.313	123	0.020	0.2677	304	0.00035
0.3086	130	0.016	0.2612	363	0.00023
0.3042	137	0.013	0.2546	435	0.00015
0.2998	145	0.010	0.2481	526	9.21E-05
0.2953	153	0.0079	0.2416	640	5.64E-05
0.2909	162	0.0061	0.235	787	3.38E-05
0.2865	171	0.0047	0.2285	977	1.96E-05
0.2821	181	0.0035	0.222	1227	1.11E-05
0.2777	193	0.0026	0.2154	1563	6.01E-06
0.2733	205	0.0019	0.2089	2023	3.13E-06
0.2689	219	0.0013	0.2024	2666	1.56E-06
0.2645	235	0.00092	0.1958	3591	7.33E-07
0.26	253	0.00061	0.1893	4961	3.23E-07
0.2556	274	0.00040	0.1828	7065	1.32E-07
0.2512	299	0.00024			
0.2468	329	0.00014			
0.2424	366	7.71E-05			
0.238	414	3.82E-05			
0.2336	477	1.66E-05			
0.2291	567	6.03E-06			
0.2247	708	1.63E-06			

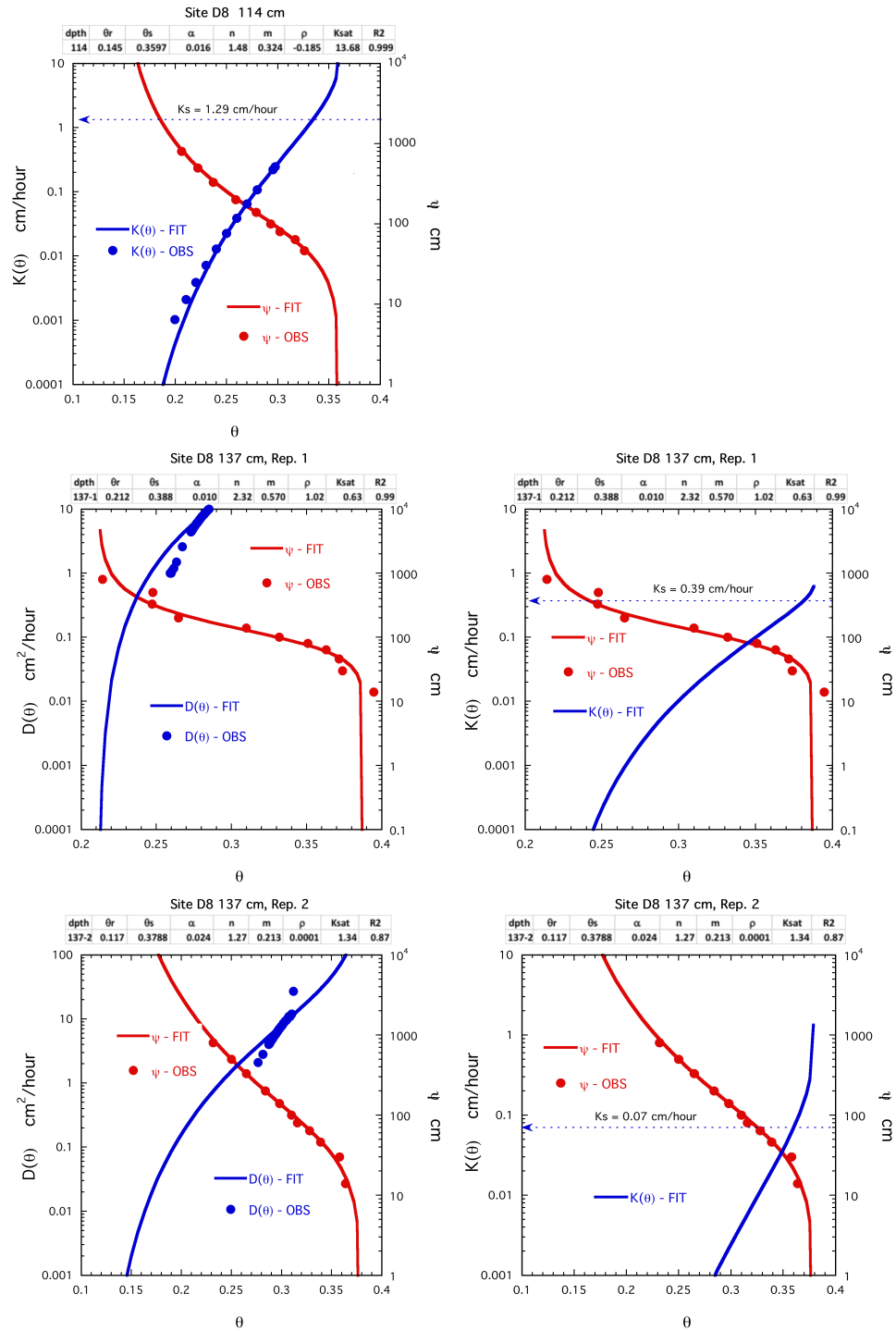


Figure D8-1. Measured laboratory data and fitted VG functions for  $\theta(\psi)$  and  $K(\theta)$  data (114 cm); and  $\theta(\psi)$  and  $D(\theta)$ , and fitted  $K(\theta)$  curves (137-cm Rep. 1 and 137-cm, Rep. 2). Note:  $\psi$  corresponding to  $K(\theta)$  on the graph is determined by first tracking vertically from  $K(\theta)$  (blue curve) to the corresponding  $\theta(\psi)$  curve (red), and then locating (horizontally right) the  $\psi$  value corresponding to that  $\theta$  and  $K(\theta/\psi)$  value.

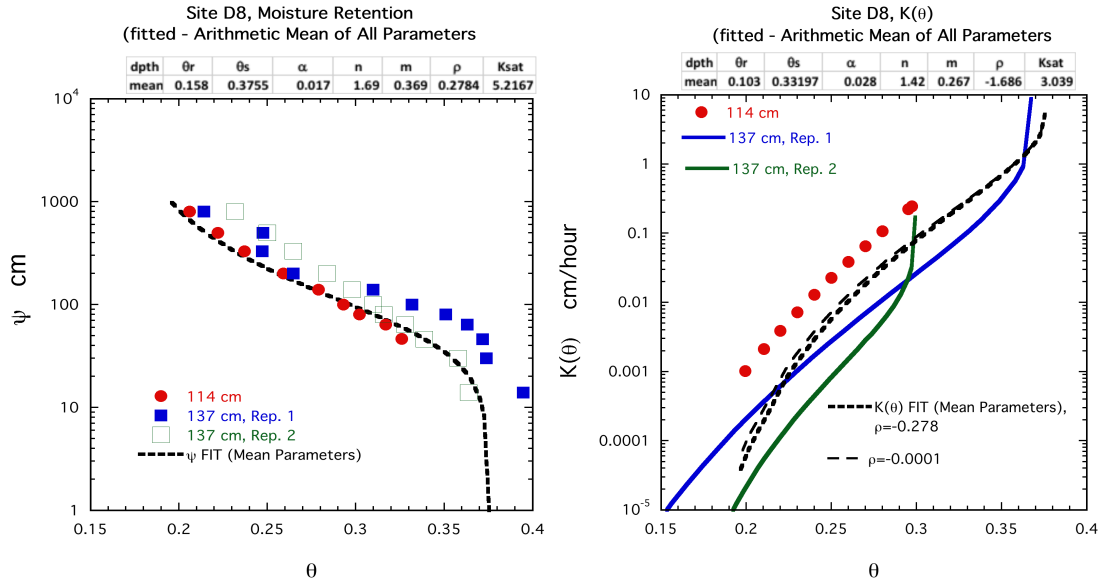


Figure D8-2. Comparison of measured  $\psi(\theta)$  (left) and  $K(\theta)$  (right) data for D8-114 cm, D8-137 cm, Rep. 1, and D8-137 cm, Rep. 2. This figure uses the mean water content, fits the mean suction using the mean of the VG parameters for the three samples.  $K(\theta)$  is calculated using the mean fitted  $K$ , and mean  $\rho$  parameter for the three depths. Fitted  $K(\theta)$  are also calculated using the most common  $\rho$  ( $\rho = 0.0001$ ).

Site D9. Evaluation Comments, Hydraulic Data, and VG Functions

- All  $\theta(\psi)$  fits are excellent (Figure D9-1).
- $K_s$  for the 114-cm depth corresponds to  $\theta_s \sim 0.385$ , air entry/inflection values at  $\psi \sim 20$  cm: Excellent fit with  $K(\theta)$  over the entire measured range.
- $K_s$  for 137-cm Rep.1 sample corresponds to  $\theta_s \sim 0.381$ , and air entry/inflection value at  $\psi \sim 31$  cm: Excellent fit with  $K(\theta)$  over the entire measured range.
- $K_s$  for 137-cm Rep.2 corresponds to  $\theta_s \sim 0.35$ ; air entry/inflection value at  $\psi \sim 45$  cm: Excellent fit with  $K(\theta)$  over the entire measured range..
- $\theta(\psi)$  and  $K(\theta)$  data for 114 cm and 137-cm Rep. 2 are closely concordant (Fig. D9-1). The 137-cm Rep. 1 sample has a much steeper  $\theta(\psi)$  curve, which corresponds to a lower  $K(\theta)$  distribution (more porosity in the high suction low-flow range). VG curves calculated using both the mean  $\rho$  ( $\rho = -0.883$ ) for the three samples, and the most common  $\rho$  ( $\rho = 0.0001$ ), both fit reasonably well to the data 114 m and 137 cm Rep. 2 data.

Table D9-1. Measured  $\theta(\psi)$  and  $K(\theta)$  determined from laboratory data.

114 cm				137 cm Rep. 1				137 cm Rep. 2			
$K_s=2.86$ cm/h				$K_s=0.15$ cm/h				$K_s=3.13$ cm/h			
$\theta$	$\psi$	$\theta$	$K(\theta)$	$\theta$	$\psi$	$\theta$	$K(\theta)$	$\theta$	$\psi$	$\theta$	$K(\theta)$
	cm		cm/h		cm		cm/h		cm		cm/h
0.3968	0	0.3497	0.88	0.3992	0	0.2448	0.00095	0.3549	1	0.3104	0.40
0.3881	14	0.3474	0.80	0.3765	14	0.2409	0.0011	0.3478	14	0.2963	0.24
0.3744	30	0.3237	0.40	0.3627	30	0.2372	0.00076	0.3307	30	0.2862	0.17
0.342	46	0.3077	0.24	0.3467	46	0.2315	0.00041	0.3221	46	0.2784	0.12
0.3268	64	0.2957	0.16	0.3359	64	0.2294	0.00032	0.3113	64	0.2721	0.096
0.305	80	0.2863	0.12	0.3262	80	0.2242	0.00017	0.2938	80	0.2624	0.064
0.2884	100	0.2786	0.088	0.3206	100	0.2191	0.000089	0.2755	100	0.255	0.047
0.266	140	0.2722	0.069	0.3105	140	0.219	0.000087	0.2528	140	0.2519	0.041
0.2294	200	0.2667	0.056	0.2957	200	0.2117	0.000032	0.2108	200	0.2442	0.030
0.2023	330	0.2619	0.046	0.2815	330			0.1787	330	0.242	0.027
0.185	500	0.2576	0.039	0.27	500			0.1597	500	0.24	0.025
0.1689	800	0.2538	0.034	0.258	800			0.1404	800	0.2381	0.023
		0.2504	0.029							0.2363	0.021
		0.2472	0.026							0.222	0.011
		0.2444	0.023							0.2142	0.0073
		0.2418	0.020							0.2135	0.0071
		0.2394	0.018							0.2083	0.0055
		0.2371	0.016							0.2026	0.0041
		0.2221	0.0081							0.198	0.0032
		0.2142	0.0054							0.1896	0.0021
		0.2033	0.0031							0.1858	0.0017
		0.1978	0.0022							0.1807	0.0013
		0.1918	0.0016							0.1799	0.0012
		0.1914	0.0015							0.1771	0.0010
		0.1874	0.0012							0.1757	0.0010
		0.1802	0.00076							0.1723	0.0008
		0.179	0.00070								
		0.1728	0.00046								
		0.1702	0.00038								

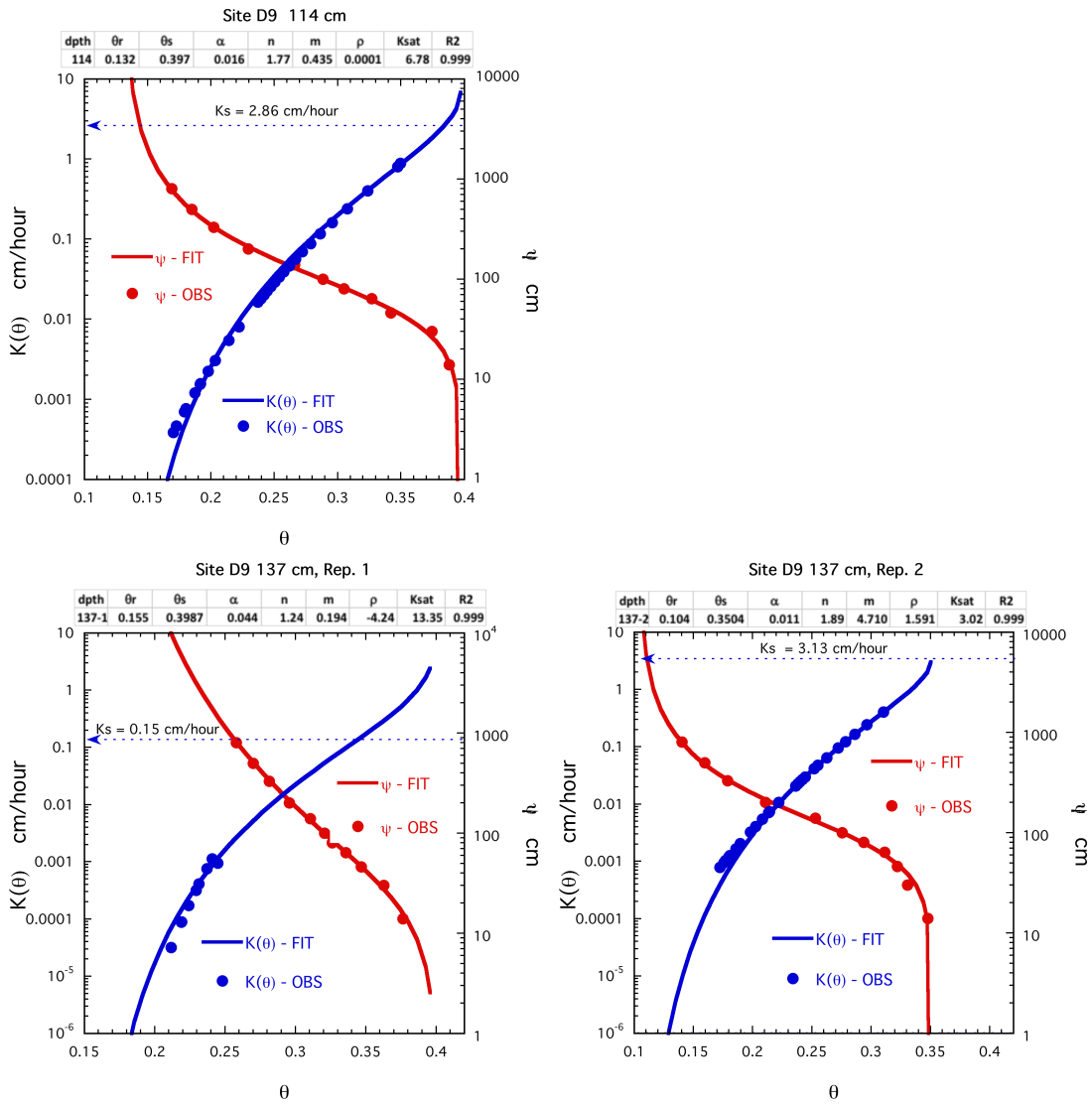


Figure D9-1. Measured laboratory data and fitted VG functions for  $\theta(\psi)$  and  $K(\theta)$  (114 cm and 137-cm, Rep. 1 and Rep. 2). VG parameters are shown in the overlying boxes. *Note:  $\psi$  corresponding to  $K(\theta)$  on the graph is determined by first tracking vertically from  $K(\theta)$  (blue curve) to the corresponding  $\theta(\psi)$  curve (red), and then locating (horizontally right) the  $\psi$  value corresponding to that  $\theta$  and  $K(\theta/\psi)$  value.*

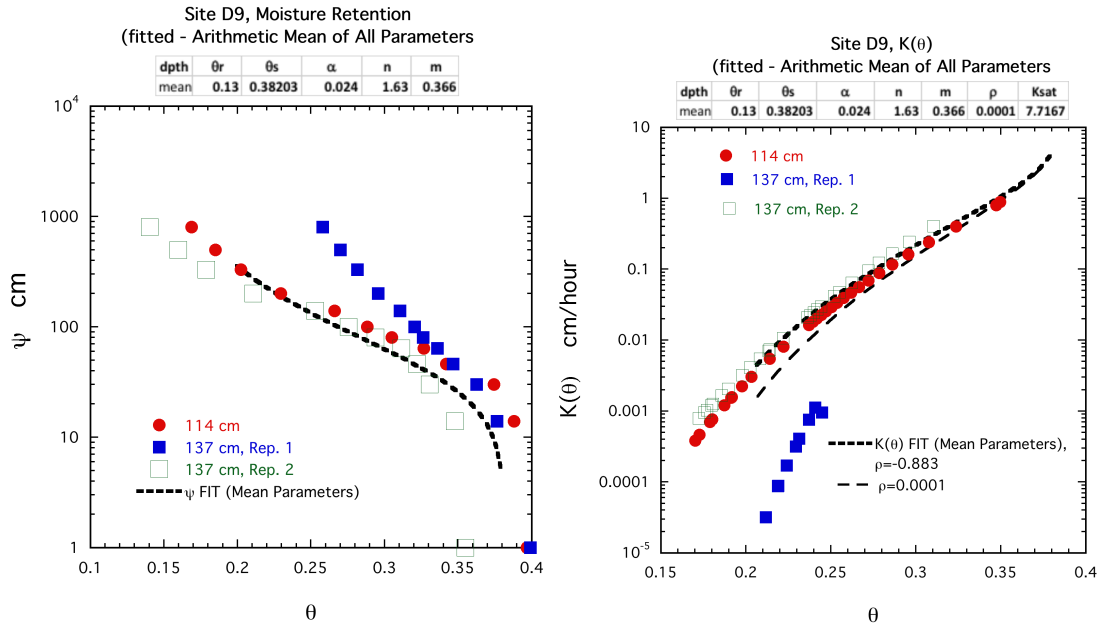


Figure D9-2. Comparison of measured  $\theta(\psi)$  (left) and  $K(\theta)$  (right) data for D9-114 cm, D9-137-cm, Rep. 1, and D9-137-cm, Rep. 2. Fitted function uses the mean of three parameter set values (including mean  $\rho = -0.883$ ), and the most common  $\rho$  value ( $\rho = 0.0001$ ).

Site D10. Evaluation Comments, Hydraulic Data, and VG Functions

- All  $\theta(\psi)$  fits are excellent (Figure D10-1).
- $K_s$  for the 114-cm depth corresponds to  $\theta_s \sim 0.362$ , air entry/inflection values at  $\psi \sim 0$  cm: Excellent fit with  $K(\theta)$  over the entire measured range.
- $K(\theta)$  for 137-cm Rep. 1 has poor fit over the entire measured range.
- $K(\theta)$  for 137-cm Rep.2 corresponds to  $\theta_s \sim 0.335$ ; air entry/inflection value at  $\psi \sim 0$  cm: Excellent fit with  $K(\theta)$  over the entire measured range.
- $\theta(\psi)$  and  $K(\theta)$  data for 114 cm, 137-cm Rep. 1, and 137-cm Rep. 2 are closely concordant (Fig. D10-2). VG  $\theta(\psi)$  curves calculated using the mean fit parameters fit well. VG  $K(\theta)$  curves calculated using both the mean  $\rho$  ( $\rho=-2.1$ ) for the three samples, fit reasonably well for the  $K(\theta)$  data. VG curve fit for the most common  $\rho$  ( $\rho=0.0001$ ), did not fit well.

Table D10-1. Measured  $\theta(\psi)$  and  $K(\theta)$  determined from laboratory data.

114 cm				137 cm Rep. 1				137 cm Rep. 2			
$K_s=2.17$ cm/h				$K_s=0.65$ cm/h				$K_s=0.25$ cm/h			
$\theta$	$\psi$	$\theta$	$K(\theta)$	$\theta$	$\psi$	$\theta$	$K(\theta)$	$\theta$	$\psi$	$\theta$	$K(\theta)$
	cm		cm/h		cm		cm/h		cm		cm/h
0.3764	0	0.3653	0.033	0.3514	0	0.3509	0.016	0.3385	1	0.3203	0.0059
0.3702	14	0.3608	0.024	0.3435	14	0.3404	0.013	0.3374	14	0.3191	0.0039
0.3526	30	0.3571	0.018	0.3227	30	0.3337	0.013	0.318	30	0.316	0.0033
0.3416	46	0.3541	0.015	0.3238	46	0.3288	0.013	0.3184	46	0.3146	0.0030
0.3347	64	0.3514	0.012	0.3152	64	0.3191	0.010	0.3139	64	0.3109	0.0023
0.3299	80	0.3491	0.010	0.3089	80	0.3129	0.0066	0.3094	80	0.3098	0.0021
0.3216	100	0.3420	0.0061	0.2977	100	0.307	0.0045	0.302	100	0.3052	0.0015
0.3088	140	0.3380	0.0045	0.2832	140	0.3028	0.0034	0.2912	140	0.3002	0.0010
0.2853	200	0.3337	0.0033	0.2523	200	0.2986	0.0025	0.2729	200	0.2974	0.00079
0.2677	330	0.3303	0.0026	0.2356	330	0.2942	0.00188	0.2592	330	0.2945	0.00063
0.2549	500	0.3275	0.0021	0.2158	500	0.2907	0.00148	0.2491	500	0.2917	0.00050
0.2407	800	0.3239	0.0016	0.1988	800	0.2903	0.00144	0.2383	800	0.2599	0.00004
		0.3209	0.0013			0.2899	0.00140			0.2542	0.00002
		0.2966	0.00022			0.2894	0.00136			0.2502	0.00002
		0.2899	0.00015			0.2784	0.00065			0.2487	0.00002
		0.2817	0.00010			0.2678	0.00034			0.246	0.00001
		0.2788	0.00009			0.2619	0.00025			0.2448	0.00001

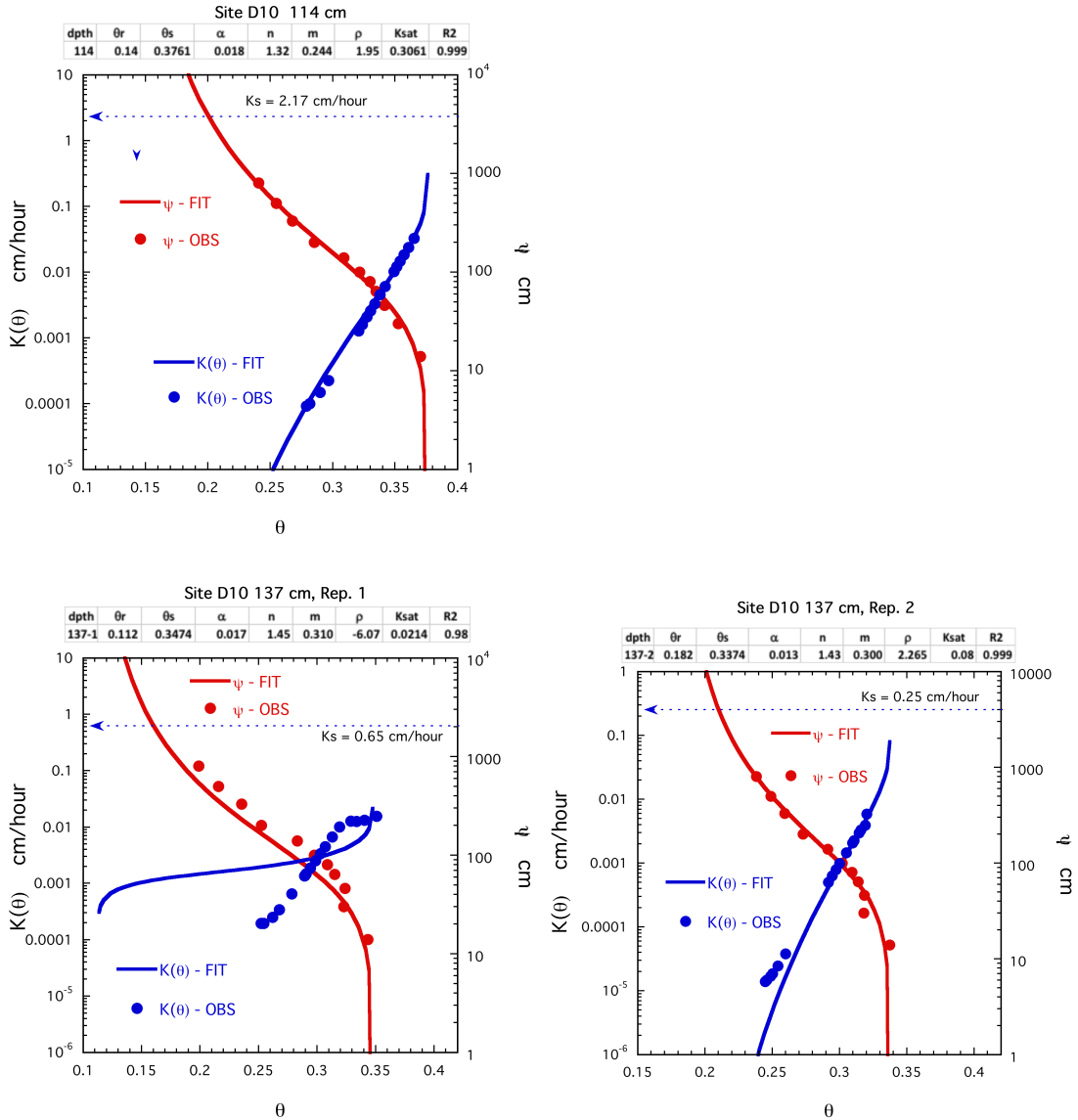


Figure D10-1. Measured laboratory data and fitted VG functions for  $\theta(\psi)$  and  $K(\theta)$ . *Note:  $\psi$  corresponding to  $K(\theta)$  on the graph is determined by first tracking vertically from  $K(\theta)$  (blue curve) to the corresponding  $\theta(\psi)$  curve (red), and then locating (horizontally right) the  $\psi$  value corresponding to that  $\theta$  and  $K(\theta/\psi)$  value.*

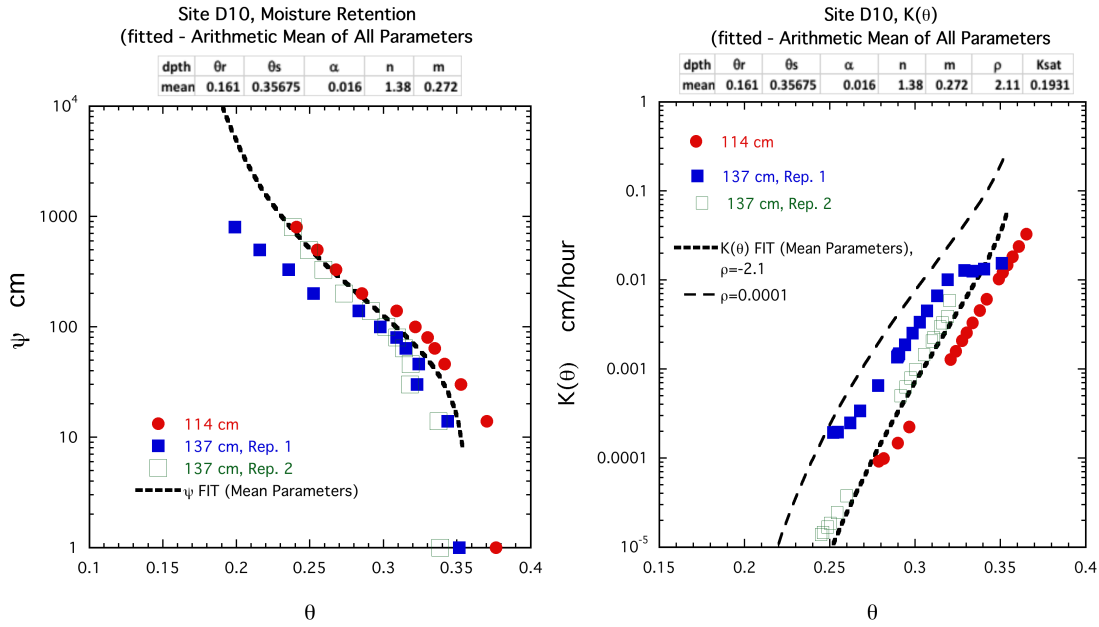


Figure D10-2. Comparison of measured  $\theta(\psi)$  (left): measured  $K(\theta)$  for D10-114 cm, D10-137-cm, Rep. 1, and D10-137-cm, Rep. 2, and fitted VG functions determined using the mean of the VG parameters for the three samples.  $K(\theta)$  is calculated using the mean fitted  $K$ , and mean  $\rho$  ( $\rho = -2.1$ ) parameter for the three depths. Fitted  $K(\theta)$  are also calculated using the most common  $\rho$  ( $\rho = 0.0001$ ).

Site D11. Evaluation Comments, Hydraulic Data, and VG Functions

- All  $\theta(\psi)$  fits are excellent (Figure D11-1).
- $K_s$  for the 114-cm depth corresponds to  $\theta_s \sim 0.335$ , air entry/inflection values at  $\psi \sim 040$  cm: Excellent fit with  $K(\theta)$  over the most of the measured range.
- $K_s$  for the 137-cm Rep. 1 corresponds to  $\theta_s \sim 0.300$ ; air entry/inflection values are  $\psi \sim 55$  cm: Excellent fit with  $K(\theta)$  over the most of the measured range
- $K_s$  for 137-cm Rep. 2 is 0.56 cm/h on the saturated sample, 1 cm/h on the unsaturated measurement (a translation of only 0.44 cm/h).  $K_s=0.56$  cm/h corresponds to  $\theta_s \sim 0.33$ ; air entry/inflection value at  $\psi \sim 60$  cm.  $K_s = 1$  cm/h corresponds to  $\theta_s \sim 0.345$ , and an air entry/inflection value at  $\psi \sim 50$  cm: Excellent fit over the entire measured range.
- Data for  $\theta(\psi)$  at 114 cm, 137-cm Rep. 1, and 137-cm Rep. 2 are closely concordant near saturation; 137-cm Rep. 2 diverges and is somewhat higher with decreasing moisture content (Fig. D11-2). Data for  $K(\theta)$  at 114 cm, 137-cm Rep. 1, and 137-cm Rep. 2 are closely concordant near saturation, but 137-cm samples diverge and are lower than the 114-cm sample with decreasing moisture. The mean parameter  $\theta(\psi)$  VG curve fit well with the three data sets. The mean parameter  $K(\theta)$  VG curves fit well for the mean  $\rho$  ( $\rho=1.383$ ), and reasonably well, particularly in the wet range, for the most common  $\rho$  ( $\rho=0.0001$ ).

Table D11-1. Measured  $\theta(\psi)$  and  $K(\theta)$  determined from laboratory data.

114 cm				137 cm Rep. 1				137 cm Rep. 2			
$K_s=1.25$ cm/h				$K_s=0.58$ cm/h				$K_s=0.56$ cm/h			
$\theta$	$\psi$	$\theta$	$\psi$	$\theta$	$\psi$	$\theta$	$\psi$	$\theta$	$\psi$	$\theta$	$\psi$
	cm		cm		cm		cm		cm		cm
0.3877	0	0.3463	2.26	0.3824	0	0.3371	2.33		0	0.3463	1.16
0.3778	14	0.3151	0.99	0.3731	14	0.3153	1.05	0.35	46	0.3173	0.31
0.3599	30	0.2966	0.58	0.3299	30	0.3023	0.62	0.3321	64	0.3031	0.15
0.3108	46	0.2839	0.38	0.3135	46	0.2936	0.42	0.3128	80	0.2938	0.094
0.2882	64	0.2744	0.28	0.2964	64	0.2872	0.30	0.3042	100	0.287	0.065
0.2644	80	0.2671	0.21	0.2811	80	0.2822	0.24	0.2808	140	0.2818	0.048
0.253	100	0.2611	0.17	0.267	100	0.2782	0.19	0.2569	200	0.2774	0.038
0.2266	140	0.2560	0.14	0.245	140	0.2721	0.13	0.2305	330	0.2738	0.031
0.1919	200	0.2518	0.12	0.2126	200	0.2697	0.12	0.2096	500	0.2707	0.025
0.1599	330	0.2481	0.100	0.1888	330	0.2676	0.10	0.2018	800	0.2679	0.022
0.138	500	0.2420	0.076	0.1731	500	0.2641	0.081			0.2655	0.019
0.1254	800	0.2394	0.068	0.1556	800	0.2627	0.073			0.2633	0.016
		0.2312	0.046			0.2614	0.067			0.2613	0.014
		0.2280	0.039			0.2571	0.049			0.2595	0.013
		0.2207	0.027			0.2511	0.029			0.2579	0.012
		0.2162	0.021			0.2506	0.028			0.2549	0.0096
		0.2103	0.014			0.2501	0.027			0.2524	0.0081
		0.2073	0.012			0.2497	0.026			0.2512	0.0075
		0.202	0.0083			0.2439	0.014			0.2501	0.0070
		0.2017	0.0081			0.2403	0.0093			0.2471	0.0057
		0.2003	0.0073			0.2388	0.0076			0.2462	0.0054
		0.199	0.0066			0.2366	0.0055			0.238	0.0030
		0.1936	0.0043							0.232	0.0020
		0.191	0.0035							0.2254	0.0012
		0.189	0.0029							0.2187	0.00071
		0.1857	0.0021							0.2122	0.00042
		0.1842	0.0018							0.2099	0.00034
		0.1841	0.0018							0.2074	0.00028

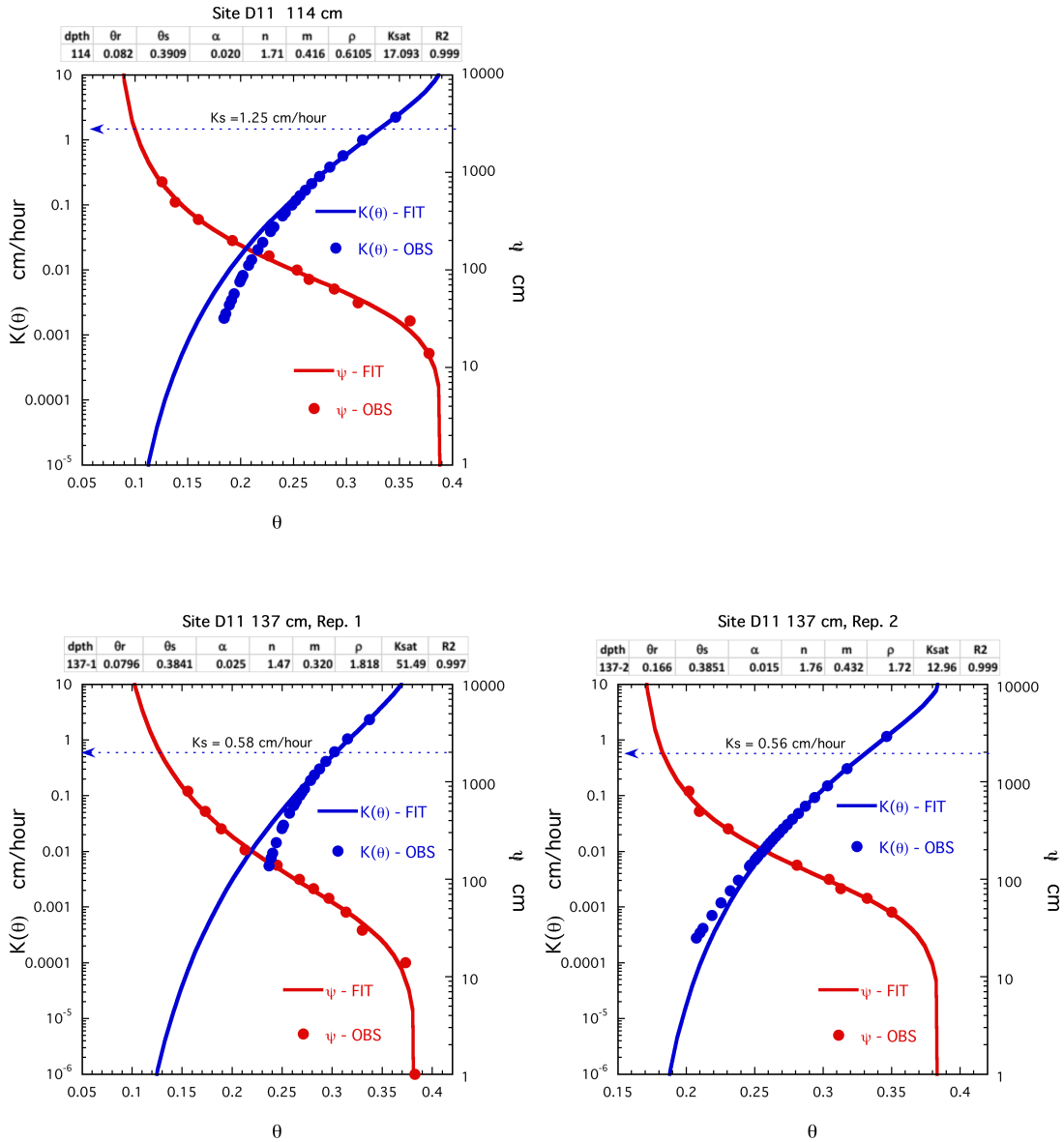


Figure D11-1. Measured laboratory data and fitted VG functions for  $\theta(\psi)$  and  $K(\theta)$ . Note:  $\psi$  corresponding to  $K(\theta)$  on the graph is determined by first tracking vertically from  $K(\theta)$  (blue curve) to the corresponding  $\theta(\psi)$  curve (red), and then locating (horizontally right) the  $\psi$  value corresponding to that  $\theta$  and  $K(\theta/\psi)$  value.

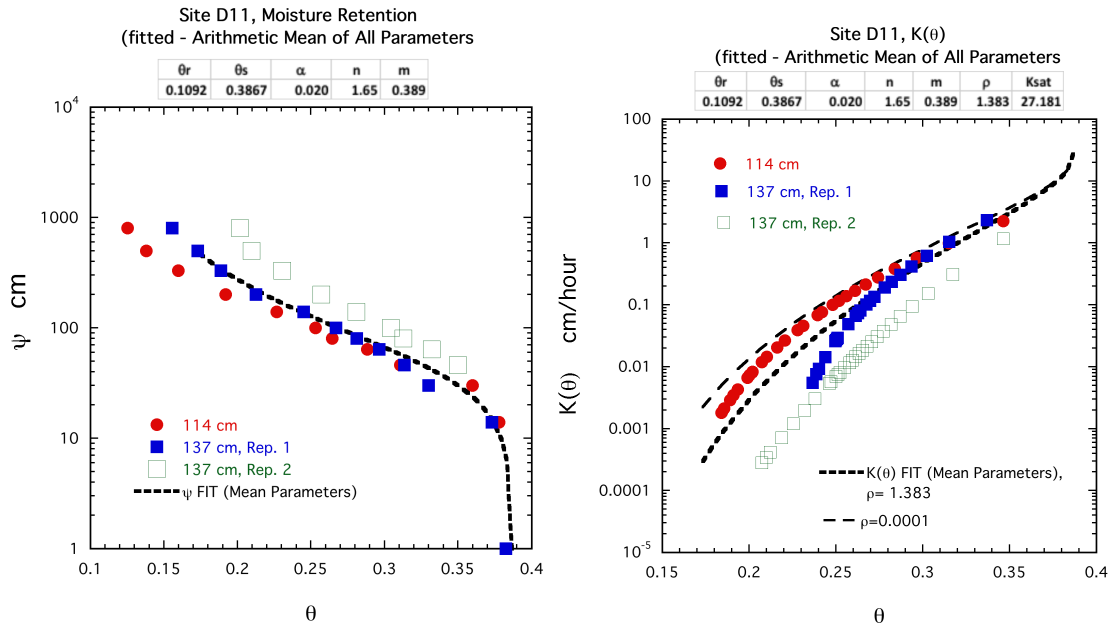


Figure D11-2. Comparison of measured  $\theta(\psi)$  (left): measured  $K(\theta)$  for D11-114 cm, D11-137-cm, Rep. 1, and D11-137-cm, Rep. 2, and fitted VG functions determined using the mean of the VG parameters for the three samples.  $K(\theta)$  is calculated using the mean fitted  $K$ , and mean  $\rho$  parameter for the three depths. Fitted  $K(\theta)$  are also calculated using the most common  $\rho$  ( $\rho = 0.0001$ ).

## **Soil Water-Retention and Unsaturated Soil Hydraulic-Conductivity Parameter: Analysis and Summary**

VG parameters, presented in tabular form and shown visually for each individual site in Sections C3, C4, C5, C6, C7, C8, D6, D7, D8, D9, D10, and D11 above, and an evaluation of their adequacy are summarized on Table 23.

As demonstrated on the previous figures (sites C3 through D11), almost all of the water-retention fits are excellent. Analysis of covariance indicated no differences in  $\theta(\psi)$  VG fit parameters ( $\theta_r$ ,  $\theta_s$ ,  $\alpha$ ,  $m$ ,  $n$ ) between 114-cm and 137-cm (composite sample) depths.

Table 23. VG parameter summary.  $\theta(\psi)$  and  $K(\theta)$  quality are subjective assessments of suitability of fit. Sample C6 Rep. 2 moisture parameters (yellow) are the same as Rep. 1 – used for K fit in both.

Site	Depth	Rep.	$\theta_r$	$\theta_s$	$\alpha$	n	m	$\rho$	Fitted Ks	R2	$\theta(\psi)$ quality	$K(\theta)$ quality
C3	114		0	0.406	0.0441	1.22	0.18	0.0001	22.8	0.995	1	2
C3	137	1	0.1788	0.413	0.0514	1.55	0.355	2.38	26.9	0.963	1	1
C3	137	2	0.1315	0.3851	0.032	1.49	0.329	8.12	247	0.999	1	1
C4	114		0.158	0.372	0.027	1.65	0.394	-2.95	7.05	0.99	1	3
C4	137	1	0.158	0.3724	0.0266	1.65	0.394	-0.623	3.65	0.98	3	2
C4	137	2	0	0.3575	0.023	1.17	0.145	-	-	-	1	N
C5	114		0.119	0.3746	0.024	1.45	0.31	0.0001	7.75	0.99	1	1
C5	137	1	0.093	0.3479	0.018	1.28	0.22	0.0001	4.3	0.96	1	4
C5	137	2	0.0471	0.3554	0.019	1.43	0.301	0.0001	5.51	0.99	1	3
C6	114		0.118	0.3876	0.031	1.52	0.342	-1.12	2.86	0.99	1	3
C6	137	1	0.061	0.3594	0.0325	1.37	0.27	0.0001	11.4	0.99	1	2
C6	137	2	0.061	0.3594	0.0325	1.37	0.27	2.97	16	0.999	1	1
C7	114		0.135	0.4072	0.0327	1.54	0.3506	4.56	8.03	0.996	1	1
C7	137	1	0.072	0.3774	0.04	1.227	0.185	-2.98	11.2	0.999	1	1
C7	137	2	0.086	0.563	0.043	1.17	0.1453	29.07	130	0.999	1	4
C8	114		0	0.4377	0.0166	1.45	0.31	-	-	-	1	N
C8	137	1	0	0.339	0.014	1.3	0.231	-	-	-	1	N
C8	137	2	0.164	0.4035	0.043	1.36	0.2647	0.0001	3.22	0.995	1	2
D10	114		0.14	0.3761	0.018	1.32	0.244	1.95	0.3061	0.999	1	1
D10	137	1	0.112	0.3474	0.017	1.45	0.31	-6.07	0.0214	0.98	2	N
D10	137	2	0.182	0.3374	0.013	1.43	0.3	2.265	0.08	0.999	1	1
D11	114		0.082	0.3909	0.02	1.71	0.416	0.611	17.09	0.999	1	1
D11	137	1	0.0796	0.3841	0.025	1.47	0.32	1.82	51.49	0.997	1	1
D11	137	2	0.166	0.3851	0.015	1.76	0.432	1.72	12.96	0.999	1	1
D6	137	1	0.118	0.524	0.542	1.36	0.265	-	-	-	1	N
D6	137	2	0	0.395	0.950	1.09	0.084	0.0001	597.6	0.75	1	2
D7	114		0.178	0.3293	0.011	1.83	0.453	0.442	0.157	0.999	1	1
D7	137	1	0	0.3673	0.019	1.18	0.153	-1.73	8.79	0.999	1	1
D7	137	2	0.131	0.2993	0.054	1.24	0.196	-3.77	0.17	0.999	1	1
D8	114		0.145	0.3597	0.016	1.48	0.324	-0.185	13.68	0.999	1	1
D8	137	1	0.212	0.388	0.01	2.32	0.57	1.02	0.63	0.99	1	2
D8	137	2	0.117	0.3788	0.024	1.27	0.213	0.0001	1.34	0.87	1	1
D9	114		0.132	0.397	0.016	1.77	0.435	0.0001	6.78	0.999	1	1
D9	137	1	0.155	0.3987	0.044	1.24	0.194	-4.24	13.35	0.999	1	1
D9	137	2	0.104	0.3504	0.011	1.89	4.71	1.591	3.02	0.999	1	1

A statistical summary of VG water-retention parameters is provided on Table 24. Mean and median values are closely correspondent.

Table 24. Statistical summary of the distribution of VG fits for  $\theta(\psi)$  data.

	Depth	N	Mean	Median	Std. Dev	Std. Err	Lower 10th %tile	Upper 10th %tile	Lower 25th %tile	Upper 25th %tile	Min.	Max.
$\theta_r$	114	11	0.1097	0.1320	0.0594	0.0179	0	0.166	0.0910	0.1438	0.0000	0.1780
	137	23	0.1011	0.1120	0.0641	0.0134	0	0.17944	0.0610	0.1573	0.0000	0.2120
$\theta_s$	114	11	0.3853	0.3876	0.0283	0.0085	0.34754	0.4194	0.3727	0.4038	0.3293	0.4377
	137	23	0.3843	0.3774	0.0566	0.0118	0.33868	0.4352	0.3559	0.3933	0.2993	0.5630
n	114	11	1.54	1.52	0.19	0.06	1.28	1.794	1.45	1.70	1.22	1.83
	137	23	1.40	1.36	0.26	0.05	1.17	1.672	1.24	1.47	1.09	2.32
$\alpha$	114	11	0.023	0.020	0.010	0.003	0.014	0.03726	0.016	0.030	0.011	0.044
	137	23	0.091	0.027	0.216	0.045	0.0138	0.1516	0.018	0.043	0.010	0.950

Spearman Rank correlation coefficients are shown on Table 25. Critical value (two-tail) for  $p < 0.05$  is 0.35 and for  $p < 0.1$  0.29,  $df = 32^6$ . Aside from the  $m = 1 - 1/n$  relationship which is trivial,  $\alpha$  is strongly negatively correlated with  $n, m$ , and positively correlated with fitted  $K_s$  and  $\theta_s$ .  $n$  and  $m$  are also strongly correlated with  $\theta_r$ . As suggested by the  $\alpha$  relationship,  $K_s$  and  $\theta_s$  have a strong positive correlation.  $\theta_r$  is strongly correlated only to  $n, m$ . “ $\rho \forall$  for the  $K(\theta)$  fit function is weakly positively correlated only with  $n, m$  and fitted  $\theta_s$ . VG parameters are thus not, in this data set, statistically independent.

<sup>6</sup> Probability analysis for Spearman Rank Correlation from the Wiley Online Library; <http://onlinelibrary.wiley.com/store/10.1002/9781118643624.app2/asset/app2.pdf;jsessionid=67929B364482F4293AAF383A6A86FB8B.f01t03?v=1&t=j6hxxdgr&s=8396b1b7c76957bde34a6dbd22370610dce2400d>, accessed on August 18<sup>th</sup>, 2017.

Table 25. Spearman Rank Correlation values for 34 samples:  $p < 0.05$  (green),  $p < 0.1$  (yellow).

	$\theta_r$	$\theta_s$	$\alpha$	n	m	$\rho$	Ks
$\theta_r$	1						
$\theta_s$	0.055	1					
$\alpha$	-0.16	0.472	1				
n	0.571	-0.006	-0.495	1			
m	0.56	-0.009	-0.49	0.999	1		
$\rho$	0.209	0.292	-0.094	0.305	0.309	1	
Ks	-0.283	0.507	0.517	-0.151	-0.147	0.32	1

A statistical summary of  $\rho$  values is provided on Table 26. Sequential analysis of covariance for  $\rho$  with depth indicates no significant change with depth, adjusted for quality of fit (from Table 23). The median value for the best fits (Group 1) is  $\rho = 0.611$ , very close to Mualem's (1976) empirical value of  $\rho = 0.5$ . Seventy-five percent of the  $\rho$  values in Group 1 are between -0.14 and 2.19. The most common single  $\rho$  value is 0.0001 which occurred in 8 out of 30 (26%) samples. Of these 6 were in Groups 1 and 2, (3 each), and two were poor fits. In Group 2 (six samples), for which  $K(\theta)$  values tend to drift slightly in the drier range, 75% of all Group 2 values are 0.0001. Spearman Rank correlation coefficients (Table 25) indicate that  $\rho$  is weakly ( $p < 0.1$ ) positively correlated only with fitted n, m and  $\theta_s$ .

Table 26. Statistical summary of the distribution of VG fits for the r parameter. Groups (Grp.) are the quality of fit categories from Table 11.

Grp.	N	Mean	Median	Std.Dev	Std. Err	Lower 10th %tile	Upper 10th %tile	Lower 25th %tile	Upper 25th %tile	Min.	Max.
1	19	0.82	0.611	2.90	0.66	-3.45	3.92	-0.14	2.19	-4.24	8.12
2	6	0.07	0.0001	0.53	0.22	-0.56	0.92	0.0001	0.0001	-0.62	1.02
3	3	-1.36	-1.120	1.49	0.86	-2.95	0.0001	-2.49	-0.28	-2.95	0.00
4	2	14.54	14.535	20.56	14.54	0.0001	29.0700	0.0001	29.07	0.00	29.07

**From a practical standpoint, for general modeling using a single function, applying the median values would likely be the best approach.**

### ISOTOPIC INDICATORS OF DENITRIFICATION

In late October of 2004 the SARE-ACE experiment site was dismantled. Monitoring wells were removed and vadose samplers were abandoned. Before dismantling, final nitrate samples were collected from all sites, with one field duplicate. Results of that sampling are shown on Table 27.

Table 27. Final nitrate samples collected on the Carrington SARE-ACE Site on Oct. 26, 2004 by W.M. Schuh and Merlyn Skaley, SWC. Treatments are: B (biological), C (conventional), and I (integrated).

Site	Depth m	Sample Volume mg	Nitrate-N mg/L	Treatment	Isotope Method
101	2	125	3.6639	I	bioassay
101	4	1500	39.5	I	standard
101	6	4000	27.3	I	standard
102	6	3500	0.12	C	bioassay
201	2	250	1.99	B	bioassay
201	4	500	21.5	B	standard
201	6	3500	17.6	B	standard
202	4	1000	32	C	standard
202	6	3000	0.06	C	bioassay
203	2	125	30.4	I	standard
203	4	1000	16.3	I	standard
203	6	3000	7.8	I	standard
301	2	250	2.34	I	bioassay
301	4	1000	18.9	I	standard
301	6	3000	8.3	I	standard
302	6	3000	2.96	B	standard
303	2	500	30.7	C	standard
303	4	1000	18.8	C	standard
303	6	3000	0.54	C	standard
401	2	500	3.9	C	standard
401	4	1000	2.05	C	standard
401	6	3000	0.9	C	standard
403	2	500	54.8	B	standard
403	4	500	14.9	B	standard
403	6	3000	5.79	B	standard

Water samples were sent to the Environmental Isotope Lab at the University of Waterloo, ON, CAN for determination of  $^{18}\text{O}$  and  $^{15}\text{N}$  isotopic composition of the nitrate content. Previous model simulations (Schuh and Klinkbiel, 2003) indicated that nitrate moved to the Carrington aquifer in a manner predicted, but that its retention was shorter than expected. The authors speculated that denitrification was occurring within the aquifer. It was hoped that isotopic status would help to clarify this possibility. Sample volumes and concentrations were used, in consultation with the Waterloo lab, to select samples and methods for isotope analysis.

Some difficulties were encountered with the samples. First, because of limited sample volume due to small amounts extractable in vadose samplers, some  $^{18}\text{O}$  samples could not be determined. Also, desired replication was not possible, so that the laboratory placed the following caveat at the bottom of the table.

*The results for these samples are not as good as we hoped; unfortunately, there is not enough material to do repeats. If you can provide us with more water, we could do repeats*

In addition, a new worker in the lab mistook water samples for glassware that needed cleaning and disposed of the contents, destroying some of the samples before they could be analyzed. Unfortunately, because the samples were collected just before dismantling the site, the lost samples and desired replications were not possible

In addition, as the samples represent a single time and baseline isotopic signatures are unknown for fertilizer input, temporal analysis and denitrification rates cannot be determined.

Available isotope data are provided on Table 28. Information of interest on local denitrification can still be discerned from the available data.

Table 28. Carrington isotope data. <sup>15</sup>N reported as ‰ Mean Atmospheric Nitrogen (MSAN). <sup>18</sup>O reported as ‰ Standard Mean Oceanic Water (SMOW). Results are from University of Waterloo Isotope Lab, April and May, 2015.

Sample	Lab#	<sup>18</sup> O	Result	Repeat	2H	Result	Repeat	<sup>18</sup> O	Result	Repeat	<sup>15</sup> N	Result	Repeat	Corrected	Result	Repeat	Fe	Result
		SMOW						NO3			NO3			DOC				
101-2	105513							X	1.17		X	6.99						
101-4	105514							X	0.58		X	7.46						
101-6	105515							X	1.68		X	8.22	8.1					
102-6	105516							X	Too Low to Run		X	Too Low to Run						
201-2	105517							X	NES		X	NES						
201-4	105518							X	3.27		X	9.27						
201-6	105519							X	3.81		X	9.45	9.58	X	7.98	8.05	X	<0.05 ppm
202-4	105520							X	2.89		X	6.68	6.64					
202-6	105521							X	Too Low to Run		X	Too Low to Run						
203-2	105522							X	Lost		X	Lost - can't repeat						
203-4	105523							X	2.93		X	6.14						
203-6	105524							X	15.41		X	8.12						
301-2	105525							X	4.80		X	3.1						
301-4	105526							X	Coming		X	8.42						
301-6	105527							X	5.46		X	12.91	12.57					
302-6	105528							X	0.82		X	12.56						
303-2	105529							X	1.32		X	6.84						
303-4	105530							X	3.93		X	9.19	8.81					
303-6	105531							X	Too Low to Run		X	Too Low to Run						
401-2	105532							X	0.50		X	9.10						
401-4	105533							X	21.07		X	23.48						
401-6	105534							X	Too Low to Run		X	21.03	20.72					
403-2	105535							X	Lost		X	Lost - can't repeat						
403-4	105536							X	4.07		X	10.41	10.06					
403-6	105537							X	-0.48		X	13.29	12.97					
Subsample from 105515	105538	X	-12.52	-12.72	X	-93.53	-94.36											
Subsample from 105523	105539	X	-13.03	-13.2	X	-96.78	-97.12											

While quantitative changes in nitrate due to denitrification cannot be determined from these data, principles of isotope fractionation can be used to draw some general conclusions. Both  $^{15}\text{N}$  and  $^{18}\text{O}$  undergo what is known as Raleigh distillation (USGS, 2004) during the process of microbial denitrification. It is thermodynamically more favorable and more energy conservative for the microbe to respire lighter ( $^{14}\text{N}$ ,  $^{16}\text{O}$ ) isotopes. The result is that the residual nitrate following denitrification is selectively heavier with respect to isotopic composition, with higher amounts of  $^{15}\text{N}$  and  $^{16}\text{O}$  remaining. If denitrification is occurring as nitrate moves down through the soil profile, we expect to see heavier nitrate with depth.

We will briefly examine isotope composition by proportion of nitrate-N, depth, and treatment.

### $^{15}\text{N}$ and $^{18}\text{O}$ vs. Nitrate-N

Fig. 18 shows that the saturated till water (4 m) and underlying Carrington aquifer (6 m), just below the till boundary, exhibit the same isotopic relationship with nitrate, and that it differs from the shallow vadose (2 m) relationship. Increasing  $^{15}\text{N}$  with decreasing nitrate-N is consistent with denitrification; i.e. as nitrate is lost through denitrification, the result would be LESS residual N, of which a higher residual  $^{15}\text{N}$  composition would be expected.

Data from the two depths, while filling the same relational curve, predominantly fill different nitrate-N ranges which is consistent with our understanding of nitrate movement within the soil-vadose-aquifer column. Solute drains from the root zone to the vadose zone where it tends to collect in dry years. During storms, water drains selectively under microtopographically determined water concentration zones, mobilizing solute beneath the root zone and carrying it to the water table in the till, where it redistributes through diffusion and lateral hydraulic movement and reaches a characteristic background nitrate concentration. During those same large storms, localized hydraulic mounds formed within the till, pushing water and nitrate locally in what we have labeled “hydraulic surges” to the aquifer. The localized pulse of solute, nitrate in this case, then gradually mixes and dilutes. This would result in an isotopic composition similar to the overlying saturated till, but in lower nitrate-N concentrations because of dilution. Near-surface aquifer concentrations of nitrate would approach those of the overlying till in locations underlying surge sites, but would be of lower concentrations later after mixing locally, or underlying sites receiving water redistributing laterally in the aquifer. Both are seen in the aquifer nitrate distribution on this figure.

The  $^{18}\text{O}$  distribution (Fig. 18) is consistent with the  $^{15}\text{N}$  distribution in nearly every aspect, but less clearly so because of less sample data and less representation in the mid-range on the curve. However, it is supportive of the same interpretations as the  $^{15}\text{N}$  indicators. An exception is the 2 m data in which  $^{15}\text{N}$  and  $^{18}\text{O}$  are inverse. Three samples and a very sparse range render the 2-m

data difficult to evaluate, except to note that both isotope distributions are in the lower range, indicating little or no denitrification

The picture we derive from this figure is that denitrification is occurring and substantial. It is occurring mainly in the saturated till, as indicated by the fact that isotopic signature in the aquifer is not perceptibly different from the overlying saturated till from which it receives nitrogen. Nitrate in the vadose zone (2 m) seems to be heavier with greater concentrations, possibly indicating a different dynamic such as more denitrification with more nitrate added, but not much can really be drawn from three samples. The fact that they are generally lighter than the underlying layers supports the inference that denitrification is mainly occurring in the saturated till layer.

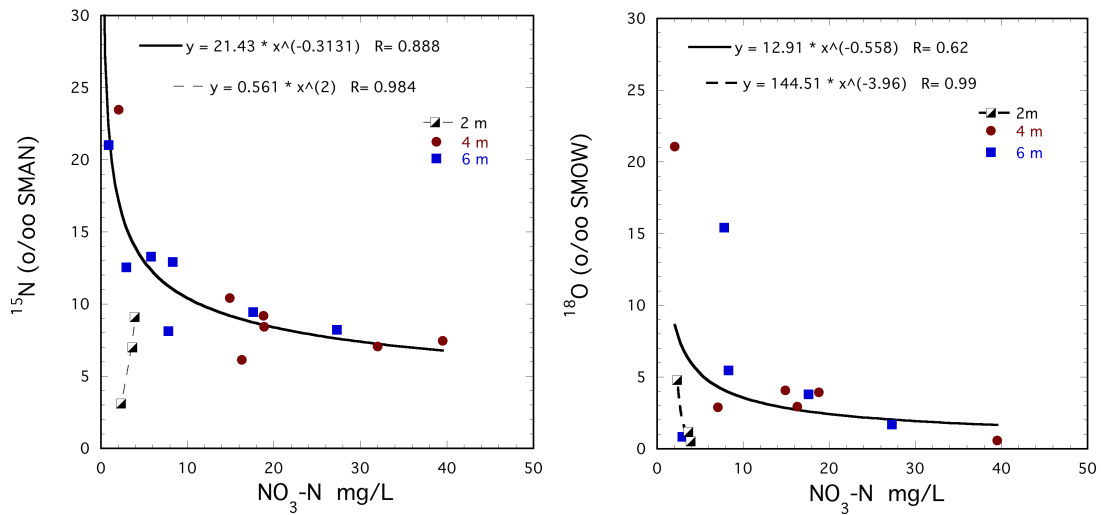


Figure 18. <sup>15</sup>N and <sup>18</sup>N isotope vs. nitrate-N by depth.

### <sup>15</sup>N and <sup>18</sup>O vs. Depth

<sup>15</sup>N isotopes, plotted by individual sites, were heavier with depth (Fig. 19). Three sites represented all three depths and one additional represented two. Indications of somewhat heavier nitrate in the aquifer may indicate that some denitrification is occurring within the aquifer itself, although the similarity of <sup>15</sup>N vs. nitrate distributions (Fig. 18) would suggest that it is minor. The <sup>18</sup>O trends are similar (Fig. 19), except that one site, 301, exhibits decreasing <sup>18</sup>O from 2 m to 6 m. Generally, heavier nitrate with depth is indicative that denitrification is occurring progressively as nitrate moves more deeply into the till and the aquifer.

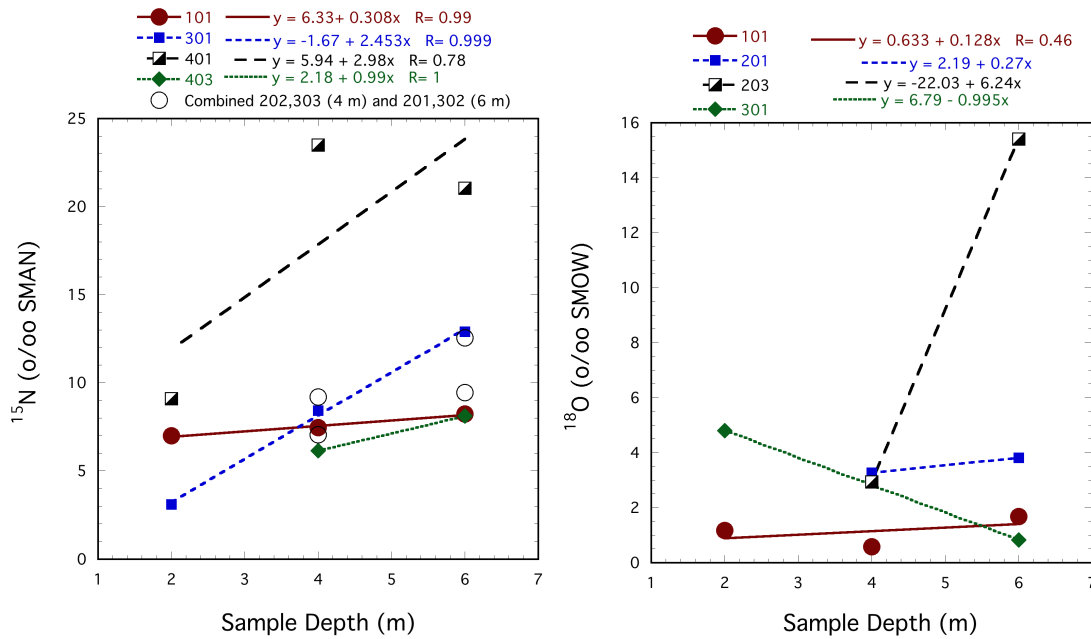


Figure 19. <sup>15</sup>N and <sup>18</sup>O vs. depth by individual treatment site.

### <sup>15</sup>N and <sup>18</sup>O vs. Nitrate-N by Treatment

<sup>15</sup>N isotopes, plotted vs. Nitrate-N by plot treatments are shown (Fig. 20). The Integrated treatment plots, which consisted mainly of green manure N, with some fertilizer supplements (Schuh and Klinkebiel, 2003) showed no identifiable isotopic trends indicative of denitrification. The Conventional treatment plots (conventional N applications and tillage) and Biological Treatment plots, both individually (not shown) and combined (Fig. 20) showed <sup>15</sup>N decreasing as a power function of nitrate-N in a relationship very similar to the separation by depth (Fig. 18 above), indicative of denitrification. <sup>18</sup>O isotope trends were not discernible.

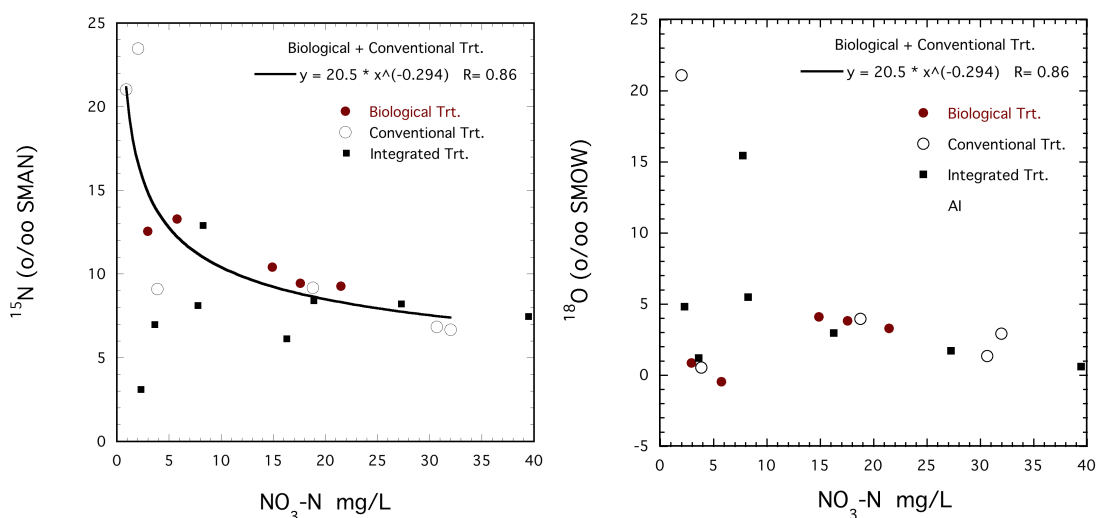


Figure 20. <sup>15</sup>N and <sup>18</sup>O vs nitrate-N by Treatment.

### Denitrification Conclusions

Isotopic distributions (heavier isotopes with lower nitrate concentrations) indicate denitrification activity on the Carrington SARE-ACE sites. <sup>15</sup>N and <sup>18</sup>O vs. nitrate-N trends indicate that little denitrification is occurring in the vadose zone (2 m), with most occurring in the saturated till at about 4 m, and some (heavier with depth) likely continuing to occur in the upper aquifer below the till boundary, although the similarity of till and aquifer isotope vs. nitrate-N trends for both the saturated till and the aquifer, indicate that most denitrification likely occurs before it reaches the aquifer. Denitrification in groundwater was not indicated for the Integrated field treatment, which would have resulted in slow field release of nitrogen from plant sources. The Conventional and Biological Treatments both exhibited groundwater denitrification with similar trends in relation to nitrate-N concentrations: i.e. N heavier with decreasing nitrate-N, according to the same power function.



## CITATIONS

- Brooks, R. H., and A. T. Corey. 1964. Hydraulic properties of porous media. Hydrology Paper No. 3, Colorado State Univ., Fort Collins, Colorado. 27 pp.
- Burdine, N. T. 1953. Relative permeability calculations from pore-size distribution data. *Petrol. Trans., Am. Inst. Min. Eng.* 198:71-77.
- Doering, E.J. 1965. Soil-water diffusivity by the one-step method. *Soil Sci.* 99:5:322-326.
- Green, R.E., and J.C. Corey. 1971. Calculation of hydraulic conductivity: a further evaluation of some predictive methods. *Soil Sci. Soc. Am. Proc.* 35:3-8.
- Hillel, D., V.D. Krentos, and YU. Stylianou. 1972. Procedure and test of an internal drainage method for measuring soil hydraulic characteristics in situ. *Soil Sci.* 114:395-400.
- Kendall, Carol. 2004. Resources on Isotopes. U.S. Geological Survey. <https://wwwrcamnl.wr.usgs.gov/isoig/res/funda.html>. Last changed Jan. 2004. Accessed August 29, 2017 by W.M.S., North Dakota State Water Commission.
- Klinkebiel, D.L., W.M. Schuh, and B.D. Seelig. 1994. Report of the Carrington CARE-Ace experiment, 1992-1993: I. Influence of agricultural management practices on agronomic parameters. NDSU Carrington Research Extension Center, Carrington, N.D.
- Klute, A. 1965a. Water retentivity of soils at specified values of matric suction: In (Ed.) C.A. Black: *Methods of soil analysis, Part 1. Agronomy 9.* American Society of Agronomy, Madison WI. pp. 129-137.
- Klute, A. 1965b. Laboratory measurement of hydraulic conductivity of a saturated soil. In (Ed.) C.A. Black: *Methods of soil analysis, Part 1. Agronomy No. 9.* American Society of Agronomy, Madison WI. pp. 210-220.
- Marshall, T.J. 1958. A relation between permeability and size distribution of pores. *J. Soil Sci.* 9:1-8.
- Millington, R.J., and J.P. Quirk. 1961. Permeability of porous solids. *Trans. Faraday Soc.* 57:1200-1207.
- Mualem, Y. 1976. A new model for predicting the hydraulic conductivity of unsaturated porous media. *Water Resour. Res.* 12:513-522.
- Philip, J.R. 1966. Sorption and infiltration in heterogeneous media. *Aust. J. Soil Res.* 5, 1-10.

Rose, C.W., W.R. Stern, and J.E. Drummond. 1965. Determination of hydraulic conductivity as a function of depth and water content for soil in situ. *Aust. J. Soil Res.* 3:1-9.

Schuh, W.M. 1987. Apparatus for extraction of undisturbed samples on noncohesive subsoils. *Soil Sci. Soc. Am. J.*, 51:6:1678-1679.

Schuh, W.M., and R.L. Cline. 1991a. Effect of Soil Properties on Unsaturated Hydraulic Conductivity Pore-Interaction Factors. *Soil Sci. Soc. Am. J.*, 54:6:1509-1519. doi:10.2136/sssaj1990.03615995005400060001x.

Schuh, W.M., R.L. Cline, and M.D. Sweeney. 1991b. Unsaturated soil hydraulic properties and parameters for the Oakes area, Dickey County, North Dakota. Water Resources Investigations No. 18. North Dakota State Water Commission. Bismarck, ND. 343 pp. [http://www.swc.nd.gov/info\\_edu/reports\\_and\\_publications/pdfs/wr\\_investigations/wr18\\_report.pdf](http://www.swc.nd.gov/info_edu/reports_and_publications/pdfs/wr_investigations/wr18_report.pdf). Accessed Sept. 12, 2017.

Schuh, W.M., R.F. Meyer, M.D. Sweeney, and J.C. Gardner. 1993a. Spatial variation of root-zone and shallow vadose-zone drainage on a loamy glacial till in a sub-humid climate. *J. Hydrol.* 148:1-4:1-26. [https://doi.org/10.1016/0022-1694\(93\)90251-4](https://doi.org/10.1016/0022-1694(93)90251-4).

Schuh, W.M., D.L. Klinkebiel and J.C. Gardner. 1993b. Use of an integrated transient flow and water budget procedure to predict and partition components of local recharge. *J. Hydrol.* 148:1-4:27-60. [https://doi.org/10.1016/0022-1694\(93\)90252-5](https://doi.org/10.1016/0022-1694(93)90252-5).

Schuh, W.M., D.L. Klinkebiel, and B.D. Seelig. 1994. Report of the Carrington SARE-ACE experiment, 1992-1993: II. Effect of agricultural management practices on ground-water quality. NDSU Carrington Research Extension Center, Carrington, N.D.

Schuh, W.M., Klinkebiel, D.L., J.C. Gardner, and R.F. Meyer. 1997. Tracer and nitrate movement to groundwater in the Northern Great Plains. *J. Environ. Qual.* 26(5), 1335-1347.

Schuh, W. M., and Klinkebiel, D. L. (2003). Effects of microtopographically concentrated recharge on nitrate variability in a confined aquifer: Model simulations. *Nat. Resour. Res.*, 12(4), 257-272. DOI: 10.1023/B:NARR.0000007805.12546.13.

Schuh, W.M., and D.L. Klinkebiel. 2004. Hydraulic effects of crop management systems on nitrate variability in a confined aquifer. *Nat. Resour. Res.* 1:13:29-43.

Schuh, W.M., R.L. Cline, and M.D. Sweeney. 2005. Infiltration data and functions, and soil moisture and matric potential data during wetting for selected soils in the Oakes area, Dickey County, North

Dakota. Water Resources Investigations No. 18A. North Dakota State Water Commission. Bismarck, ND. 153 pp.  
[http://www.swc.nd.gov/info\\_edu/reports\\_and\\_publications/pdfs/wr\\_investigations/wr18a\\_report.pdf](http://www.swc.nd.gov/info_edu/reports_and_publications/pdfs/wr_investigations/wr18a_report.pdf). Accessed Sept. 12, 2017.

Van Genuchten, M. Th. 1980. A closed-form equation for predicting the hydraulic conductivity of unsaturated soils. Soil Sci Soc. Am J. 44:892-898.

Van Genuchten, M. Th., F.G. Leij, and S.R. Yates. Dec. 1991. The RETC code for quantifying the hydraulic functions of unsaturated soils. EPA/600/2-91/065. U.S. Salinity Laboratory, USDA-ARS, Riverside, CA. Van Genuchten, M. Th., F.G. Leij, and S.R. Yates. Dec. 1991. <https://www.pc-progress.com/Documents/programs/retc.pdf>, accessed July 28, 2017.



Lab #'s: 10021-10048.

Project: Carrington Proj.

Soil-ID	LAB #	Horiz.	DT	DB	USDA TEXT. NIDP CLASS	Size Class and Particle Diameter (microns)										
						VCOS 2000- 1000	CCS 1000- 500	MS 500- 250	FS 250- 100	VFS 100- 50	SAND 2000- 50	SILT 50- 2	CLAY < 2	FSI 20- 2	OSI 50- 20	CS-C < 2
(PERCENT)																
NW	10021	A	0	6	3.0 L	0.7	3.7	7.3	13.0	11.1	36.0	49.8	15.2	24.2	24.7	0.0
NW	10022	A	6	12	9.0 SIL	0.6	3.1	6.4	11.1	10.1	31.3	52.6	16.1	22.7	29.9	0.0
NW	10023	B	12	16	14.2 SIL	0.3	2.3	4.5	8.4	9.8	25.3	60.0	14.8	23.0	35.0	0.0
NW	10024	CK	16	29	22.4 L	1.0	2.0	4.2	8.5	10.0	25.7	49.8	24.5	20.6	29.2	11.3
NW	10025	C1	29	49	38.5 FSL	5.1	6.1	10.4	19.5	13.4	54.5	37.6	7.9	18.6	19.1	0.8
NW	10026	C2	49	62	55.3 FSL	4.4	5.5	12.9	24.0	14.0	60.7	33.3	6.1	16.0	17.2	0.0
NW	10027	C3	62	71	66.5 L	2.9	3.5	7.3	17.3	14.3	45.4	37.9	16.6	17.9	20.0	0.0
NW	10028	C4	71	78	74.3 L	3.1	3.9	7.5	19.3	16.4	50.2	36.4	13.4	19.7	17.7	0.0
NW	10029	C5	78	85	81.0 L	1.3	1.6	3.0	9.0	27.4	42.3	49.7	7.9	16.5	33.2	0.0
NW	10030	C6	85	96	90.3 L	2.6	3.3	6.0	14.9	16.0	42.8	38.8	18.4	20.4	18.4	0.0
NW	10031	C7	96	110	102.8 L	1.5	2.5	4.9	19.1	22.5	50.6	39.7	9.7	19.3	20.4	0.0
NE	10032	A	0	12	6.0 SIL	1.4	3.6	7.1	11.8	10.4	34.2	50.8	15.0	21.6	29.2	0.0
NE	10033	B	12	21	16.3 SIL	1.0	2.0	4.1	6.6	8.8	22.5	57.9	19.6	22.7	35.2	0.0
NE	10034	C	21	33	26.8 SIL	1.6	3.5	4.3	6.2	11.4	27.0	56.5	16.5	22.5	34.0	7.0
NE	10035	C1	33	51	41.8 SL	11.3	10.3	13.2	15.4	8.2	58.6	33.3	8.2	17.0	16.3	0.0
NE	10036	C2	51	68	59.3 FSL	2.1	5.2	17.2	29.8	14.1	68.4	29.5	2.0	11.8	17.8	0.0
NE	10037	C3	68	84	76.0 FSL	4.0	3.6	11.9	21.8	13.9	57.0	32.9	18.1	16.8	16.1	0.0
NE	10038	C4	84	97	90.3 L	2.4	4.0	6.8	15.8	14.6	43.5	39.3	17.2	22.1	17.2	0.0
SE	10039	A	6	12	9.0 SIL	1.9	3.7	6.9	11.8	10.6	34.9	51.4	13.7	23.1	28.3	0.0
SE	10040	B	14	20	16.8 SIL	1.7	2.7	4.7	7.4	10.2	26.6	58.3	15.2	23.9	34.4	0.0
SE	10041	CK	20	31	25.5 SL	18.1	8.4	7.3	9.9	9.5	53.1	34.2	12.7	11.8	22.4	0.8
SE	10042	C1	31	36	33.5 FSL	2.4	7.5	13.2	24.3	15.4	62.8	35.7	1.5	13.7	22.0	0.0
SE	10043	C1	31	48	39.3 FSL	6.7	7.8	12.7	22.2	12.7	62.1	35.1	2.8	15.7	19.4	0.0
SE	10044	C2	52	72	62.0 FSL	1.2	2.3	8.5	29.4	19.8	61.3	33.0	5.7	12.9	20.1	0.0
SE	10045	C3	72	78	75.0 FSL	1.8	3.8	10.5	25.3	14.9	56.2	31.8	11.9	11.0	20.9	0.0
SE	10046	C4	78	90	83.8 LS	1.1	3.4	12.9	42.4	20.3	80.1	19.6	0.2	9.4	10.3	0.0
SE	10047	C5	90	93	91.3 L	3.1	3.5	6.5	16.4	15.1	44.5	34.7	20.9	16.2	18.4	0.0
SE	10048	C6	94	106	100.0 L	2.2	2.9	6.1	16.0	16.5	43.7	43.2	13.1	20.6	22.6	0.0

APPENDIX A-1: Soil Particle Size, Texture, Organic Carbon, Specific Conductance, and 15-Bar Gravimetric Water Content for Recharge Experiment Sites - NW, NE, and SE Hydraulic Measurement Sites.

Lab #s: 10021-10048,  
Project: Carrington Proj.

WALKEY-BLACK  
ORGANIC CARBON ANALYSES

Soil-ID	LAB #	Horiz.	DT	DB	KIDP in	MB-C,C, -%	Tot-OC -%	D.M. -%
NW	10021	A	0	5	3.0	1.57	2.06	3.55
NW	10022	A	6	12	9.0	1.52	1.98	3.42
NW	10023	B	12	15	14.2	1.01	1.31	2.25
NW	10024	CK	16	29	22.4	0.47	0.61	1.05
NW	10025	C1	29	49	38.5	0.18	0.24	0.41
NW	10026	C2	49	62	55.3	0.24	0.31	0.54
NW	10027	C3	62	71	65.5	0.52	0.67	1.16
NW	10028	C4	71	78	74.3	0.18	0.24	0.41
NW	10029	C5	78	85	81.0	0.09	0.12	0.20
NW	10030	C6	85	96	90.3	0.18	0.24	0.41
NW	10031	C7	96	110	102.8	0.21	0.28	0.48
NE	10032	A	0	12	6.0	1.58	2.02	3.49
NE	10033	B	12	21	16.3	1.01	1.31	2.26
NE	10034	C	21	33	25.8	0.46	0.59	1.02
NE	10035	C1	33	51	41.8	0.17	0.22	0.37
NE	10036	C2	51	68	59.3	0.17	0.22	0.37
NE	10037	C3	68	84	76.0	0.18	0.24	0.41
NE	10038	C4	84	97	90.3	0.21	0.28	0.48
SE	10039	A	3	12	9.0	0.78	0.99	1.71
SE	10040	B	14	20	16.8	0.94	1.23	2.12
SE	10041	CK	20	31	25.5	0.82	1.06	1.83
SE	10042	C1	31	36	33.5	0.17	0.22	0.37
SE	10043	C2	31	43	39.3	0.09	0.12	0.20
SE	10044	C2	52	72	62.0	0.17	0.14	0.24
SE	10045	C3	72	78	75.0	0.09	0.10	0.17
SE	10046	C4	78	90	83.8	0.09	0.09	0.09
SE	10047	C5	90	93	91.3	0.09	0.09	0.09
SE	10048	C6	94	106	100.0	0.00	0.00	0.00

APPENDIX A-1: Soil Particle Size, Texture, Organic Carbon, Specific Conductance, and 15-Bar Gravimetric Water Content for Recharge Experiment Sites - NW, NE, and SE Hydraulic Measurement Sites.

Lab #'s: 10021-10048.  
 Project: Carrington Proj.

Soil-ID	LAB #	Horiz.	DT	DS	MISF in	pHse	pH:1	ECse -dS/m-	EC1:1 -dS/m-	15-bar H2O -%
NW	10021	A	0	6	3.0	8.1		891		10.35
NW	10022	A	6	12	9.0	8.1	8.1	1108	656	11.19
NW	10023	B	12	16	14.2	8.1		663		5.15
NW	10024	CK	16	29	22.4	8.3	8.3	602	426	8.05
NW	10025	C1	29	49	38.5	8.2	8.2	792	317	4.42
NW	10026	C2	49	62	55.3	8.1	8.1	682	332	7.01
NW	10027	C3	62	71	66.5	8.3	8.2	1069	542	8.76
NW	10028	C4	71	78	74.3	8.3	8.3	1525	593	7.57
NW	10029	C5	78	85	81.0	8.4	8.4	1629	697	6.44
NW	10030	C6	85	96	90.3	8.2	8.1	1108	629	9.68
NW	10031	C7	96	119	102.8	8.2	8.1	1383	607	5.57
NE	10032	A	0	12	6.0	8.0	7.7	1108	598	10.41
NE	10033	B	12	21	14.3	8.4	8.4	890	554	11.51
NE	10034	C	21	33	26.6	8.6	8.3	798	507	7.32
NE	10035	C1	33	51	41.8	8.1		919		4.45
NE	10036	C2	51	69	59.7	8.2	8.2	658	294	2.76
NE	10037	C3	69	69	76.0	8.4	8.4	809	366	6.80
NE	10038	C4	84	97	90.3	8.0	8.0	631	399	9.51
SE	10039	A	6	12	9.0	8.1		1179		11.61
SE	10040	B	14	20	16.8	8.1	8.0	943	519	9.04
SE	10041	CK	20	31	25.5	8.2		672		5.75
SE	10042	C1	31	36	33.5	8.3		653		3.29
SE	10043	C1	31	48	39.3	8.3	8.1	613	322	2.73
SE	10044	C2	52	72	62.0	8.6	8.6	554	297	5.01
SE	10045	C3	72	78	75.0	8.2		731		6.83
SE	10046	C4	78	90	83.8	8.4		530		2.46
SE	10047	C5	90	93	91.3	8.6	8.4	590	326	9.68
SE	10048	C6	94	106	100.0	8.5	8.4	624	384	7.90

APPENDIX A-1: Soil Particle Size, Texture, Organic Carbon, Specific Conductance, and 15-Bar Gravimetric Water Content for Recharge Experiment Sites - NW, NE, and SE Hydraulic Measurement Sites.

Lab # s: 48-77  
 Project: M.Sweeney-Carrington Project

Soil-ID	LAB #	Horiz.	DT	DB	TEXT. MIDP CLASS in	USDA Size Class and Particle Diameter (microns)										
						WCSS 2000- 1000	CS 1000- 500	MS 500- 250	FS 250- 100	VFS 100- 50	SAND 2000- 50	SILT 50- 2	CLAY < 2	FSI 20- 2	CEC 50- 20	OC-C < 2
(PERCENT)																
103	48		0	3	1.5 L	1.2	3.1	6.9	14.1	12.9	38.0	47.1	14.7	19.2	27.3	0.0
	49		3	6	4.5 SiL	1.7	3.0	7.0	13.8	12.6	38.3	51.4	10.4	23.3	28.1	0.0
	50		6	12	9.0 SiL	0.8	2.3	5.5	12.7	13.3	34.7	51.3	14.1	19.5	31.8	0.0
	51		12	24	18.0 L	2.2	3.6	8.2	16.0	14.0	44.0	44.4	11.6	19.5	24.9	1.7
	52		24	48	36.0 L	3.5	4.4	8.2	17.0	14.7	48.1	40.9	11.0	17.3	23.6	3.3
104	53		0	3	1.5 L	1.5	2.7	5.6	12.0	13.0	34.8	48.7	16.5	17.8	28.9	0.0
	54		3	6	4.5 L	2.1	2.8	5.4	11.2	11.4	32.8	48.3	18.9	18.8	31.5	0.8
	55		6	12	9.0 SiL	0.7	1.9	3.8	8.9	10.8	26.2	58.1	15.7	23.6	34.5	0.8
	56		12	24	18.0 SiL	1.2	1.8	4.9	11.4	14.8	34.1	51.5	14.4	22.9	28.6	1.6
	57		24	48	36.0 L	1.9	3.5	7.1	14.7	12.2	39.4	39.4	21.2	19.9	19.6	5.0
103	58		0	3	1.5 SiL	1.7	3.1	6.1	11.1	11.5	33.4	50.9	15.6	25.6	25.3	0.0
	59		3	6	4.5 SiL	1.1	2.6	5.5	10.7	11.9	31.7	51.7	16.5	21.0	20.7	0.0
	60		6	12	9.0 SiL	0.7	1.7	4.3	8.8	10.0	25.6	57.3	17.0	26.2	31.1	0.0
	61		12	24	18.0 SiL	0.7	2.0	4.2	9.0	11.6	27.5	56.2	13.3	23.8	35.4	0.0
	62		24	48	36.0 L	1.6	3.5	8.2	18.2	15.7	47.1	40.9	12.0	17.6	23.2	0.0
302	63		0	3	1.5 L	2.4	7.3	6.6	15.7	13.4	41.4	44.0	14.6	20.8	23.2	0.0
	64		3	6	4.5 L	1.8	3.9	7.1	15.4	12.6	40.7	44.4	14.8	18.8	25.7	0.0
	65		6	12	9.0 SiL	0.9	2.3	5.2	13.3	12.8	34.5	50.1	15.3	23.6	26.5	0.8
	66		12	24	18.0 SiL	0.9	2.5	5.5	12.8	12.3	34.0	54.0	12.0	24.0	30.0	0.8
	67		24	48	36.0 L	1.9	3.7	8.2	21.3	16.5	51.6	41.2	7.2	18.3	22.9	0.0
304	68		0	3	1.5 L	9.4	3.2	6.6	12.9	11.0	34.2	49.8	16.0	26.9	22.9	0.0
	69		3	6	4.5 SiL	0.7	2.9	6.5	11.8	11.3	33.2	51.6	15.2	26.4	25.2	0.0
	70		6	12	9.0 SiL	0.9	3.0	6.4	11.0	8.6	29.9	54.5	15.6	26.3	28.1	0.9
	71		12	24	18.0 SiL	0.6	2.9	5.9	9.3	7.7	26.4	56.7	16.9	22.6	34.0	0.0
	72		24	48	36.0 L	3.3	4.3	8.5	15.7	12.1	44.0	48.9	7.1	21.5	27.4	0.0
311	73		0	3	1.5 L	1.1	3.3	7.2	15.7	14.0	41.4	43.7	14.9	15.4	28.3	0.0
	74		3	6	4.5 L	3.3	3.9	7.2	14.6	12.5	41.4	46.2	12.3	18.1	28.1	0.0
	75		6	12	9.0 SiL	1.7	3.2	6.8	13.1	12.0	36.7	51.8	11.5	20.2	31.6	0.0
	76		12	24	18.0 L	2.3	3.3	7.0	12.9	12.2	37.8	49.9	12.3	18.0	31.9	0.0
	77		24	48	36.0 L	3.0	5.2	10.0	16.9	15.2	50.2	39.4	10.4	18.2	21.2	0.0

APPENDIX A-2: Soil Particle Size, Texture, Organic Carbon, Specific Conductance, and 15-Bar Gravimetric Water Content for Recharge Experiment Sites - Vadose Sampler Sites.

Lab #'s: 48-77		WALKER-BLACK						SATURATION EXTRACT			
Project: M.Sweeney-Carrington Project		ORGANIC CARBON ANALYSES						DATA			
Soil-ID	LAB #	Horiz.	DT	DB	MIDP	WB-O.C.	Tot-OC	O.M.	S.P.	pH	EC
					in	%	%	%	%		dS/m-1
103	48		0	3	1.5	1.03	1.34	2.31	33	7.1	1.04
	49		3	6	4.5	1.00	1.30	2.24	38	6.7	0.68
	50		6	12	9.0	0.97	1.26	2.17	40	7.3	0.88
	51		12	24	18.0				34	8.1	0.90
	52		24	48	36.0				30	8.1	0.62
104	53		0	3	1.5	1.31	1.70	2.93	42	6.6	1.03
	54		3	6	4.5	1.21	1.58	2.72	40	6.4	0.67
	55		6	12	9.0	1.00	1.30	2.25	41	7.6	0.66
	56		12	24	18.0				39	7.7	1.13
	57		24	48	36.0				37	8.1	1.11
109	58		0	3	1.5	1.55	2.01	3.47	43	6.8	1.02
	59		3	6	4.5	1.49	1.94	3.34	42	6.2	0.66
	60		6	12	9.0	0.91	1.19	2.04	42	7.1	0.57
	61		12	24	18.0				40	6.9	0.51
	62		24	48	36.0				35	7.9	0.79
302	63		0	3	1.5	1.50	1.97	3.40	44	7.1	1.33
	64		3	6	4.5	1.45	1.97	3.27	45	7.2	1.30
	65		6	12	9.0	0.88	1.14	1.97	42	7.6	1.13
	66		12	24	18.0				39	7.5	1.13
	67		24	48	36.0				30	7.9	0.92
304	68		0	3	1.5	1.67	2.18	3.75	47	6.5	0.79
	69		3	6	4.5	1.47	1.94	3.34	47	6.2	0.60
	70		6	12	9.0	0.76	0.99	1.70	41	6.4	0.55
	71		12	24	18.0				42	7.1	0.48
	72		24	48	36.0				36	7.6	0.89
311	73		0	3	1.5	1.40	1.82	3.13	41	7.1	1.14
	74		3	6	4.5	1.52	1.97	3.40	42	6.6	0.74
	75		6	12	9.0	0.97	1.26	2.18	42	6.8	0.62
	76		12	24	18.0				40	8.0	0.79
	77		24	48	36.0				33	7.9	0.62

APPENDIX A-2: Soil Particle Size, Texture, Organic Carbon, Specific Conductance, and 15-Bar Gravimetric Water Content for Recharge Experiment Sites - Vadose Sampler Sites.



APPENDIX B: SARE-ACE LABORATORY WATER RETENTION DATA FOR EACH CORE SAMPLE

Table B-1. Water retention and bulk data for each individual core sample for the SARE-ACE experiment.

Ident	depth cm	subsample	sample	Site	$\psi$ cm	0	14	30	46	64	80	100	140	200	330	500	800	BD
						cm	cm											
107	107	1	1	C3		0.3649	0.3247	0.3143	0.2741	0.2651	0.2487	0.2353	0.2189	0.1936	0.1683	0.1475	0.1281	1.62
107	107	2	1	C3		0.3843	0.3783	0.3768	0.2755	0.2681	0.2502	0.2458	0.2294	0.2041	0.1832	0.1698	0.1549	1.58
122	122	1	1	C3		0.4304	0.4185	0.3843	0.3545	0.3411	0.3307	0.3262	0.3143	0.3009	0.283	0.2681	0.2621	1.57
122	122	2	1	C3		0.4334	0.4245	0.3977	0.3724	0.3575	0.347	0.3411	0.3307	0.3172	0.3024	0.283	0.2651	1.48
122-2	122	1	2	C3		0.3813	0.3664	0.3664	0.3024	0.283	0.2621	0.2502	0.2324	0.213	0.1743	0.1549	0.137	1.69
122-2	122	2	2	C3		0.3917	0.3753	0.3753	0.2919	0.2726	0.2547	0.2458	0.2324	0.207	0.1847	0.1698	0.1579	1.57
152-1	152	1	1	C3		0.3917	0.3426	0.3217	0.2904	0.277	0.2621	0.2577	0.2458	0.2338	0.216	0.2041	0.1921	1.52
152-1	152	2	1	C3		0.4468	0.3887	0.2949	0.2338	0.2204	0.2085	0.2026	0.1877	0.1758	0.1534	0.146	0.134	1.4
152-1	152	1	2	C3		0.3485	0.347	0.2904	0.2741	0.2606	0.2502	0.2398	0.2279	0.2085	0.1936	0.1802	0.1698	1.67
152-2	152	2	2	C3		0.3738	0.3575	0.2919	0.286	0.2755	0.2666	0.2577	0.2472	0.2234	0.2055	0.1906	0.1698	1.63
152-2	152	3	2	C3		0.3798	0.3738	0.3381	0.3366	0.3277	0.3247	0.3187	0.3098	0.2904	0.2815	0.2711	0.2562	1.86
107-1	107	1	2	C4		0.3798	0.3619	0.3575	0.2994	0.2755	0.2502	0.2353	0.2145	0.1996	0.1728	0.1564	0.14	1.7
107-1	107	2	2	C4		0.4096	0.3902	0.3887	0.2919	0.2666	0.2487	0.2353	0.2175	0.21	0.1832	0.1817	0.1594	1.52
107-2	107	1	3	C4		0.3753	0.356	0.3485	0.2621	0.2353	0.21	0.1981	0.1802	0.1519	0.1236	0.1102	0.0909	1.54
107-2	107	2	3	C4		0.3455	0.3366	0.3366	0.2785	0.2577	0.2398	0.2279	0.213	0.1832	0.1564	0.1385	0.1221	1.64
122-1	122	1	3	C4		0.347	0.347	0.3321	0.3336	0.3292	0.3277	0.3232	0.3172	0.3024	0.2919	0.283	0.2741	1.84
122-1	122	2	3	C4		0.3753	0.3515	0.3455	0.3411	0.3336	0.3262	0.3217	0.3143	0.3053	0.2904	0.2815	0.2681	1.92
122-2	122	1	4	C4		0.3575	0.3277	0.3172	0.2904	0.2726	0.2562	0.2502	0.2324	0.2175	0.1892	0.1772	0.1594	1.83
122-2	122	2	4	C4		0.3858	0.3545	0.347	0.3351	0.3232	0.3158	0.3098	0.3024	0.2889	0.2741	0.2651	0.2517	1.59
152-1	152	1	2	C4		0.3381	0.3381	0.3053	0.3009	0.2919	0.286	0.2785	0.2621	0.2368	0.213	0.1951	0.1772	1.77
152-1	152	2	2	C4		0.3664	0.3649	0.3232	0.3143	0.3024	0.2904	0.277	0.2592	0.2264	0.2041	0.1862	0.1668	1.74
152-2	152	1	3	C4		0.3768	0.3336	0.3202	0.2934	0.277	0.2562	0.2487	0.2279	0.2055	0.1832	0.1653	0.1564	1.74
152-2	152	2	3	C4		0.347	0.3247	0.3202	0.2994	0.277	0.2517	0.2398	0.216	0.1921	0.1698	0.1519	0.134	1.78

APPENDIX B: SARE-ACE LABORATORY WATER RETENTION DATA FOR EACH CORE SAMPLE

Table B-2. Water retention and bulk data for each individual core sample for the SARE-ACE experiment.

Ident	depth cm	subsample	sample	Site	$\nu$	0 cm	14 cm	30 cm	46 cm	64 cm	80 cm	100 cm	140 cm	200 cm	330 cm	500 cm	800 cm	BD g/cm <sup>3</sup>
107	114	1	1	C5		0.4066	0.3902	0.3902	0.2949	0.283	0.2606	0.2502	0.2264	0.1951	0.1623	0.1415	0.1251	1.53
122-1	107	1	1	C5		0.3649	0.3545	0.3545	0.3232	0.3187	0.3113	0.3053	0.2949	0.2815	0.2666	0.2532	0.2353	1.82
122-1	107	2	1	C5		0.35	0.347	0.3113	0.3098	0.2994	0.2964	0.2875	0.277	0.2577	0.2443	0.2353	0.2219	1.8
122-2	107	1	2	C5		0.3575	0.3545	0.3381	0.3396	0.3351	0.3321	0.3247	0.3158	0.3009	0.2904	0.2815	0.2681	1.8
122-2	107	2	2	C5		0.3709	0.347	0.3307	0.2964	0.277	0.2562	0.2458	0.2219	0.1921	0.1564	0.1326	0.1072	1.7
122-2	107	1	3	C5		0.3709	0.3545	0.3545	0.3024	0.2904	0.2755	0.2681	0.2532	0.2294	0.1996	0.1832	0.2219	1.7
122-2	107	2	3	C5		0.3858	0.3738	0.3738	0.3143	0.2979	0.28	0.2726	0.2592	0.2338	0.2041	0.1847	0.2681	1.62
152-1	153	1	1	C5		0.3321	0.3336	0.3083	0.3053	0.2949	0.2904	0.2741	0.2606	0.2279	0.2026	0.1936	0.1251	1.73
152-1	153	2	1	C5		0.3292	0.3262	0.3068	0.3009	0.286	0.2785	0.2696	0.2502	0.2204	0.2145	0.1951	0.2353	1.78
152-2	152	1	2	C5		0.3053	0.3024	0.2889	0.286	0.2785	0.2755	0.2666	0.2547	0.2309	0.2175	0.1996	0.1802	1.95
152-2	152	2	2	C5		0.3381	0.3381	0.3321	0.3292	0.3187	0.3068	0.2949	0.277	0.2413	0.2264	0.1966	0.1802	1.85
123-1	122	1	1	C6		0.3232	0.3232	0.3098	0.3009	0.2934	0.28	0.2666	0.2398	0.2115	0.1892	0.1743	0.1504	1.69
123-1	122	2	1	C6		0.3455	0.3232	0.3113	0.2875	0.2681	0.2517	0.2458	0.2294	0.2085	0.1787	0.1564	0.14	1.72
123-2	122	1	2	C6		0.3679	0.3649	0.3038	0.2845	0.2696	0.2592	0.2443	0.2338	0.2041	0.1906	0.1877	0.1653	1.52
123-2	122	2	2	C6		0.3604	0.3575	0.2651	0.2517	0.2353	0.2264	0.21	0.1951	0.1713	0.1519	0.137	0.1221	1.51
123-3	122	1	3	C6		0.3575	0.353	0.3053	0.2979	0.286	0.28	0.2681	0.2547	0.2279	0.2115	0.1877	0.1713	1.6
123-3	122	2	3	C6		0.3753	0.3753	0.3083	0.2934	0.2755	0.2621	0.2517	0.2368	0.21	0.1892	0.1862	0.146	1.47

APPENDIX B: SARE-ACE LABORATORY WATER RETENTION DATA FOR EACH CORE SAMPLE

Table B-3. Water retention and bulk data for each individual core sample for the SARE-ACE experiment.

Ident	depth cm	subsample	sample	Site	$\psi$														BD g/cm <sup>3</sup>
					0 cm	14 cm	30 cm	46 cm	64 cm	80 cm	100 cm	140 cm	200 cm	330 cm	500 cm	800 cm			
107	107	1	1	C7	0.4051	0.3366	0.3232	0.2889	0.2636	0.2219	0.1966	0.1609	0.146	0.1013	0.0819	0.0611	1.32		
107	107	2	1	C7	0.3664	0.3351	0.3202	0.277	0.2443	0.2175	0.1921	0.1787	0.1475	0.1057	0.076	0.064	1.51		
122-1	122	1	1	C7	0.4245	0.4036	0.3753	0.3396	0.3247	0.3113	0.3083	0.2949	0.2815	0.2681	0.2562	0.2428	1.66		
122-1	122	2	1	C7	0.4126	0.4007	0.3724	0.3426	0.3262	0.3128	0.3083	0.2949	0.2785	0.2636	0.2532	0.2368	1.65		
122-2	122	1	2	C7	0.3783	0.359	0.3247	0.3053	0.2889	0.277	0.2711	0.2592	0.2428	0.2294	0.216	0.2026	1.73		
122-2	122	2	2	C7	0.3858	0.356	0.35	0.3381	0.3247	0.3128	0.3083	0.2964	0.2815	0.2666	0.2517	0.2353	1.87		
152-1	152	1	1	C7	0.3753	0.3411	0.3351	0.3262	0.3202	0.3098	0.3038	0.2875	0.2726	0.2532	0.2413	0.2279	1.83		
152-1	152	2	1	C7	0.3768	0.3307	0.3143	0.2934	0.2755	0.2577	0.2443	0.2264	0.2041	0.1832	0.1758	0.1623	1.67		
152-2	152	1	2	C7	0.3262	0.3202	0.3158	0.3158	0.3143	0.3128	0.3068	0.2964	0.2845	0.2726	0.2666	0.2547	1.94		
152-2	152	2	2	C7	0.3336	0.3307	0.2979	0.2964	0.2919	0.2889	0.2845	0.2785	0.2681	0.2592	0.2472	0.2398	1.84		
108	107	1	1	C8	-	-	-	0.377	0.3452	0.3203	0.306	0.2837	0.245	0.1951	0.1654	0.1342	1.76		
123-1	122	1	1	C8	0.3307	0.3262	0.2904	0.2889	0.2815	0.2741	0.2666	0.2547	0.2294	0.207	0.1832	0.1564	1.7		
123-1	122	2	1	C8	0.353	0.347	0.3202	0.3143	0.3038	0.2964	0.2875	0.2696	0.2338	0.207	0.1936	0.1609	1.73		
123-2	122	1	2	C8	0.3992	0.3902	0.353	0.3307	0.3143	0.3024	0.2964	0.2845	0.2696	0.2532	0.2413	0.2279	1.8		
123-2	122	2	2	C8	0.4066	0.3694	0.359	0.3381	0.3247	0.3128	0.3068	0.2934	0.2785	0.2592	0.2472	0.2309	1.8		
122-1	122	1	1	D6	0.2964	0.2949	0.1653	0.1549	0.146	0.1415	0.134	0.1296	0.1147	0.1072	0.0998	0.0953	1.8		
122-1	122	2	1	D6	0.3217	0.3158	0.1832	0.1713	0.1609	0.1564	0.146	0.137	0.1192	0.1087	0.0983	0.0938	1.66		
122-2	122	1	2	D6	0.3024	0.3009	0.216	0.2041	0.1936	0.1892	0.1832	0.1713	0.1594	0.1519	0.1445	0.137	1.76		
122-2	122	2	2	D6	0.3068	0.3024	0.2666	0.2621	0.2562	0.2532	0.2487	0.2413	0.2264	0.2145	0.207	0.1966	1.88		
152-1	152	1	1	D6	0.3336	0.3307	0.3113	0.3143	0.3083	0.3053	0.2979	0.286	0.2651	0.2502	0.2458	0.2279	1.89		
152-1	152	2	1	D6	0.3396	0.3351	0.3351	0.3262	0.3202	0.3143	0.3053	0.2949	0.2726	0.2562	0.2428	0.2264	1.85		
152-2	152	1	2	D6	0.3366	0.3277	0.3217	0.3232	0.3217	0.3187	0.3158	0.3083	0.2964	0.286	0.277	0.2666	1.95		
152-2	152	2	2	D6	0.3262	0.3217	0.3143	0.3172	0.3143	0.3143	0.3083	0.3009	0.286	0.2741	0.2636	0.2517	1.83		

APPENDIX B: SARE-ACE LABORATORY WATER RETENTION DATA FOR EACH CORE SAMPLE

Table B-4. Water retention and bulk data for each individual core sample for the SARE-ACE experiment.

Ident	depth cm	subsample	sample	Site	Water Retention Data (w)																BD g/cm <sup>3</sup>
					0 cm	14 cm	30 cm	46 cm	64 cm	80 cm	100 cm	140 cm	200 cm	330 cm	500 cm	800 cm					
108	107	1	1	D7	0.4245	0.4111	0.4096	0.3232	0.3187	0.3083	0.3053	0.2964	0.2815	0.2636	0.2532	0.2413	1.58				
108	107	2	1	D7	0.4468	0.4304	0.4304	0.2994	0.286	0.2666	0.2592	0.2324	0.2055	0.1802	0.1653	0.1519	1.38				
123-1	122	1	1	D7	0.4245	0.4066	0.4051	0.3977	0.3887	0.3634	0.3455	0.3068	0.2577	0.1966	0.1579	0.1236	1.61				
123-1	122	2	1	D7	0.4155	0.4021	0.4007	0.3992	0.3887	0.3738	0.356	0.3098	0.2636	0.2026	0.1668	0.1579	1.65				
123-2	122	1	2	D7	0.3828	0.3604	0.3441	0.3232	0.3187	0.3128	0.3098	0.3053	0.2979	0.286	0.2785	0.2636	1.73				
123-2	122	2	2	D7	0.3768	0.359	0.359	0.3292	0.3232	0.3172	0.3113	0.3053	0.2949	0.2785	0.2681	0.2547	1.91				
154-1	152	1	1	D7	0.4007	0.3381	0.3277	0.3172	0.3143	0.3083	0.3038	0.2979	0.2889	0.2785	0.2696	0.2592	0.86				
154-1	152	2	1	D7	0.2979	0.2875	0.2666	0.2547	0.2502	0.2443	0.2428	0.2338	0.2264	0.2145	0.2041	0.1981	0.95				
154-2	152	1	2	D7	0.3321	0.3262	0.3053	0.3068	0.3053	0.3038	0.3024	0.2949	0.286	0.277	0.2711	0.2636	1.86				
154-2	152	2	2	D7	0.3366	0.3366	0.3202	0.3187	0.3158	0.3158	0.3083	0.3053	0.2934	0.283	0.2755	0.2696	1.86				
107	107	1	1	D8	-	-	-	0.3409	0.3192	0.2732	0.2568	0.2277	0.1992	0.1653	0.1498	0.137	1.76				
122-1	122	1	1	D8	0.3753	0.356	0.353	0.3455	0.3411	0.3292	0.3202	0.3083	0.2904	0.2651	0.2443	0.2175	1.76				
122-1	122	2	1	D8	0.356	0.3262	0.3187	0.2785	0.2711	0.2606	0.2547	0.2428	0.2309	0.2115	0.1966	0.1758	1.76				
122-2	122	1	2	D8	0.3917	0.3798	0.3187	0.3187	0.3083	0.3024	0.2904	0.28	0.2532	0.2338	0.2204	0.207	1.71				
122-2	122	2	2	D8	0.3798	0.3753	0.353	0.356	0.353	0.3515	0.35	0.3441	0.3262	0.3128	0.3038	0.2964	1.86				
152-1	152	1	1	D8	0.4081	0.3843	0.3798	0.3753	0.3679	0.3604	0.359	0.3515	0.3411	0.3292	0.3187	0.3053	1.9				
152-1	152	2	1	D8	0.4155	0.3887	0.3798	0.356	0.3321	0.3128	0.3053	0.2889	0.2726	0.2532	0.2398	0.2279	1.82				
152-2	152	1	2	D8	0.4319	0.4245	0.423	0.42	0.4126	0.3947	0.3664	0.3277	0.2413	0.2279	0.2532	0.1921	1.64				
152-2	152	2	2	D8	0.4081	0.3992	0.4007	0.3917	0.3783	0.3545	0.3202	0.2875	0.2383	0.2145	0.213	0.1609	1.59				

APPENDIX B: SARE-ACE LABORATORY WATER RETENTION DATA FOR EACH CORE SAMPLE

Table B-5. Water retention and bulk data for each individual core sample for the SARE-ACE experiment.

Ident	depth cm	subsample	sample	Site	$\psi$	0	14	30	46	64	80	100	140	200	330	500	800	BD
						cm	cm	cm										
107	107	1	1	D9	0.42	0.4141	0.4141	0.3128	0.2904	0.2458	0.2249	0.1877	0.14	0.1117	0.0923	0.0804	1.49	
122-1	122	1	1	D9	0.42	0.4007	0.3798	0.3604	0.3426	0.3307	0.3247	0.3113	0.2949	0.28	0.2666	0.2517	1.81	
122-1	122	2	1	D9	0.426	0.4126	0.3873	0.356	0.3366	0.3232	0.3158	0.3038	0.2875	0.2726	0.2606	0.2487	1.58	
122-2	122	1	2	D9	0.3664	0.3634	0.3515	0.3441	0.3411	0.3232	0.2934	0.2711	0.2204	0.1743	0.1504	0.1296	1.68	
122-2	122	2	2	D9	0.3515	0.35	0.3396	0.3366	0.3232	0.3024	0.283	0.2562	0.2041	0.1728	0.1549	0.134	0.72	
152-1	152	1	1	D9	0.3873	0.3619	0.3575	0.3485	0.3455	0.3366	0.3321	0.3232	0.3068	0.2904	0.2755	0.2651	1.98	
152-1	152	2	1	D9	0.3634	0.3307	0.3262	0.3217	0.3187	0.3143	0.3098	0.3038	0.2934	0.283	0.277	0.2666	2	
152-2	152	1	2	D9	0.347	0.3411	0.3024	0.2889	0.2741	0.2577	0.2428	0.2204	0.1772	0.1519	0.1355	0.1192	1.61	
152-2	152	2	2	D9	0.3545	0.3366	0.3292	0.3187	0.3068	0.2919	0.283	0.2636	0.2413	0.216	0.1981	0.1787	1.74	
107	107	1	1	D10	0.4051	0.3947	0.3932	0.3351	0.3262	0.3158	0.3083	0.2949	0.2741	0.2577	0.2428	0.2279	1.5	
107	107	2	1	D10	-	-	-	-	0.3392	0.3183	0.3074	0.2865	0.2639	0.2475	0.23	0.2208	1.5	
122-1	122	1	1	D10	0.3515	0.3441	0.3336	0.3366	0.3321	0.3307	0.3232	0.3083	0.2755	0.2502	0.2338	0.216	1.91	
122-1	122	2	1	D10	0.3569	0.3494	0.3315	0.3345	0.3271	0.3241	0.3107	0.2958	0.2645	0.2407	0.2228	0.207	1.93	
122-2	122	1	2	D10	0.3977	0.3932	0.3545	0.35	0.3426	0.3381	0.3307	0.3202	0.3024	0.2934	0.2875	0.277	1.7	
122-2	122	2	2	D10	0.3709	0.3694	0.35	0.3515	0.3455	0.3411	0.3351	0.3247	0.3098	0.2964	0.2875	0.2755	1.83	
152-1	152	1	1	D10	0.3426	0.3366	0.3113	0.3098	0.2979	0.2889	0.277	0.2636	0.2368	0.2413	0.2115	0.1921	1.87	
152-1	152	1	1	D10	0.3545	0.3441	0.3143	0.3143	0.3038	0.2919	0.28	0.2651	0.2324	0.21	0.1951	0.1802	1.77	
152-2	152	2	2	D10	0.2919	0.2919	0.2845	0.2875	0.2815	0.2726	0.2562	0.2368	0.2026	0.1758	0.1564	0.143	1.82	
152-2	152	2	2	D10	0.2934	0.2845	0.283	0.2845	-	-	-	0.283	0.277	0.2651	0.2577	0.2577	1.94	
152-3	152	1	3	D10	0.3843	0.3664	0.3649	0.3277	0.3158	0.3068	0.2994	0.2904	0.2755	0.2606	0.2487	0.2398	1.81	

APPENDIX B: SARE-ACE LABORATORY WATER RETENTION DATA FOR EACH CORE SAMPLE

Table B-6. Water retention and bulk data for each individual core sample for the SARE-ACE experiment

Ident	depth cm	subsample	sample	Site	$\psi$																BD
					0 cm	14 cm	30 cm	46 cm	64 cm	80 cm	100 cm	140 cm	200 cm	330 cm	500 cm	800 cm	g/cm <sup>3</sup>				
108	107	1	1	D11	0.417	0.4081	0.4066	0.3515	0.3381	0.3172	0.3053	0.2845	0.2472	0.213	0.1802	0.1504	1.6				
108	107	2	1	D11	0.4319	0.4185	0.4066	0.2889	0.2696	0.2443	0.2294	0.2011	0.1623	0.1266	0.1072	0.0909	1.41				
123-1	122	1	1	D11	0.3351	0.3277	0.3053	0.2815	0.2621	0.2413	0.2324	0.21	0.1787	0.143	0.1132	0.1147	1.81				
123-1	122	2	1	D11	0.3634	0.353	0.3172	0.2875	0.2636	0.2443	0.2338	0.2115	0.1758	0.1519	0.1445	0.1043	1.65				
123-2	122	1	2	D11	0.3932	0.3828	0.3664	0.3277	0.2949	0.2651	0.2547	0.2204	0.1877	0.1579	0.1385	0.1623	1.51				
123-2	122	2	2	D11	0.3858	0.3768	0.3575	0.3277	0.3009	0.2741	0.2621	0.2324	0.1996	0.1668	0.1445	0.1296	1.56				
152-1	152	1	1	D11	0.4051	0.3947	0.347	0.3381	0.3217	0.3098	0.2815	0.2532	0.2145	0.1936	0.1802	0.1638	1.52				
152-1	152	2	1	D11	0.426	0.417	0.35	0.347	0.3381	0.3292	0.3202	0.3053	0.2815	0.2666	0.2547	0.2398	1.64				
152-2	152	1	2	D11	0.4573	0.4364	0.4319	0.4275	0.42	0.4081	0.4007	0.3828	0.3664	0.3441	0.3158	0.2949	1.63				
152-2	152	2	2	D11	0.3575	0.3262	0.3217	0.3172	0.3128	0.3038	0.2994	0.2875	0.2741	0.2532	0.2398	0.2204	1.84				